

## Politecnico di Torino

Master's Degree: Electrical Engineering Curriculum: Smart Grids and E-Mobility Academic Year: 2024–2025 Graduation Session: October 2025

# Charge Accumulation in Polymers for $SF_6$ -Free Hybrid Gas/Solid Insulation System

**Supervisors:** Rachelle Hanna Fabio Freschi

**Candidate:** Maria Lupo

#### **Abstract**

Climate change is pushing the electrical engineering community to replace sulfur hexafluoride, the most potent greenhouse gas currently used in high- and medium-voltage insulation systems. In this context, hybrid insulation systems—combining a solid dielectric, typically a polymer, with an environmentally friendly gas—represent a promising alternative. However, ensuring their reliability requires a deep understanding of charge accumulation phenomena at gas/solid interfaces, which strongly influence the initiation of electrical discharges.

This thesis investigates surface charge dynamics in polymeric materials (PP, PVC, PVDF, PTFE) through surface potential decay (SPD) measurements. The decay curves were analyzed to estimate the trap density within the dielectrics and fitted using a bi-exponential model to extrapolate the potential evolution over extended time periods. The extracted surface charge densities serve as input for a numerical model developed in COMSOL Multiphysics<sup>®</sup>, enabling the simulation of a realistic electric field distribution in a triple point configuration where surface charge accumulation is taken into account. Based on this model, the streamer inception criterion is evaluated.

The results contribute to a deeper understanding of pre-breakdown mechanisms in  $SF_6$ -free hybrid insulation systems and support the design of more reliable and sustainable high- and medium-voltage insulation systems.

## **Contents**

1	Intr		1				
	1.1	G2Elal	)	1			
	1.2	Report	Outline	2			
2	Phys	Physical Principles of Gas Discharge and Interaction with Solids 3					
	2.1		rge in gases	3			
		2.1.1	Ionization process	3			
		2.1.2	Electron avalanches	4			
		2.1.3	Townsend theory	5			
		2.1.4	From electronic avalanches to streamers	5			
		2.1.5	Streamer phenomenon	7			
		2.1.6	Streamer-to-Leader Transition	8			
		2.1.7		10			
	2.2			12			
	2.2	2.2.1		12			
		2.2.2		13			
	2.3			14			
	2.3	2.3.1	$\boldsymbol{\varepsilon}$	14			
		2.3.2		14			
		2.3.2	Discharge recurrent and velocity				
3	Surf			17			
	3.1	Overvi	ew of SPD	17			
		3.1.1	Corona Charging	17			
		3.1.2	Kelvin Probe	18			
		3.1.3	1	19			
		3.1.4	Limits of the model	22			
	3.2	Data Ir	nterpretation	24			
		3.2.1	Trap Energy Distribution	24			
		3.2.2	Surface Charge Density and Influence on Electric Field	26			
		3.2.3	Influence of different parameters on Charge Decay	27			
4	E			30			
4	_	eriment					
	4.1 4.2	-	1	30			
		-		33			
	4.3			34			
		4.3.1		34			
		4.3.2	·	38			
		4.3.3	•	39			
		4.3.4	J J	41			
		4.3.5	1 00	44			
		4.3.6	Surface Charge Density	48			

5	Sim	ulation		50		
	5.1	COMS	${\sf SOL}$ Multiphysics $^{ ext{@}}$	50		
	5.2		ode in Air without Solid			
		5.2.1	Geometry	50		
		5.2.2	Validation of the model	53		
		5.2.3	Results	54		
	5.3	5.3 Electrode in Air with Solid				
		5.3.1	The triple point	56		
		5.3.2	Geometry	. 57		
		5.3.3	Validation of the model	59		
		5.3.4	Results	60		
Co	onclus	sions		65		
Re	eferen	ces		67		

## **Glossary**

- **Hybrid insulation** Insulation system that combines solid and fluid materials (gas or liquids) to achieve better electrical and mechanical performance.
- **Space charge** is an accumulation of free electric charges in a region of space that is not immediately neutralized by opposite charges, causing a disturbance in the local electric field.
- **Relative Permittivity** or dielectric constant, quantifies the factor by which the electric field is reduced inside a material compared to air [1]. This reduction results from the polarization of the material's molecules in response to the applied electric field.
- **Conductivity** Measure of a material's ability to conduct electric current. Quantitatively is defined as the inverse of resistivity. It depends on the presence and mobility of charge carriers within the material.
- **Triple Point** The interface where gas, solid dielectric and conductor meet.
- **Deep Traps** Energy states in an insulator that capture charge carriers for long times, affecting long-term charge storage.
- **Shallow Traps** Energy states that capture charges briefly and release them quickly, influencing short-term conduction.
- **Breakdown** Phenomenon in which an insulator loses its insulating capability and becomes conductive.
- **Streamer** Rapidly growing ionized channel initiating electrical breakdown. Velocity  $\approx 10^5$ .
- **Leader** Slower, highly conductive channel that follows streamers and leads to full breakdown. Velocity  $\approx 10^2$ .

#### 1 Introduction

Climate change is one of the greatest challenges of the new century. Scientists and engineers need to find new and innovative solutions for big problems, like replacing sulfur hexafluoride  $(SF_6)$ . Sulfur hexafluoride is the most impactful greenhouse gas: 1 kg of  $SF_6$  is equivalent to 23,5 tons of  $CO_2$  [2]. About 80% of the  $SF_6$  gas produced worldwide is used in high-voltage circuit breakers (CB) and Gas Insulated Switchgear (GIS) mainly due to its high dielectric strength. While this gas is still considered a standard because of its outstanding dielectric properties, there are new compounds that are more eco-friendly options, especially for medium-voltage electrical equipment. The insulation in such systems is hybrid, consisting of a pressurized gas — most commonly  $SF_6$ , which is expected to be replaced by compressed air — and a solid dielectric, typically a polymer.

G2Elab is conducting research to identify more sustainable alternatives to replace this gas since 1990. However, achieving optimal performance in these new systems requires a thorough understanding of the pre-breakdown and breakdown mechanisms at gas/solid interfaces. These complex phenomena depend on various parameters, including the relative permittivity and surface and volume conductivity of the solid, as well as the nature and pressure of the gas. In these configurations, charge accumulation on the surface of the solid plays a key role by altering the local electric field, directly affecting the initiation and propagation of electrical discharges, leading to system breakdown.

This study aims to assess the influence of solid dielectric properties on surface charge accumulation and thus on electric field reinforcement. The scientific approach of this work combines experimental investigations with electric field simulations to gain a deeper understanding of how charge accumulation in solid insulators affects field evolution in hybrid insulation systems. This will ultimately enable more accurate design of high and medium voltage electrical equipment without relying on  $SF_6$ . This work also contributes to ongoing studies (particularly Phd study of N. Moubarak) at G2ELab aimed at analyzing the impact of surface charge accumulation on pre-breakdown and breakdown processes under impulse voltage stress.

#### 1.1 G2Elab

My internship took place at the Grenoble Electrical Engineering Laboratory (G2Elab) from February 10, 2025, to July 25, 2025, located in GreEN-ER building in Grenoble.

The laboratory is nationally and internationally recognized in the field of electrical engineering.

G2Elab is structured into six specialized teams that cover key areas such as energy systems, materials, modeling, and innovative technologies. SYREL (Electrical Systems and Networks) works on the evolution, control, and optimization of electrical grids, integrating new technologies for future smart networks. EP (Power Electronics) is dedicated to the design and modeling of energy conversion systems, developing compact and high-performance semiconductor and power electronics devices. MADEA (Materials, Machines and Advanced Electromagnetic Devices) is a multidisciplinary team working on the design of innovative electromagnetic systems, combining expertise in materials science, modeling, and experimentation. MAGE (Models, Methods and Methodologies Applied to Electrical Engineering) focuses on computational modeling for electrical machines, control systems, and building applications. Finally, the Micro-Magnetic Systems team develops magnetic micro-electromechanical systems, combining

miniaturization with advanced functionality. The MDE (Dielectric and Electrostatic Materials) team investigates electric field-induced phenomena in dielectric materials—solid, liquid, or at interfaces—focusing on experimental methods and industrial applications like HVDC (High Voltage Direct Current) and energy recovery.

I had the honor of carrying out my internship within the MDE research department, under the supervision of Ms. Hanna Rachelle.

The MDE team consists of 7 researchers, along with 10 PhD students and post-doctoral researchers. The team's research finds applications in the sectors of electrical energy transmission, conversion, and storage, and is essential for understanding electrical discharge phenomena and the multi-physical aging processes of materials. My internship perfectly integrates with this department's activities, as my work focuses on the analysis of insulating dielectric materials.

#### 1.2 Report Outline

In the following, we will begin by a state of art on gas discharge phenomena, followed by an examination of the physical principles governing charge accumulation in solid insulators. Subsequently, we will investigate the gas-insulator system to understand how the gas discharge is influenced by the presence of the solid. These theoretical concepts are essential for understanding how the presence of the solid affects the gas discharge, as well as the mechanisms of charge accumulation in insulating polymers, which will subsequently be investigated experimentally through the surface potential decay method.

The potential decay experiment will be conducted on 4 samples with different electrical properties. The objective is to assess their electrical properties, with a particular focus on the spatiotemporal evolution of charge density, as this can significantly affect the initiation of gas discharges in hybrid insulation systems.

Based on the obtained data, trap density will be evaluated to identify the presence of deep or shallow traps, which govern the evolution of charge accumulation within the material.

Surface charge density will also be derived and used to simulate the electric field in COMSOL Multiphysics  $^{\$}$ .

## 2 Physical Principles of Gas Discharge and Interaction with Solids

#### 2.1 Discharge in gases

The following describes the phenomena related to discharge in gases without a solid. The break-down usually follows the pre-breakdown phenomena: electron avalanches, streamers, leaders. These mechanisms may take place individually or sequentially, depending on the environmental conditions (electric field, gas type and pressure, temperature, etc.).

Consider two metallic electrodes, an anode and a cathode, divided by a gap filled with gas. The behavior of the gas depends on the threshold value of the applied electric field: initially, the gas acts as an insulator, but once this threshold is exceeded, its conductivity changes rapidly within fractions of a microsecond, turning into a conductor.

#### 2.1.1 Ionization process

In theory, a gas should behave as an ideal insulator, without free electrons. However, in practice, free electrons are present due to background ionization (cosmic rays, natural radioactivity: in air, at normal temperature and pressure is about 10<sup>3</sup> free electrons/cm<sup>3</sup>) and play a crucial role in the discharge process, which begins at the cathode. These electrons are accelerated by the electric field along its lines, and during their motion, they can collide with gas molecules. As a result, they lose energy and decelerate [3].

The energy gained by an electron with charge e while moving a mean free path h in an electric field of strength E is given by the equation:

$$W = eEh$$

Here, the mean free path h is generally inversely proportional to the number density of gas molecules N, meaning  $h \propto 1/N$ . Therefore, the energy can be expressed as:

$$W \propto \frac{E}{N}$$

This ratio, E/N, is referred to as the energy parameter (reduced electric field) and defines the interaction between the electric field and the gas particles.

For an ideal gas, the number density N is related to the gas pressure p by the equation:

$$P = Nk_bT$$

where  $k_b$  is the Boltzmann constant and T is the absolute temperature. Since pressure P can be directly measured, while N cannot, it is more convenient in practice to express the energy parameter in terms of the ratio E/P, which represents the strength of the electric field per unit pressure. This form is commonly used in gas discharge studies.

The key processes active in gases during discharge can be summarized as follows [4].

**Ionization** occurs when an electron gains enough energy to ionize a neutral gas molecule

A, resulting in the formation of a positive ion  $A^+$  and an additional free electron. This process is referred to as "primary" ionization, and the electrons produced are termed "primary" electrons. The equation for this process is:

$$A + e^- \rightarrow A^+ + 2e^-$$

**Attachment** takes place when a free electron encounters a gas molecule with an available outer energy level. In this process, the electron attaches to the molecule, forming a negative ion  $A^-$  and reducing the number of free electrons in the system:

$$A + e^- \rightarrow A^-$$

**Excitation** occurs when an electron collides with a molecule but does not impart enough energy to ionize it. Instead, the molecule is excited to a higher-energy state. The molecule later decays to its ground state, emitting a photon of light in the process. The corresponding reactions (where *hv* is the photon energy) are:

$$A + e^- \rightarrow A^* + e^-$$
 and  $A^* \rightarrow A + h\nu_l$ 

**Photoionization** happens when a photon with energy greater than or equal to the ionization energy of a gas molecule strikes it, resulting in ionization and the release of a free electron:

$$A + h\nu_2 \rightarrow A^+ + e^-$$

At the cathode, two main processes occur: photoemission, where light causes electrons to be released from the surface, and ion impact, where positive ions hit the cathode and release electrons.

#### 2.1.2 Electron avalanches

The electron avalanche is a crucial process in gas discharges. Electrons, under the influence of an electric field, gain enough energy to ionize the gas molecules, thereby generating more free electrons [4].

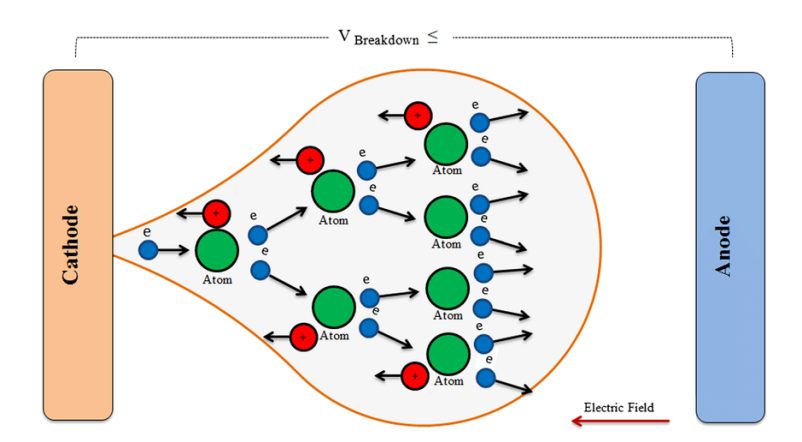


Figure 1: Electron Avalanche process [5].

As shown in figure 1 the process begins with a free electron. Under the influence of the electric field, this free electron can collide with gas molecules, ionizing them. As a result, a

group of new electrons, known as an "avalanche," is generated. In less than a microsecond, the number of electrons in an avalanche can increase to millions. This electron avalanche takes the form of a spherical cloud and, as it moves toward the anode, leaves behind positive ions that move slowly compared to the electron cloud. These electrons create a "space-charge field" that can influence the overall electric field. The avalanche phenomenon is difficult to predict due to the unpredictability of the collisions. However, the number of electrons at the head of the avalanche grows exponentially with increasing distance.

Let's consider the case where a gas only creates positive ions: a single electron from the cathode generates M electrons at the anode. d is the distance between the cathode and the anode, and  $\alpha$  is the primary ionization coefficient, which represents the average number of ionizing collisions an electron undergoes as it moves towards the anode. This coefficient is known for most gases. We can write:

$$M = e^{d\alpha} \tag{1}$$

M-1 is the number of new electrons and positive ions formed.

#### 2.1.3 Townsend theory

The Townsend theory provides a mathematical and theoretical description of how electron avalanches can lead to the breakdown of the gas.

The electron released from the cathode by a photon or a positive ion is called a secondary electron. Secondary electrons generate secondary avalanches. The Townsend criterion for gas breakdown can be expressed as:

$$\gamma(M-1) \ge 1 \tag{2}$$

where  $\gamma$  can be seen as the probability that a secondary electron is released due to the impact of a positive ion. By substituting (2) in (1) we obtain the breakdown condition [4]:

$$11 \le \alpha d \le 18 \tag{3}$$

#### 2.1.4 From electronic avalanches to streamers

As the electrons move toward the anode, the unbalanced distribution of electrons evolves into a state of near equilibrium [6]. This process is driven by both the applied external electric field and collisions with gas molecules. During this time interval, the space-charge field is significantly smaller than the applied field, and the development of avalanches is practically the same as that obtained by neglecting the space charges. Therefore, the growth of electrons is exponential. The electric field in the radial direction (normal to the electric field) is entirely due to the space charge, while in the longitudinal direction (tangential to the electric field), it is governed by the applied electric field. The reason for this lies in the different influences of the space charge and the applied electric field: in the radial direction, the space charge accumulates as electrons are accelerated and collide with gas molecules, creating a local electric field that affects the radial direction. In the longitudinal direction, the external electric field is the main driving force for the movement of electrons toward the anode. In this direction, the contribution of the space

charge to the electric field is relatively small compared to the applied field.

As more and more electrons are generated, the avalanche starts to deviate from this exponential growth. This happens because, as the number of electrons increases, they begin to shield the applied electric field inside the avalanche. This shielding reduces the overall electric field in the center, causing the rate of electron production to decrease. As the space-charge effect becomes significant, the total field inside the avalanche decreases, with a concomitant decrease in the mean energy. It is observed that the electric field reaches a minimum inside the avalanche due to the shielding effect of the space charge. Anyway, at higher pressures, the decrease in ionization in the center of the avalanche is balanced out by an increase in ionization at the edges of the avalanche, where the electric field is stronger.

At this stage of the process, the formation of the anode-directed streamer can be observed. The electric field in the region near the avalanche head is at least 1.3 times stronger than the externally applied field. The intense increase in the electric field at the streamer tip is due to the high ion density and the small radius of curvature of the streamer tip. This increase in electric field intensity facilitates both the acceleration of free electrons already present and the generation of new electrons through ionization.

The cathode-directed streamer occurs shortly after, when the photoelectrons generated at the rear of the avalanche initiate new secondary avalanches. However, the anode-directed streamer propagates at nearly twice the velocity of the cathode-directed streamer.

Below, we will analyze the streamer criterion, also known as the Meek criterion [7]. The effective ionization coefficient  $\alpha_{eff}$  represents the net electron grow rate. In other words it is the difference between the ionisation coefficient  $\alpha$  and the attachment coefficient  $\eta$ :

$$\alpha_{eff}(E) = \alpha(E) - \eta(E) \tag{4}$$

 $\alpha_{eff}$  accounts for all processes influencing the number of free electrons, such as electron capture. It represents a net avalanche growth rate: if  $\alpha_{eff}$  is positive, the avalanche grows; otherwise it decreases. During a time t, the center of the avalanche drifts a distance  $d = \mu_e Et$  (where  $\mu_e$  is the electron mobility), and the number of electrons is multiplied by a factor  $\exp(\alpha_{eff}(E)d)$ .

When the space charge density of the avalanche creates an electric field comparable to the external field, the discharge transitions into the streamer phase.

In ambient air, this happens when the **Meek criterion** k is verified:

$$\alpha_{eff}(E)d \approx 20$$
 (5)

When a single electron develops an avalanche in an inhomogeneous electric field  $E(\mathbf{r})$ , the local multiplication rates  $\alpha_{eff}(E)$  add up over the electron trajectory L, as expressed by the integral  $\int_I \alpha_{eff}(E(s)) ds$ .

The Meek criterion for the avalanche-to-streamer transition in air at standard temperature and pressure then becomes:

$$\int_{L} \alpha_{eff}(E(s))ds \approx 20 \tag{6}$$

The value in (6) is higher for  $SF_6$  because this gas is strongly electronegative, so it requires higher ionization to became a streamer.

The value of  $\alpha_{eff}$  in air can be estimated with the analytical model presented by [8] as follows:

$$\alpha_{eff}/N = 4 \cdot 10^{-20} \exp(-985/(E/N + 43)) - 30 \cdot 10^{-24} \text{ [m}^2\text{]}$$
 (7)

where N is the neutral gas density  $(N = 2, 47 \cdot 10^{25})$  and E is the Electric field.

#### 2.1.5 Streamer phenomenon

Streamers are fast electron avalanches that may lead to electric breakdown. They occur in less than a microsecond at high pressure-distance ( $P \times d$ ) values above 10 kPa. Streamers have a filamentary shape and propagate at a higher velocity than both electron avalanches and leaders. Unlike the gradual development in Townsend's model, streamers form when the space charge at the avalanche head generates an electric field comparable to the applied field. According to the Meek criterion [9], the transition from avalanche to streamer occurs when the number of electrons exceeds the critical threshold of  $N_{cr} = 10^8$  in air. Breakdown occurs because of these narrow, filamentary plasmas, which propagate faster than in the Townsend mechanism, because they do not rely on ion migration to the cathode to produce secondary electrons.

Positive and negative streamers are different (Figure 2).

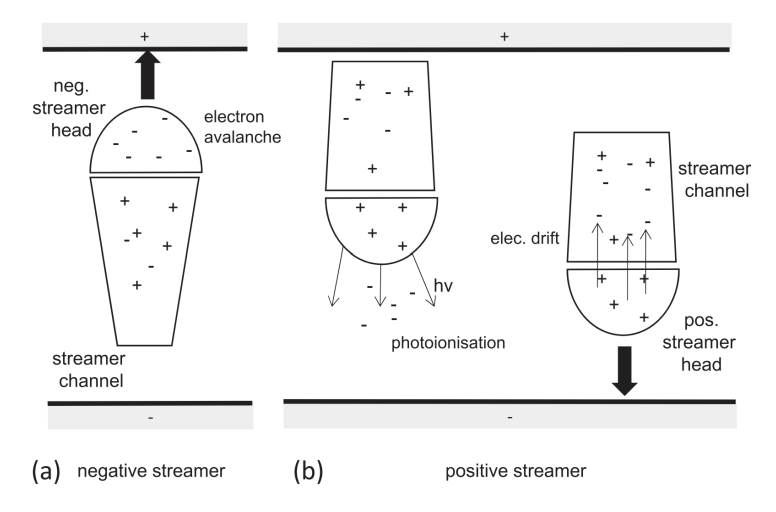


Figure 2: Negative and Positive Streamers. [10].

**Negative streamers** [11] are generated once the Meek criterion is met in the vicinity of the cathode. As illustrated in Figure 2, the negative streamer head propagates in the same direction as the electron drift. The electric field at the streamer head plays a crucial role in accelerating electrons and sustaining the propagation of the discharge.

In Figure 2, the two stages of the **Positive streamers** process are clearly visible. On the left, the ionization wave can be observed to propagate in the opposite direction to the motion of electrons. Positive streamers primarily rely on the photo-ionization mechanism: during the primary avalanche, photons are emitted, which can ionize surrounding neutral molecules, thereby facilitating the advancement of the streamer. The total electric field, which results from the sum of the applied electric field and the field generated by the space charge, reaches its maximum value in front of the space charge. After an ionized channel is formed, while the space-charge zone appears very bright. When the newly formed channel touches the cathode, secondary streamers are transported within it, illuminating the channel again. However, these

secondary streamers propagate at a lower velocity and with an energy approximately 5 to 10 times lower than the primary ones. A photo of the positive streamer in dried air is shown in the Figure 3.

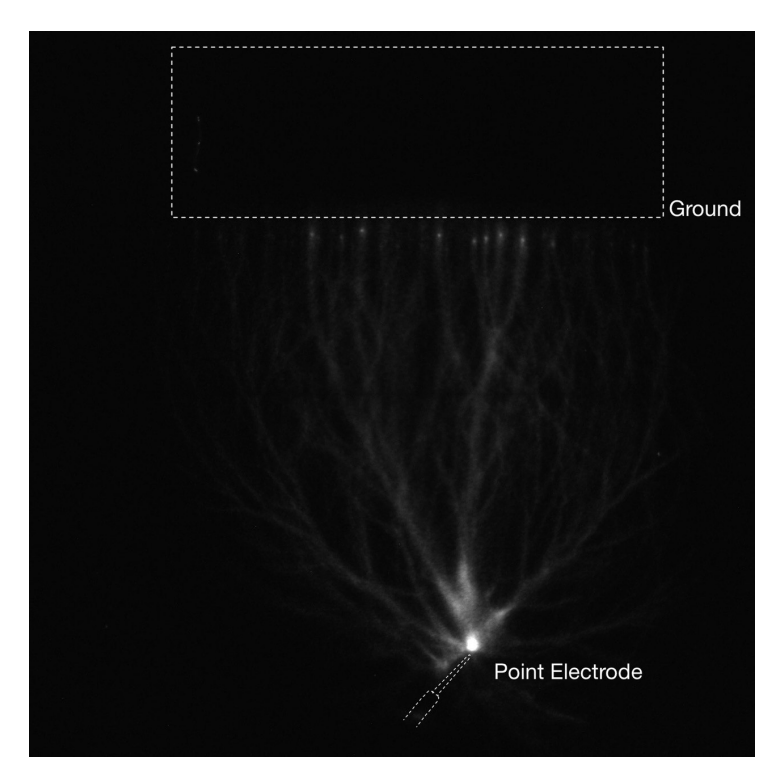


Figure 3: Streamer positive polarity in dried air between a positive needle electrode and plane, gap distance 5 cm. Applied voltage 38 kV. Photo courtesy of G2Elab.

#### 2.1.6 Streamer-to-Leader Transition

The discharge in the gas is closer to breakdown after the development of the second streamer; in fact, the transition from streamer to leader is observed. Leaders represent self-propagating electrical discharge phenomena, capable of extending for kilometric distances and commonly observed in the atmosphere in the form of lightning.

A necessary condition for the transition from streamer to leader is the heating of surrounding gas. A temperature of about 1500 K is required in dry air, or around 2000 K in humid air [12]. The temperature increase in the channel is associated with the rise in voltage: non-recombined electrons gain energy and ionize neutral molecules. As more electrons are produced through ionization, the gas in the channel heats up and expands. This expansion lowers the number of neutral particles in the channel, which increases the value of E/N that is the electric field divided by the neutral particle density. If E/N exceeds the critical threshold, a new phase of massive ionization may occur, leading to breakdown [11].

The leader's structure is primarily composed of three distinct components [13] as we can see in Figure 4:

The streamer zone: a region composed of a multitude of small ionized filaments. The propagation of these filaments generates an electric current that contributes to the heating of the main leader channel.

**The leader head:** the region where the phase transition from streamers, characterized by low temperatures, to a conductive channel with high temperature occurs.

**The channel:** a high-temperature plasma filament, typically ranging between 5000 K and 7000 K. This channel acts as a conductor, allowing the flow of electricity from the source to the leader head.

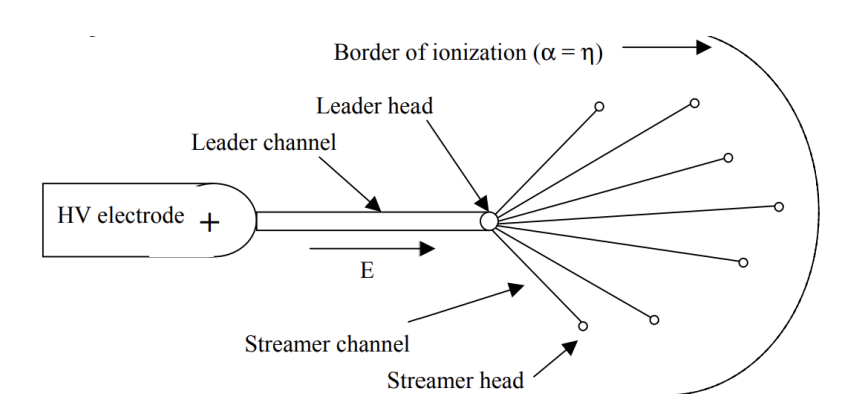


Figure 4: The structure in front of a leader discharge [14].

Finally, leaders can be distinguished on the basis of their polarity, classified as positive or negative. The process of heating the surrounding air constitutes a fundamental mechanism for the propagation of both types of leaders. In positive leaders, this heating is concentrated in the head, adjacent to the main channel. In negative leaders, heating is associated with the formation and growth of a space leader that precedes the main channel.

The studies by Gallimberti and Wiegart [15] confirm that the streamer-to-leader transition occurs both in air and in electronegative gases such as sulfur hexafluoride, although the mechanisms involved are markedly different.  $SF_6$  is a highly electronegative gas, which means that it tends to capture free electrons, thereby hindering the propagation of discharge. As a result, the streamer-to-leader transition in  $SF_6$  is more complex, yet it can still take place. Under these conditions, an intermediate phenomenon known as the leader precursor has been observed, a luminous region with no measurable current that consistently precedes the formation of a leader channel. In contrast, in air, the transition can occur more directly and rapidly as a result of the higher availability of free electrons and positive ions.

Compared to streamers, leaders are ionized channels with higher temperature and conductivity, and they are capable of sustaining the flow of even very large currents. For a leader propagation in air with a typical velocity of  $(1-3) \times 10^6$  cm/s, the time required to heat the gas to the necessary temperature is less than  $3 \times 10^{-7}$  seconds.

In the Figure 5, the leader obtained by applying a voltage of 52 kV in dry air with an electrode gap of 5 cm is shown.

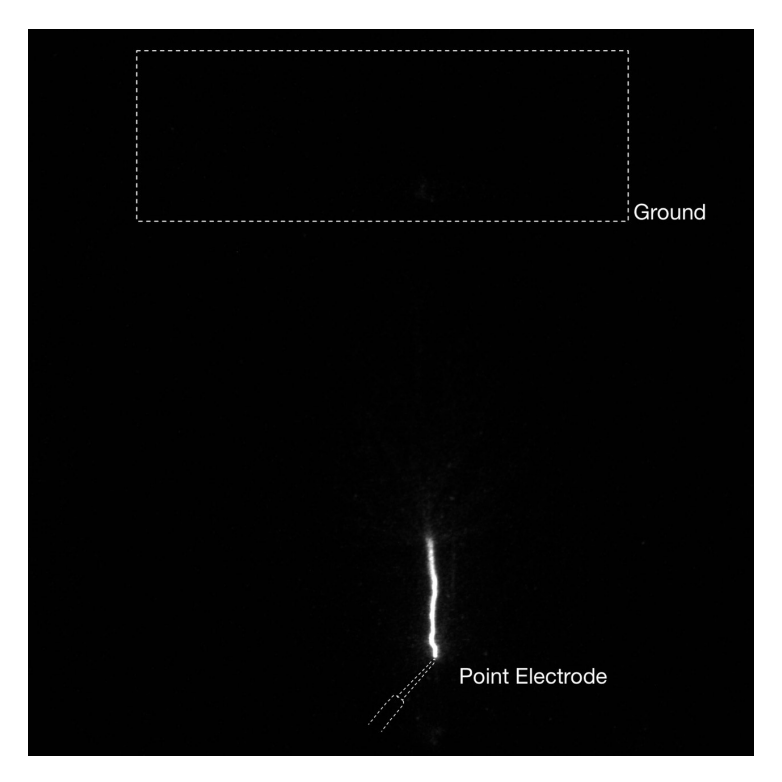


Figure 5: Leader in dried air between a positive needle electrode and plane, gap distance 5 cm. Applied voltage 52 kV. Photo courtesy of G2Elab.

#### 2.1.7 Breakdown Mechanisms

As previously discussed, the breakdown of a gas requires an applied electric field strong enough to initiate a self-sustaining ionization process. Breakdown in gases can occur through different physical mechanisms. The dominant mechanism depends on factors such as the product of the gas pressure P and the distance between the electrodes d.

In 1889, Friedrich Paschen documented his studies on the minimum voltage required to initiate a discharge in a gas [16]. He observed that both the gas pressure and the distance between the electrodes affect the breakdown process, and concluded that the relevant parameter is the product  $P \times d$ , rather than the two variables considered independently. Paschen's study was entirely empirical, but it was later confirmed by Townsend through the development of the electron avalanche theory.

From the Figure 6, we can observe that the curves exhibit a minimum breakdown voltage. For the Air, with values of  $P \times d$  lower than this minimum, the breakdown voltage increases. The left side of the curve can be explained by the fact that, as the pressure decreases, the mean free path of electrons becomes very long, resulting in very few collisions between electrons and neutral molecules. As a result, an higher voltage is required to initiate the discharge. On the right side of the curve, the increase in pressure leads to a shorter mean free path for electrons. This reduces the effective space available for ionization, and a higher voltage is again needed to achieve breakdown.

As expected, the breakdown curve for  $SF_6$  is above that of air. This is because  $SF_6$  is an excellent insulating gas, making it more difficult to ionize.

It is commonly accepted that the different mechanisms of breakdown in air at atmospheric

pressure depend on the  $P \times d$  parameter as follows [11]:

- $10^{-4} < P \times d < 0.3 \, \text{bar} \cdot \text{cm}$ : Townsend's breakdown;
- $0.3 < P \times d < 5.0$  bar · cm: Townsend and Streamer on different condictions;
- $5.0 < P \times d < \approx 100 \, \text{bar} \cdot \text{cm}$ : Streamer breakdown;
- $P \times d > \approx 100 \, \text{bar} \cdot \text{cm}$ : Leaders breakdown;

In the Figure 7, the breakdown obtained by applying a voltage of 60 kV in dry air with an electrode gap of 5 cm is shown.

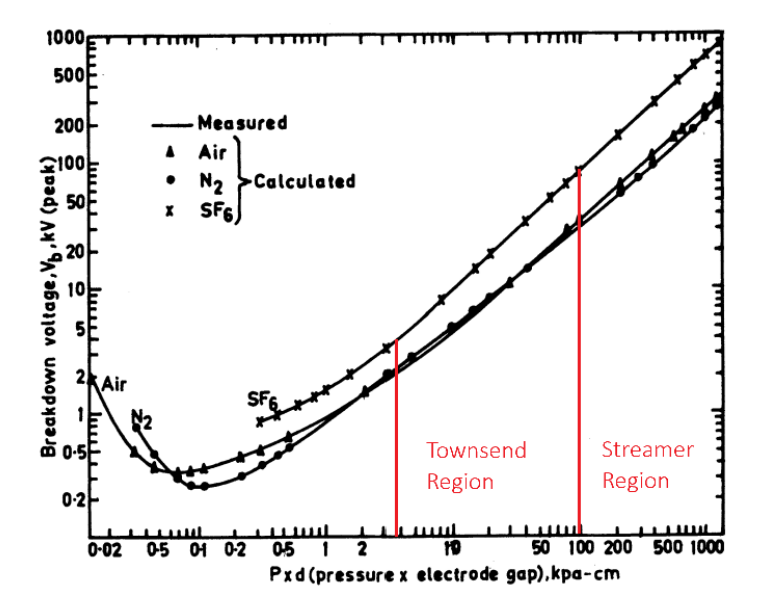


Figure 6: Paschen's law for several gases [17]

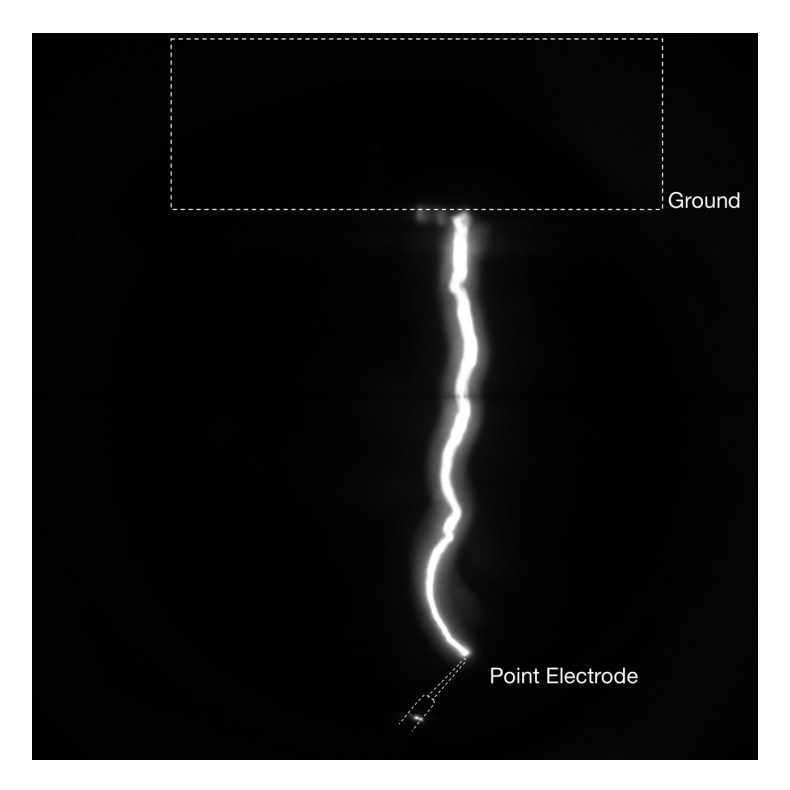


Figure 7: Breakdown in dried air between a positive needle electrode and plane, gap distance 5 cm. Applied voltage 60 kV. Photo courtesy of G2Elab.

#### 2.2 Relevant Physical Phenomena in Solids

#### 2.2.1 Trapping and Detrapping of Free Electrons

In polymers [18], the conductivity value is typically low ( $< 10^{-11}$  S/m) because of the limited number of free charge carriers with low mobility. This mobility is significantly influenced by the presence of energetic traps within the material's structure. Consequently, the overall electrical properties of polymers are closely related to the energy distribution of these trapping states.

Two types of trapes exist in polymers: shallow traps (related to physical defects within the material) and deep traps (related to chemical defects). Shallow traps correspond to low-energy location and deep traps to higher energy depth, as we can see in the Figure 8.

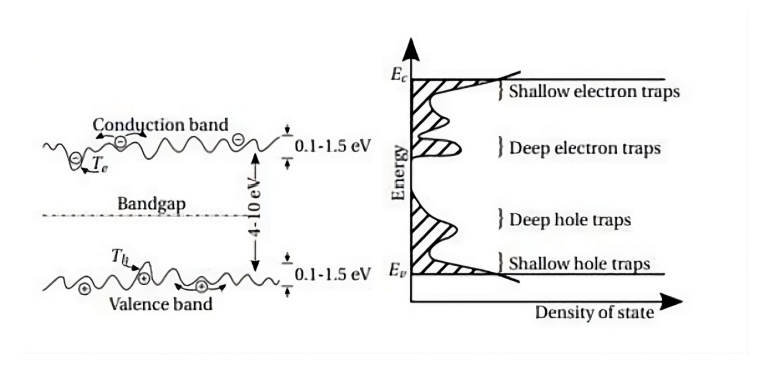


Figure 8: Distribution of traps and relative energy level [19].

When charges are injected into an insulating polymer, they rapidly dissipate their excess energy and settle within these traps. The depth to which these charges can penetrate the material is determined by the distribution of the traps themselves, the intensity of the applied electric field, and the timescale of observation. It is also important to note the phenomenon of retrapping, where charges, after being released from one trap, can be recaptured by another. Finally, isothermal discharge experiments, which monitor the decrease in surface potential at a constant temperature, represent a crucial experimental technique for obtaining detailed information about the distribution of trapping states within the polymer.

For simplicity, we will consider charge decay in the absence of retrapping. Following a rapid injection of electrons into a polymer, the electrons distribute themselves among the available energy states, which include shallow traps and deep traps. Electrons in shallow traps are easily released (detrapped) due to thermal energy. Under the influence of the electric field, once released, they gain kinetic energy and can contribute to the external discharge current. The total number of deep trapping states is generally greater than that of shallow traps, and consequently, at longer times, the majority of injected electrons tend to remain trapped in the deep states. However, electrons trapped in deep states can also be excited (e.g., thermally) and transition to higher energy levels, as up to the conduction band, but this process typically requires more energy and occurs on longer timescales.

#### Considering:

 $E_0$ : Mobility Edge, a property of the disordered material that separates extended conduction states with high mobility from those with low mobility (traps).

 $E_d$ : Demarcation Energy, Depends on time. Represents the energy above which traps have released their charge carrier so have been emptied at time t after carrier injection. As time increases,  $E_d$  decreases, meaning that progressively deeper traps begin to empty.

We get for the Energy level of electron traps  $E_t$ :

$$E_t = E_0 - E_d = kT \ln(\gamma t) \tag{8}$$

where  $\gamma$  is the attempt frequency, of order 4,  $17 \cdot 10^{13} s^{-1}$  [20]. The intensity of the observed electric current is related to the speed with which the demarcation energy  $E_d$  changes over time, and it is also related to the local density of states, that is, the number of free places for electrons at each energy level:

$$I(t) \propto N(E)dE/dt \tag{9}$$

and from (8), we get:

$$I(t) \propto N(E)KT/\nu t$$
 (10)

Therefore, the factor I(t)t is related to the number of traps occupied by electrons at the energy  $E_d$ . Accumulated electrons can be released by ion bombardment or photoemission. These emitted electrons from the solid can affect secondary avalanches and aid streamer propagation.

#### 2.2.2 Charge Accumulation

The sequential application of voltage pulses leads to a gradual accumulation of charge within the solid insulating material. This charge accumulation can significantly influence the initiation and propagation of discharges in the gaseous medium, as it alters the pre-existing spatial distribution

of the electric field. As discussed in the preceding paragraph, the trapping and detrapping processes of charges influence the charge distribution within the insulating polymer. The charges that remain trapped lead to a net accumulation of charge within the material. This accumulation is not constant but depends on the difference in rates between the charges being trapped and those being released at different energy levels. Deeper traps, for example, can trap charge for prolonged periods. This accumulation of trapped charge creates a non-uniform charge distribution and contributes to the creation of an internal electric field within the material. It is also important to note that the charge accumulation is strongly dependent on factors such as the trap concentration and the material's inhomogeneity.

#### 2.3 Influence of Solid on Gas Discharge

#### 2.3.1 Distorted Electric Field

Placing a dielectric solid parallel to an electrode axis alters the electric field lines due to the solid's higher relative permittivity compared to air. This difference in permittivity causes the field lines to concentrate towards the dielectric's surface. Consequently, if the electrode features a sharp point, this concentration of field lines becomes particularly pronounced at the tip, resulting in a significantly more intense electric field in that localized region [11].

The phenomenon of electric field line distortion along the solid can be observed in Figure 9.

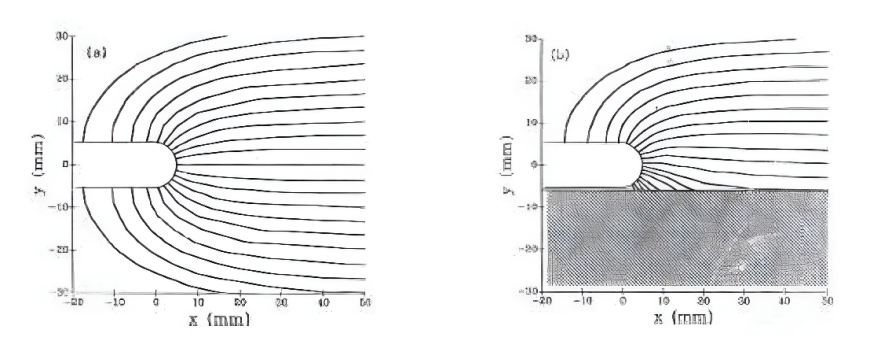


Figure 9: Electric field near the point electrode in air without solid and in presence of the solid [21].

The electric field distortion caused by the presence of a solid dielectric intensifies the field in specific areas. This phenomenon arises from the need to satisfy electrostatic boundary conditions, resulting in a stronger electric field at irregular surfaces. Consequently, this creates a preferential path for discharge, characterized by a higher electric field.

#### 2.3.2 Discharge localization and velocity

The presence of the insulating dielectric significantly influences the streamer's propagation path. This is because the streamer will, in part, propagate along the surface of the solid insulator. This phenomenon occurs in response to the physical effects induced by the solid's presence. However, the path followed by the streamer depends on the type of gas used, the geometry under study, the dielectric's properties, and also the pressure. Additionally, it's observed that in the presence of a solid, positive discharges initiate more easily than negative ones. [7]

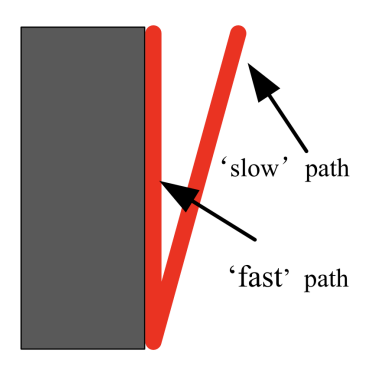


Figure 10: Streamer propagation paths [22].

As we can see in Figure 10, when a streamer propagates along an insulating surface, two distinct paths are observed [22]: a fast component and a slow component. The fast component propagates directly along the surface of the dielectric material, exhibiting a higher velocity ( $\sim 10^5 \, m/s$ ). The slow component, conversely, propagates in the air adjacent to the surface, with a lower velocity ( $\sim 10^2 \, m/s$ ). Measurements utilizing photomultipliers 10 have detected two light peaks at the cathode, corresponding to these two components. The first peak is associated with the fast component, and the second with the slow component. Photographs captured with stroboscopic ICCD [23] camera have visually confirmed these propagation paths (Figure 11). Furthermore, higher values of relative permittivity have been observed to increase the probability of discharge along the dielectric surface.

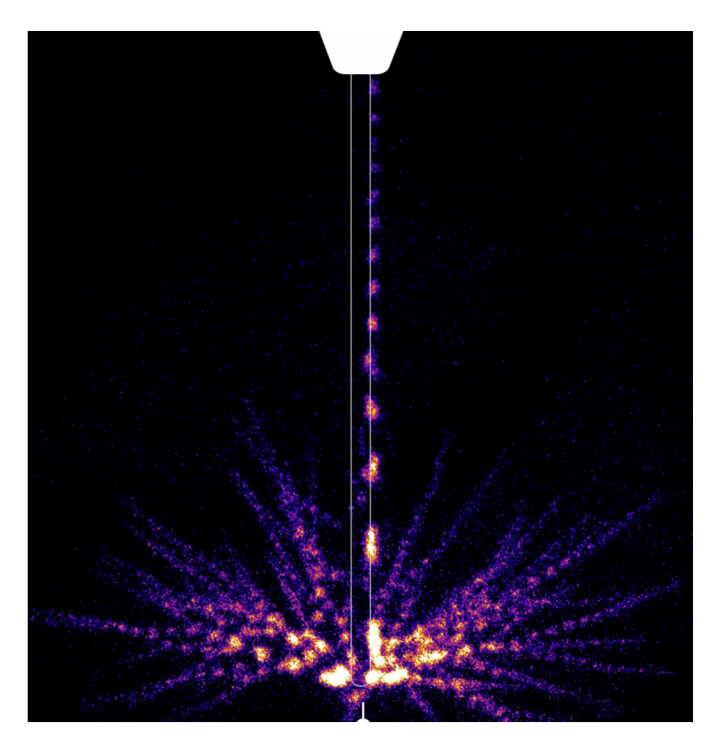


Figure 11: Discharge at 600 mbar in air for the rod with TiO2 filler, with relative permittivity  $\epsilon_r = 8$ . A positive surface streamer can be observed and its velocity is clearly much larger than the velocity of the bulk streamers [23].

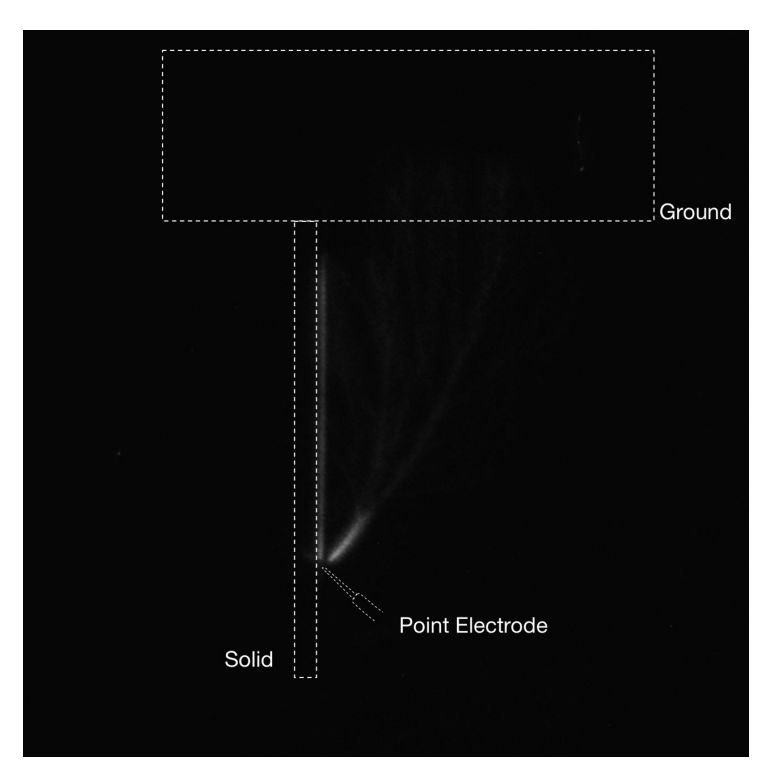


Figure 12: Streamer propagation in presence of solid. Dried air and gap distance of 5 cm between a positive needle electrode and plane. Applied voltage 46 kV. Photo courtesy of G2Elab.

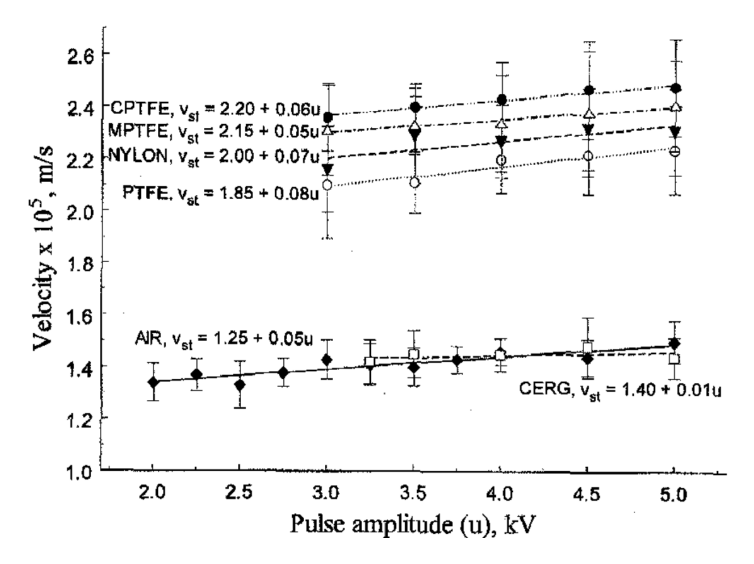


Figure 13: Propagation velocities at traverse up to the cathode as a function of the pulse voltage amplitude [24].

As shown in Figure 13, the streamer velocity at the cathode increases only weakly with the pulse amplitude [24]. It is clear that streamers propagate at a higher velocity along the insulator surface (like for materials CPTFE, MPTFE, NYLON, PTFE) than in air. Furthermore, different values of relative permittivity correlate with distinct velocities at the cathode. An exception is the ceramic insulator (CERG), which exhibits behavior comparable to that obtained in the absence of a solid insulator.

### **3 Surface Potential Decay**

The environmental concerns surrounding  $SF_6$  mean we urgently need to find new solutions and insulating materials, especially those suitable for conditions near the triple point.

Surface potential decay (SPD) is widely considered when selecting solid insulators for high-voltage applications. This experiment allows us to obtain important information regarding the dielectric properties of an insulating material. The advantage of surface potential measurement is its sensitivity to charge location, unlike current measurement, which records charge displacement. Several physical processes are involved: volume polarization, surface conduction, atmospheric neutralization, charge injection at the interface, and surface irregularities.

#### 3.1 Overview of SPD

#### 3.1.1 Corona Charging

A corona discharge is an electrical discharge that forms when a sufficiently high voltage is applied between asymmetrical electrodes, such as a sharp point and a flat plate [25].

This discharge creates two distinct regions. Near the point or wire, a small ionization zone produces ions and excited molecules. The numerous collisions between these charged particles and neutral gas molecules also initiate gas movement. This region is characterized by the presence of charge carriers of a single polarity. These carriers have low mobilities. The specific ions produced depend on the corona's polarity: negative coronas in air primarily generate  $CO_3^-$  ions, while positive coronas mostly yield  $(H_2O)nH^+$  ions. The produced ions are then accelerated by the potential difference towards the sample, whose lower face is connected to ground.

Corona ions do not penetrate deep into the material's bulk. Instead, they transfer their charge to the surface. This excess charge can move on the surface or can be trapped in surface traps or can be neutralized by ions of the air.

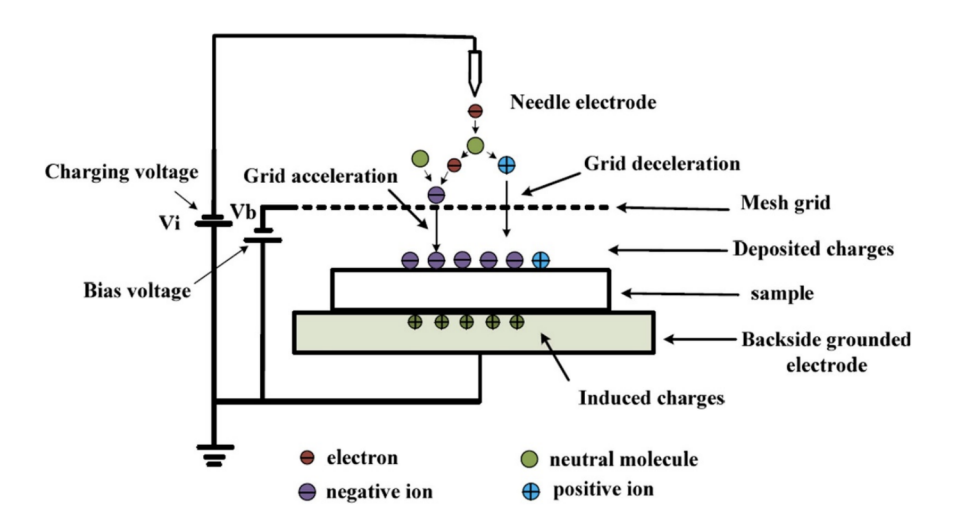


Figure 14: Diagram of a Corona Triode [26]. With a negative charging voltage both electrons and negative ions are deposited.

The metallic grid between the high-voltage point electrode and the sample to be charged, as illustrated in Figure 14, ensures a good control over the charged surface potential and the charge

uniformity across the sample. These three-electrode systems are conventionally referred to as corona triodes.

The continuous adjustment of the grid voltage,  $V_g$ , maintains a constant charging current. In such configurations, the grid voltage  $V_g$  is directly related to the sample's surface potential V(t) by the equation:

$$V_{\varrho} = V(t) + \Delta V$$

Here,  $\Delta V$  represents the potential difference between the grid and the sample's surface.

#### 3.1.2 Kelvin Probe

The Kelvin method in the last years has gained popularity as a standard surface analysis technique due to his extremely high surface sensitivity. This method is based on the noncontact and nondestructive technique. The Kelvin probe allows for the measurement of contact potential difference (CPD) without inducing electron displacement [27].

A traditional Kelvin probe is essentially a vibrating capacitor designed to measure surface potential without physical contact. It primarily consists of two key electrodes: a vibrating electrode (the probe itself) this is typically a flat, circular electrode that oscillates perpendicularly to the sample's surface and a Stationary electrode, which is the surface of the sample, usually connected to ground.

These two electrodes form a capacitor. When there is a contact potential difference ( $V_{CPD}$ ) between the vibrating probe and the sample, the probe's oscillation induces an alternating current (AC) in the external circuit  $I = V_{CPD} dC/dt$ . To counteract this, an external DC "backing" potential ( $V_b$ ) is applied and adjusted until the induced AC current is nullified. At this null point,  $V_b$  is equal in magnitude and opposite in polarity to  $V_{CPD}$ , thereby allowing for the precise determination of  $V_{CPD}$ .  $V_b$  is equal to the surface potential  $V_s$  of the material under test.

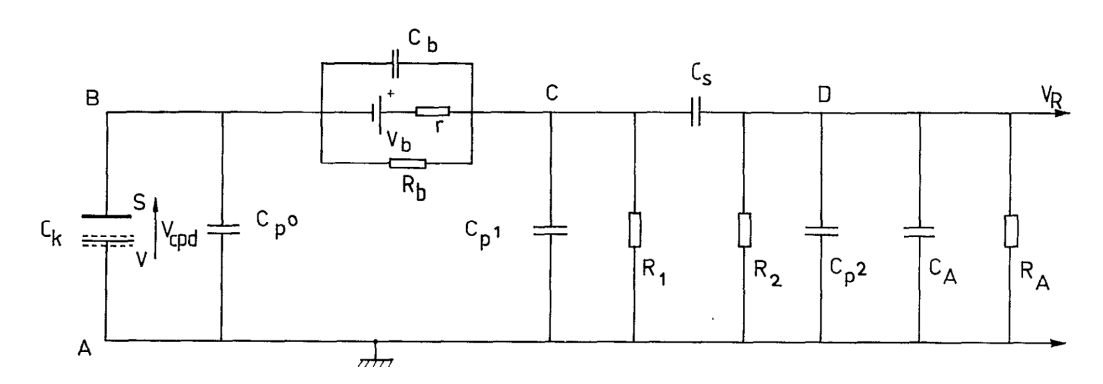


Figure 15: Kelvin Probe Circuit [27].

As we can see from Figure 15:

• AB: includes the time-varying Capacitance  $C_k(t)$  and V is the vibrating reference electrode and S is the sample electrode. The parasitic capacity to earth  $C_p^0$  is due to the probe connection wires.

- BC: Within the Kelvin probe circuit, the parameters r,  $C_b$ , and  $R_b$  are used to characterize the series resistance and parallel impedance associated with  $V_b$ . Specifically, the  $C_p^1$  term accounts for capacitances induced by the connecting cables on the  $V_b$  side, including those due to the filter.
- CD: The  $R_1$ - $C_S$ - $R_2$  filter is essential for ensuring that long time-constant voltage transients, which can arise, for instance, from  $V_b$  switching actions, decay quickly to ground.  $C_p^2$  represents the parasitic capacitance to ground on the preamplifier side. Finally,  $R_A$  and  $C_A$  denote the input resistance and parallel capacitance of the preamplifier, respectively.

#### 3.1.3 General Equations of Potential Decay

The amount of charge within an insulating material decays over time. This decay is attributed to factors of various natures (see Figure 16): bulk neutralization within the volume, surface conduction, and the neutralization of surface charges by air ions [28].

**Surface charge displacement** can occur due to carriers hopping through different traps or can be ohmic in nature. Surface conductivity allows for the quantification of this mechanism. However, it is important to remember that surface conductivity is strictly linked to external environmental conditions, particularly temperature.

**Bulk neutralization** is related to internal ionization processes and consists of charge decay within the material's volume. Internal ionisation is linked to volume conduction, which is the transport of charge within the material, and to dipolar response, which occurs in the presence of intrinsic dipoles within the material.

Finally, **Neutralization by air ions** can occur through recombination between surface charges and free ions present in the surrounding air.

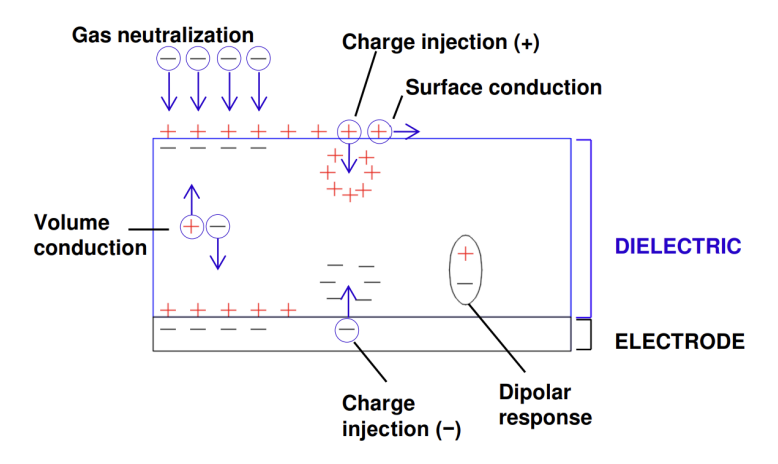


Figure 16: Mechanism of charge decay [28].

Usually, the phenomenon of surface charge displacement is the dominant discharge mechanism for polymers and insulating materials, especially when the surface is degraded or in the presence of humidity [29]. However, it's important to emphasize that through SPD, it's possible to analyze charge decay within the bulk of the insulating material. This is crucial for obtaining information regarding the **intrinsic properties** of the material. Volume conduction is an intrinsic property of the material, linked to its atomic and molecular structure, the presence of defects within the bulk, and its energy levels. Studying the potential decay through the volume allows

us to gain insights into the insulator's intrinsic quality, the mobility of charge carriers within it, and the density and distribution of traps. On the other hand, surface properties characterize the interface between the material and the external environment and are strongly dependent on environmental conditions.

The model for Surface potential decay under consideration was formulated by Philippe Molinié [30]. He examined a very thin dielectric slab of thickness d. The other dimensions are very large, allowing the problem to be treated as 1-D: all measured quantities depend solely on the distance from one of its surfaces. Boundary conditions: The lower surface of the plate is grounded, so its potential is zero, the potential on the upper surface is assumed to be zero.

The electric displacement D is a combination of the electric field in vacuum  $\epsilon_0 E$  and the internal polarization P of the material, so how the dielectric molecules align in response to the electric field. The value of D on the upper surface of the dielectric is equal to the free charge density q(t) deposited on that surface.

During potential decay, we are in an open-circuit situation: there is no current path to or from the outside. In this situation, the continuity equation describing how charges move within the dielectric is given by:

$$\frac{\partial D}{\partial t} + \left(\sigma + \sum_{i} \mu_{i} \rho_{i}\right) E = 0 \tag{11}$$

The first term,  $\frac{\partial D}{\partial t}$ , represents the time variation of the electric displacement. The second term  $(\sigma + \sum_i \mu_i \rho_i) E$  is related to the electrical conduction of the material. Here,  $\sigma$ is the intrinsic conductivity of the material, while  $\mu_i$  and  $\rho_i$  are, respectively, the mobility and the charge density of any additional charge carriers injected into the dielectric. E is the electric field. It is noted that diffusion, so the random movement of charges due to thermal agitation, is considered negligible within the model.

Insulating materials exhibit **dielectric relaxation**, meaning they do not react instantaneously to an applied electric field. This delay is primarily due to the internal molecular reorganization of polymers; their long chains are not rigid but can slowly rearrange in response to the electric field. Furthermore, there can be various regions within the material where charges accumulate, polarizing the material.

Mathematically, to describe this delay, we use the dielectric response function  $\phi_E(t)$ , which takes into account past electric fields. The electric field inside the dielectric material also depends on  $\phi_E(t)$  and can be expressed as:

$$E(t) = \frac{1}{\epsilon_0} \int_{-\infty}^{t} D(\tau) \phi_E(t - \tau) d\tau$$
 (12)

where  $\tau$  is a past time variable accounting for the material's memory effect in the dielectric response.

For a homogeneous dielectric, we assume E = V/d and thus write:

$$V(t) = \frac{d}{\epsilon_0} \int_{-\infty}^{t} q(\tau) \phi_E(t - \tau) d\tau$$
 (13)

Assuming zero conductivity, the continuity equation implies that, during decay,  $\partial D/\partial t = 0$ , so the free charge density on the surface remains constant. It can be written as  $q(t) = \Gamma_0(t)q_0$ , where  $\Gamma_0(t)$  is the Heavyside function centered at t = 0.

From the equation for V(t), we can deduce:

$$\frac{dV(t)}{dt} = \frac{dq_0}{\epsilon_0} \frac{d}{dt} \int_0^t \phi_E(\theta) d\theta = \frac{dq_0}{\epsilon_0} \phi_E(t)$$
 (14)

This relationship implies that the material does not react instantaneously to changes in the electric field. If a charge is deposited on the material, a potential step will follow, which will subsequently decrease due to internal polarization.

The simplified model we will use for data analysis is the **homogeneous conduction model**. This model focuses on how the material's intrinsic electrical conductivity influences potential decay. The primary assumptions are:

- Polarization is stabilized: This means that dielectric relaxation is no longer the dominant factor or has already occurred. Consequently, the material is simply described by its constant permittivity  $(\epsilon)$ .
- Space charge effects are neglected: We do not consider charge accumulations within the bulk of the material that could distort the electric field.

With these simplifications and with the existence of an intrinsic conductivity, (14) is transformed into:

$$\sigma E + \epsilon \frac{\partial E}{\partial t} = 0 \tag{15}$$

where  $\sigma$  is the intrinsic conductivity of the material.

This equation can be rewritten in terms of potential (V), leading to the following relationship:

$$\frac{1}{V}\frac{dV}{dt} = -\frac{\sigma}{\epsilon} \tag{16}$$

Integrating the equation, we get:

$$V_s/V_0 = e^{-t\sigma/\epsilon} \tag{17}$$

If the intrinsic conductivity  $\sigma$  is constant, this equation indicates that the potential decay will follow an exponential trend, with a time constant given by  $\epsilon/\sigma$ . A higher conductivity will result in a faster potential decay. Note that  $\sigma$  is a volume conductivity [29]. This model can only be applied on particular hypotheses:

- 1. Charge emission: from the electrodes, radiation such as gamma rays, and photoexcitation.
- 2. Recombination: charges recombine very quickly or become trapped, so they cannot move easily. This phenomenon is particularly evident on PTFE, where the charge remains trapped for long periods because there is not enough conductivity to remove it.
- 3. Mobility: the bulk of polymers is much less conductive than the surface. Exponential decay is often associated with surface conduction.

#### 3.1.4 Limits of the model

Permittivity and conductivity values are important for predicting charge decay but they aren't precise enough tools on their own. Philippe Molinié deeply studied this problem [31]. His studies reveal that simply measuring resistivity and permittivity is not enough to accurately predict how an electric charge disperses over time. Experimental data clearly shows that the potential decay in many insulating materials doesn't follow a simple exponential trend; that is, it is not merely characterized by a time constant like in an RC circuit (Figure 17).

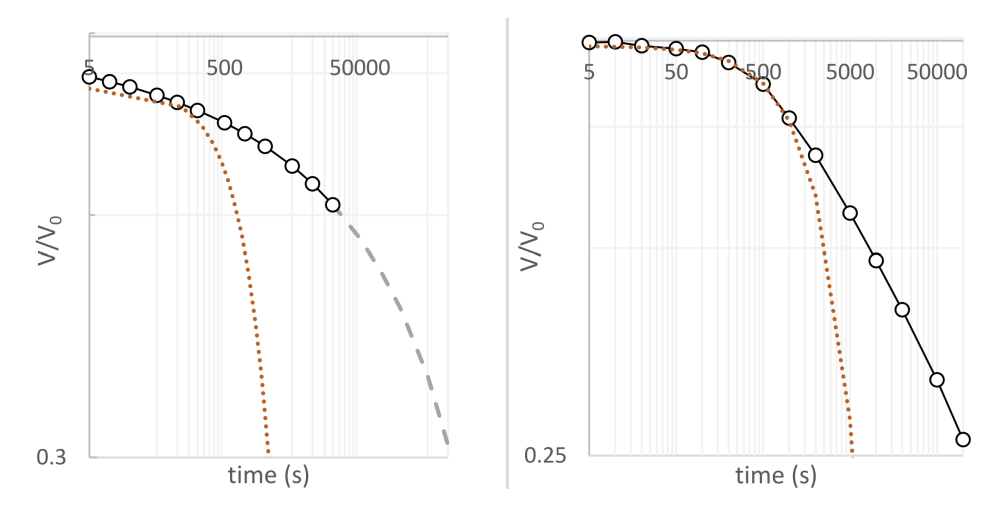


Figure 17: The graphs show the potential decay on a logarithmic scale for epoxy (left) and Cross-Linked Polyethylene XLPE (right). Black circles represent the experimental data, while red dots indicate the theoretical exponential decay according to an RC Circuit [31].

The accuracy of charge decay predictions on an insulator is significantly influenced by the surrounding environment and the measurement methods employed: the presence of a measuring device can significantly alter the recorded value.

Specifically, a field mill introduces a parasitic capacitance between the instrument and the insulator's surface, which can lead to a reduction in the measured potential. Conversely, the use of an electrostatic probe is designed to minimize interference with the field lines, thus offering a measurement closer to the insulator's intrinsic potential.

Figure 18 provides a clear illustration of how the electrostatic surface potential of a charged insulating material interacts with its environment and various measurement instruments. Each panel of the figure (a, b, c) shows a specific setup, with its corresponding capacitive circuit.

In Figure 18(a), which is the reference condition without any measurement instrument, we see a charged insulating surface, with volume charge density  $\rho_q$ . From this surface, electric field lines radiate in two main directions, represented by the blue arrows. Some of these curved arrows extend into the environment. These lines illustrate the path along which atmospheric ions of opposite polarity are drawn to the insulator's surface, aiding in charge decay. Meanwhile, other blue arrows dive directly into the solid insulator, which is a natural discharge mechanism. The equivalent circuit on the right models this scenario with a capacitance  $C_{g0}$  between the charged surface and ground and a capacitance  $C_{g1}$  between the surface and other ungrounded objects in the environment. These parallel-connected capacitances demonstrate how the charge spreads across various capacitive pathways.

In Figure 18(b) showcases how a grounded field mill affects the measurement of surface





(c) Influence of electrostatic probe.

Figure 18: Electrostatic Field Lines and influence in three different contexts [31]. Note:  $\sigma$  here is the surface charge density.

potential. When this device is placed above an insulating surface and grounded, the electric field lines from the charged surface tend to gather around it. Essentially, the Field Mill pulls in some of the field lines that would normally spread out. In terms of the equivalent circuit, this results in an added capacitance,  $C_{gFM}$ , between the insulating surface and the instrument. Since this capacitance is in parallel with  $C_{g0}$ , it boosts the overall capacitance of the system in relation to ground. As a result, for a specific amount of charge, the potential that the Field Mill measures will seem lower than what the insulator would show if the instrument weren't there, thanks to this induced capacitive effect.

Moving on to Figure 18(c), we see the electrostatic feedback potential probe (like a Kelvin probe). This probe works by keeping its potential aligned with that of the surface being measured. The goal is to prevent significant field lines from flowing between the insulator and the probe, thereby reducing disturbance. The blue arrows under the probe, diminished or absent, indicate that field lines aren't being redirected towards it but mainly interact with the ground through  $C_{g0}$  In the equivalent circuit, there's no noticeable extra capacitance linked to the probe. Because of this feature, the potential measured by the electrostatic probe is more accurate to the true surface potential, without significant instrument interference. For this reason, it usually registers higher values than a Field Mill.

In conclusion, the issue is not that the measuring instrument accelerates the decay, as we've seen this doesn't happen with a Kelvin Probe. The problem lies in the theoretical model being incomplete or incorrect under real conditions. The simplified theoretical model, which assumes the insulator behaves like an RC circuit, is inadequate because, in reality, the behavior of the insulating solid is much more complex and can be simulated with various capacitances. Furthermore, it must be remembered that charge traps, dielectric polarization, and the influence of atmospheric ions also play a fundamental role in charge decay. The intrinsic slowness of the material in releasing trapped charge is a dominant factor that makes the overall decay slower than the theoretical exponential one (Figure 17).

#### 3.2 Data Interpretation

#### 3.2.1 Trap Energy Distribution

In the context of the electrical characterization of insulating materials, one of the main results of SPD is to extract the trap density at different energy levels in the insulating polymers studied. Knowledge of this energy distribution of traps is crucial for understanding the mechanisms of charge accumulation and detrapping, which were previously explained in paragraph 2.2.2. By analyzing the trap density, we can observe and predict how charges become trapped and subsequently released within the material. As consequence, we can intuit how long will be the decay. In the following, we will analyze the models used for studying the trap energy distribution: the first is based on [32] and [20], the second is used by Philippe Molinié in [33] based on [34]. The aim is to give a comprehensive review of the methods of analysis of trap energy distribution.

**First Model:** In the model under analysis the theory of isothermal relaxation current is taken into account. It is assumed that the surface trap states are uniformly distributed in a thin layer, and the distribution is analyzed from an energy perspective.

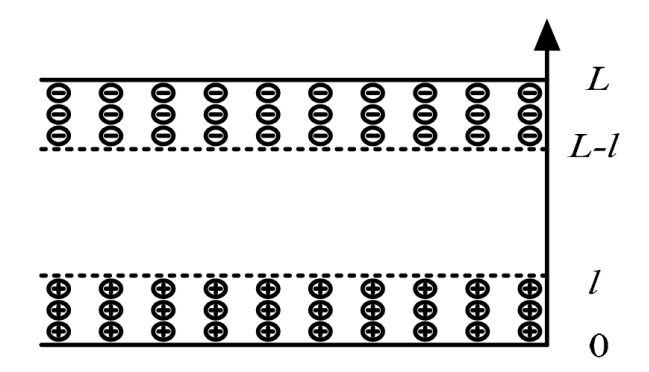


Figure 19: Space charge distribution in a sample following corona charging. [32]

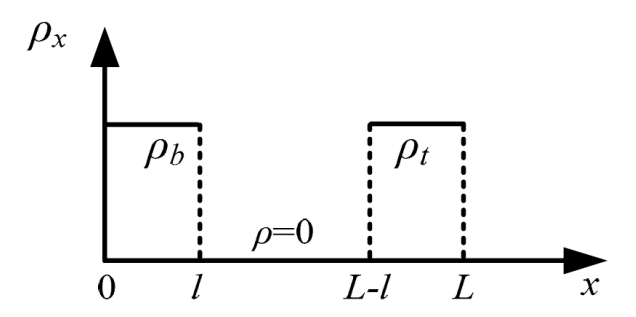


Figure 20: Uniform charge distribution [32].

In Figure 19, L represents the total thickness of the sample, while l indicates the thickness of the layer where the density of distributed charges is concentrated. Furthermore, we can observe the Schottky or Fowler-Nordheim effect<sup>1</sup>, known as double injection phenomena.

<sup>&</sup>lt;sup>1</sup>Both are field-assisted conduction mechanisms: Schottky emission occurs at the electrode-insulator interface, while Fowler-Nordheim tunneling takes place across a thin barrier within the bulk material.

The uniform charge distribution, shown in Figure 20, is usually used to obtain the trap energy distribution in the corona charged material.

Under the Theory of isothermal relaxation current we get the total rate of electron emission to conduction band as:

$$n_t' = f_0 N(E_t) k_b T / t \tag{18}$$

where  $f_0$  is the rate of initial occupancy of traps,  $k_b$  is the Boltzmann's constant, T is the external temperature, t the time and  $N(E_t)$  is the trap density at the energy level of  $E_t$ . Note that the expression for  $E_t$  comes from (8).  $f_0$  can be described as:

$$f_0(E_t) = \frac{v_r n}{v_r n + e_n} \quad \text{(for electrones)}$$

$$f_0(E_t) = \frac{v_r p}{v_r p + e_p} \quad \text{(for holes)}$$

where  $v_r p$  is the capture rate and  $e_p$  is the emission rate. The surface potential is calculated as follows:

$$V_s = \frac{1}{\epsilon_0 \epsilon_r} \left[ \int_0^l x \rho_b dx + \int_l^{L-l} x \rho dx + \int_{L-l}^L x \rho_t dx \right]$$
 (19)

We assume that  $\rho = 0$  in the bulk of the sample and  $\delta \ll 2L$ , then:

$$V_s = \frac{Ll\rho_t}{\epsilon_0 \epsilon_r} \tag{20}$$

The surface potential decay is due to the releasing of charges in the top layer. The speed of the decay can be written as:

$$\frac{dV_s}{dt} = \frac{Ll}{\epsilon_0 \epsilon_r} \frac{d\rho_t}{dt} = \frac{Ll}{\epsilon_0 \epsilon_r} q n_t'$$
 (21)

So, the Electron Trap density can be written by substituting (18) in (21):

$$N(E_t) = \frac{\epsilon_0 \epsilon_r t}{kT f_0(E_t) lLq} \frac{dV_s}{dt}$$
 (22)

where T is the absolute temperature and q is the Coulomb quantity of electrons, and  $f_0(E_t)$  is the rate of initial occupancy of the traps. The expression is applicable to both electron traps and hole traps.

The limitation of this model is the difficulty in estimating the rate of initial occupancy, that cannot be estimated using the SPD experiment alone. This value is often set to 1, but this assumption is far from reality.

**Second Model:** this model is based on Philippe Molienié approach [30].  $t \cdot dV/dt$  vs log(t) was used in the interpretation of potential decay measurements and he suggests that this plot makes it possible to evaluate peaks in the potential curves and their characteristic time. This transformation is justified by:

$$\frac{dV}{d\log t} = \ln(10) \cdot t \cdot \frac{dV}{dt} \tag{23}$$

This shows that  $t \cdot dV/dt$  is proportional to the derivative of the potential with respect to the logarithm of time. This makes the transformation useful for highlighting rapid and slow changes in voltage that are less visible on a linear scale. In the graph, each peak corresponds to a group of traps that empty around a characteristic time  $\tau$ . The amplitude of the peak is proportional to the amount of charge released and thus to the associated trap density. The position of the peak in log(t) is related to the release time, which can be linked to the trap's energy depth,  $E_t$ . The area under the  $t \cdot dV/dt$  curve is proportional to the overall potential change and, therefore, to the released charge, as indicated in:

$$\int_{\log t_1}^{\log t_2} t \cdot \frac{dV}{dt} d\log t = \frac{1}{\ln(10)} \left[ V(t_1) - V(t_2) \right]$$
 (24)

The demarcation energy is a time-dependent energy threshold that separates filled traps from empty ones. The value of  $E_t$  increases over time, meaning it shifts toward deeper traps. Shallow traps empty quickly, while deeper ones release charge over longer periods. Thanks to the demarcation energy model (8), it is possible to associate each time with a corresponding trap energy. The tentative escape frequency  $\gamma$  can be derived from surface potential decay measurements taken at different temperatures, although this type of analysis falls outside the scope of our current study.

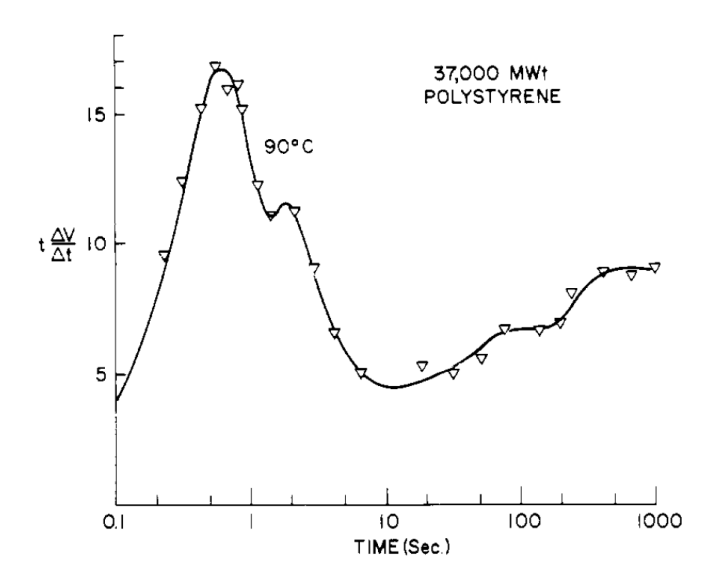


Figure 21: Density of electron trapping states in polystyrene. The energy scale can de derived from  $E_t = kT ln(\gamma t)$  [34].

#### 3.2.2 Surface Charge Density and Influence on Electric Field

Through the SPD experiment, the obtained values of  $V_s$  allow us to calculate the surface charge density. This parameter is fundamental during the simulation phase because it strongly influences the electric field, which is crucial in Meek's criterion as deeply explained in section 2.1.4.

Knowing the value of the surface potential  $V_s$ , it is possible to determine the surface charge density  $\sigma_q$  as in a parallel plate capacitor with dielectric as follows [35]. The electric field in the solid insulator can theoretically be:

$$E = V_s/d \tag{25}$$

where *d* is the thickness of the solid.

From the local Gauss Law, it is known that when the electric field is normal to the surface in a uniform electric field:

$$D\vec{n} = \sigma_q \tag{26}$$

Where  $D = \epsilon_0 \epsilon_r E$ , so we can write:

$$\sigma_q = \epsilon_0 \epsilon_r E = \epsilon_0 \epsilon_r V_s / d \tag{27}$$

The surface charge density strongly influences the value of the electric field. This is explained in detail in [36]. Experimentally, it has been observed that injecting charges into the surface of a material creates a certain charge density,  $\sigma_q$ . The accumulated charge on the surface generates an internal electric field within the dielectric. This field depends on  $\sigma_q$ , since a higher surface charge density produces a stronger electric field. The electric field originating from  $\sigma_q$  can oppose or add to the external field, thereby decreasing or increasing the surface conductivity  $\sigma$ , respectively. In COMSOL Multiphysics<sup>®</sup>,  $\sigma_q$  can be used to simulate charge accumulation within the insulating material in order to analyze the electric field.

#### 3.2.3 Influence of different parameters on Charge Decay

**Controlled humidity:** Relative humidity (RH) represents the amount of water vapor present in the air and ranges from 0% (dry air) to 100% (saturated air). Water vapor is an electronegative gas, so it captures free electrons and alters ionization and discharge phenomena. At high humidity levels (RH > 70%), fewer electrons remain free, resulting in a lower amount of charge accumulated on the solid surface.

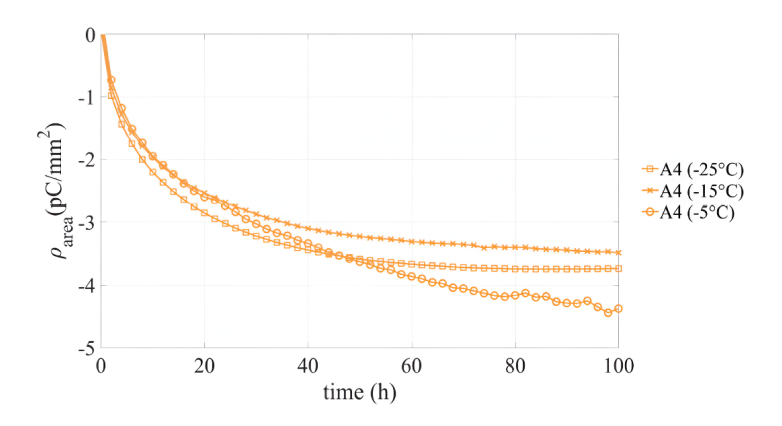


Figure 22: Charge density evaluation in area A4 for different humidity levels, under E = 5kV/m[37].

The role of humidity in the context of charge decay in an insulator is closely linked to the applied electric field [37]:

- In the case of a weak electric field  $(1800 \cdot V/m)$ , no micro-discharges are observed: the accumulated charge decays through conduction in the gas and in the solid;
- In the case of high electric fields (>  $5000 \cdot V/m$ ), humidity plays a crucial role as it can promote the onset of micro-discharges. Micro-discharges generate local charge peaks that add to the charge already present in the solid, leading to a slower overall decay;

Figure 22 shows the decay of surface charge density in area A4 at different humidity levels. The curve corresponding to the driest air condition  $(-25^{\circ}C)$  shows a faster decay. As air humidity increases  $(-5^{\circ}C)$ , a slower decay is observed due to the reinjection of charge caused by micro-discharges.

In summary, high humidity hinders air ionization: less charge reaches the solid, and the charge accumulation decreases.

**Polarity:** Experimental results [38] show that, for the same applied voltage, negative corona discharge produces current pulses with higher amplitude (Figure 23) and frequency compared to positive corona. At the same time, electric field simulations indicate that negative polarity generates a stronger local electric field than positive polarity. This phenomenon is explained by the fact that negative corona, based on electron emission, involves a more efficient and unstable ionization process. Positive corona, on the other hand, relies on slower mechanisms. As a result, negative corona is more easily initiated and produces a higher current density.

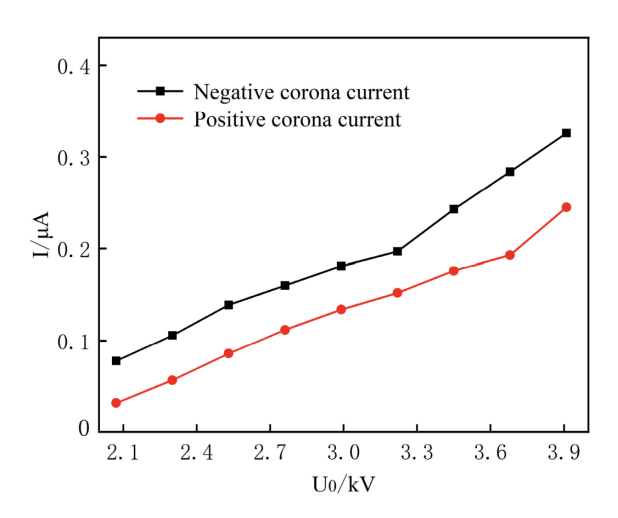


Figure 23: Applied Voltage  $U_o$  and respective Current I for different polarity [38].

The same has also been observed in [39]. This study showed that the most important ion produced by negative charging is  $COS^-$ , while a positive corona produces  $(H_2O)_nH^+$ ,  $NO^+$ , and  $NO_2^+$ ; the latter two become more abundant as the humidity decreases.

Negative charge tends to penetrate more easily into the polymer bulk: electrons exhibit a mobility that is an order of magnitude higher than that of positive charges, leading to a faster decay. The proposed model for negative charges includes both deep and shallow surface traps, and the injection into the bulk is also a significant phenomenon. In contrast, the injection of positive charges into the bulk is less pronounced, and the decay occurs mainly through surface de-trapping. The decay is slower compared to negative charge.

**Time of Ionization:** For the first time, the impact of the time ionization has be investigated in [39]. The surface potential  $V_s(t)$  at time t, is expressed as follows:

$$V_s(t) = \frac{d\sigma_q(t)}{\varepsilon} + \frac{1}{\varepsilon} \int_0^d (d-x) \, \rho_q(x,t) \, dx \tag{28}$$

where, d is the thickenss,  $\epsilon$  is the permittivity,  $\sigma_q(t)$  is the charge density at the surface and  $\rho_q(x,t)$  is the density of bulk charge at distance x below the surface. At the end of the charging period  $t_c$ , the values of  $\sigma_q(t_c)$  and  $\int_0^d (d-x) \, \rho_q(x,t_c) \, dx$  will determine the following discharge and decay of  $V_s(t)$ . The study highlights that  $\rho_q(x,t_c)$ , in particular, is strongly influenced by the time  $t_c$ : a charging time of just a few seconds leads to a significantly different charge profile compared to a charging time of several minutes.

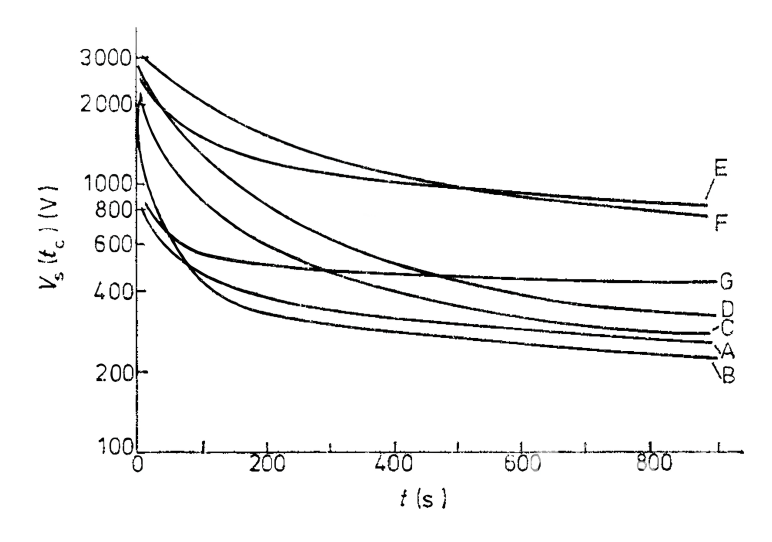


Figure 24: Influence of charging time  $t_c$  on  $V_s(t)$  decay [39] on the same sample.

In Figure 24 we will focus just on the decay curves after triode corona charging (from A to D). As the charging time  $t_c$  increases, the amount of charge trapped in both deep and surface states increases, resulting in a slower decay of the surface potential.

# 4 Experiment

## 4.1 Set-Up Experiment

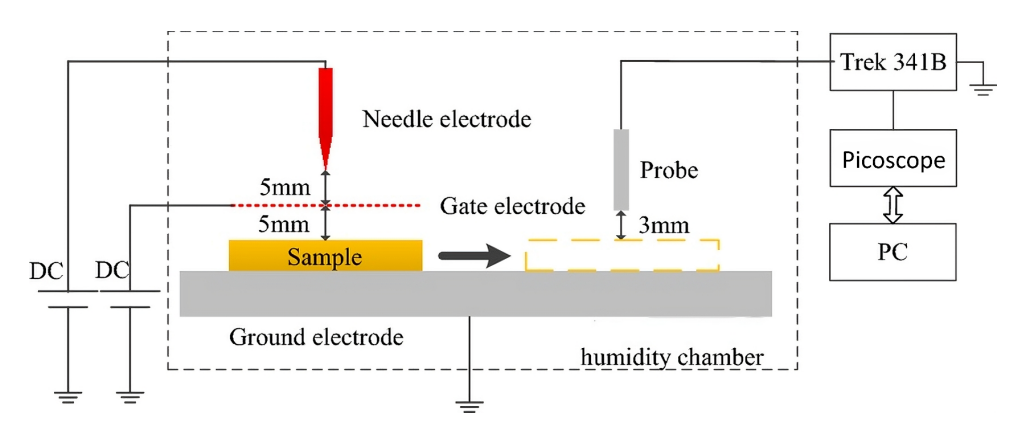


Figure 25: Experimental setup for DC corona charging and potential surface measurements.

Figure 25 shows the setup of the SPD (Surface Potential Decay). The dashed line indicates the humidity chamber, for controlled conditions. In this study, the experiments were done under ambient conditions, so with room temperature and local humidity.

For the analysis of the setup, we proceed from left to right: The sample is separated by a distance of 10mm from the needle electrode and 5 mm from the grid. The needle electrode is connected to a DC power supply for charging the sample via corona discharge. The Bench-top High Voltage Power Supply (Figure 26 (d)) allows the user to set the voltage applied by the corona triode.

The sample is placed on a ground electrode (Figure 27), which is a metallic surface connected to earth. After being charged, the sample is quickly moved underneath the probe for measurement. The distance between the sample and the probe is 3 mm. The probe is connected to an electrostatic voltmeter (Trek 341B) which measures the potential over time. The output of the Trek 341B is connected to a Picoscope, which records the potential signal over time. The Picoscope is connected to a PC for data acquisition.

Through a dedicated graphical interface (Figure 28) developed to control the experiment, it is possible to select the type of measurement (Cartography, Single point), the ionization time, and the measurement durations.

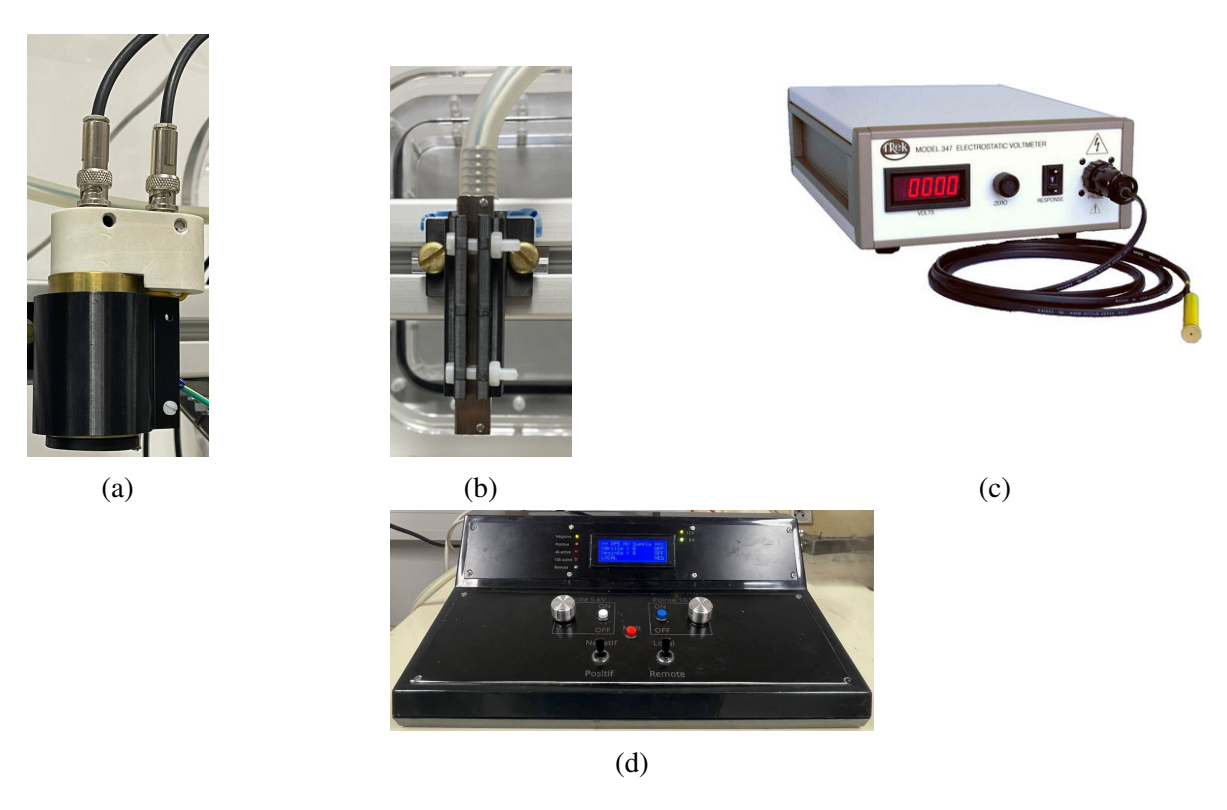


Figure 26: Instruments used in G2Elab: (a) Corona triode, (b) Kelvin Probe, (c) Electrostatic voltmeter (d) Bench-top HV Power Supply.

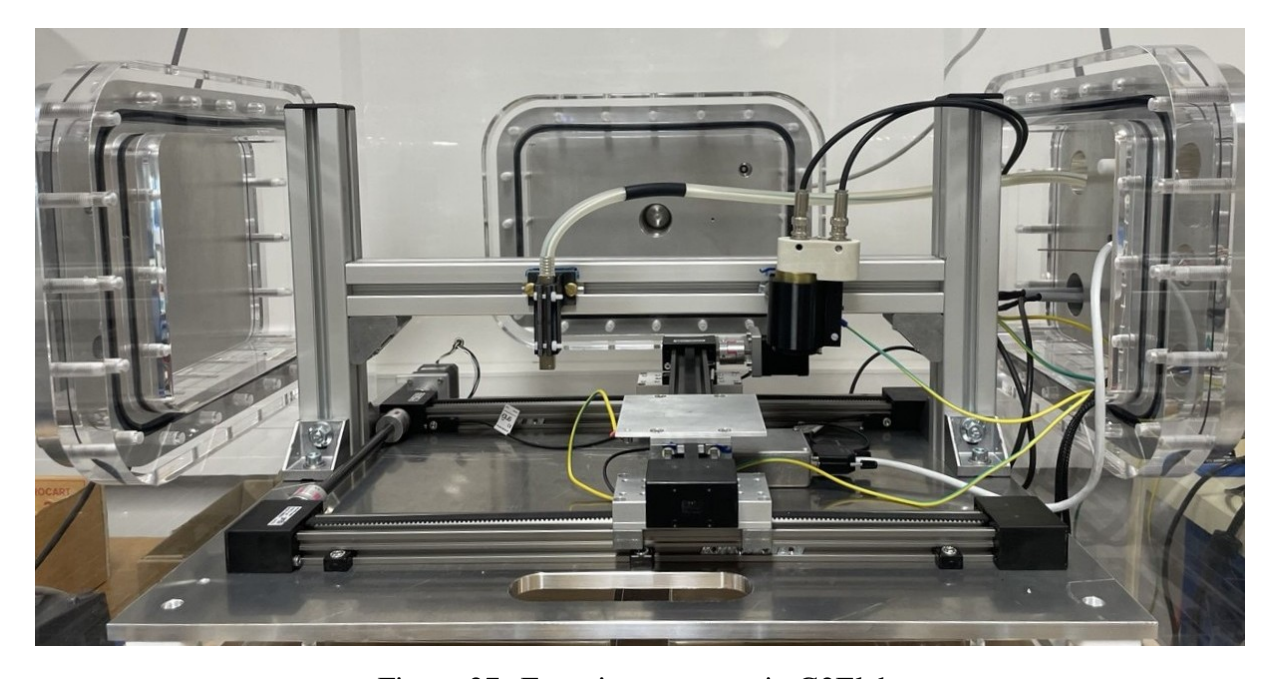


Figure 27: Experiment set-up in G2Elab.

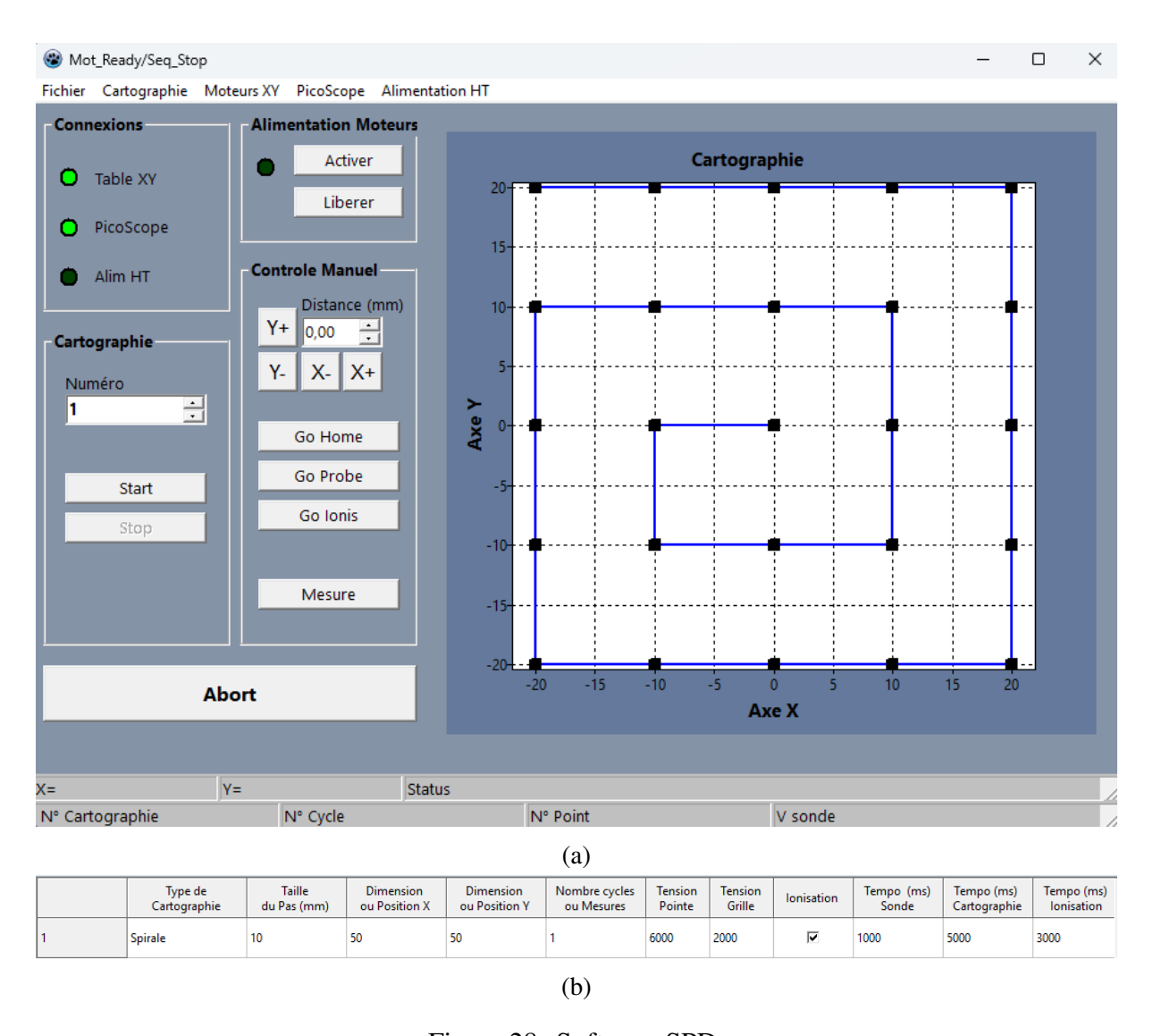


Figure 28: Software SPD.

## 4.2 Samples

The samples used are: PP, PVC, PVDF, PTFE and have dimensions of 10 cm by 10 cm and a thickness of 34 mm. These materials are shown in Figure 29.

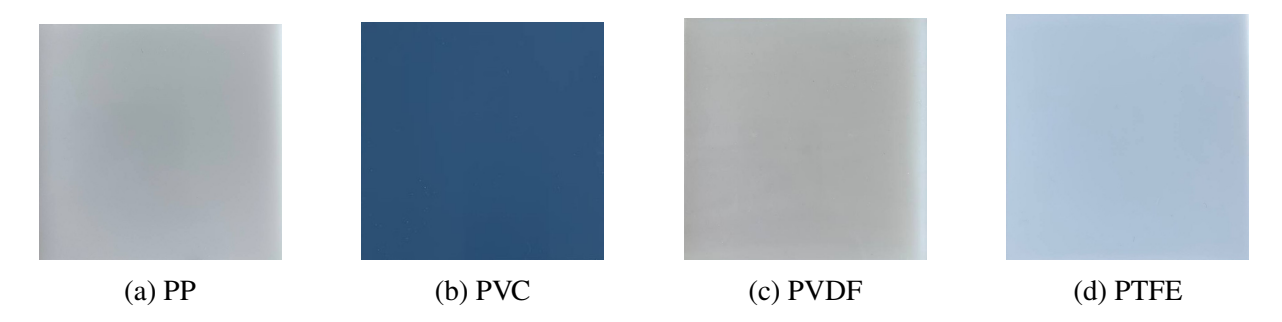


Figure 29: Samples used.

**PP: Polypropylene** [40] is a semi-crystalline polymer, translucent white in color. It is an electrical insulator with extremely low conductivity. However, its electrical properties can be drastically modified and improved through the addition of conductive fillers. Incorporating materials like carbon nanotubes (CNTs), carbon black (CB), or graphite allows PP to transform from an insulator into a semiconductor or even a conductor.

**PVC:** Polyvinyl chloride [41] is a versatile amorphous thermoplastic polymer, available in both rigid and flexible forms, gray in color. Its properties can be significantly modified through the addition of plasticizers and fillers. PVC is inherently an excellent electrical insulator, exhibiting very low electrical conductivity in its pure state. This low conductivity, combined with high dielectric strength, makes it a good insulator. However, a key characteristic of PVC is its ability to be transformed into a conductive material through the strategic incorporation of conductive fillers.

**PVDF:** Polyvinylidene fluoride [42] is a semi-crystalline thermoplastic polymer, typically translucent white in color, with a relatively low density. It possesses high mechanical, chemical, and radiation resistance. The dielectric properties of PVDF are notable, making it suitable for various electrical applications. Although it might not always be the ideal choice for high-frequency insulation, it stands out due to its high relative permittivity.

**PTFE:** Polytetrafluoroethylene [43] is a white, highly hydrophobic solid polymer. This material boasts superb thermal stability, making it suitable even for extreme applications. PTFE is an excellent electrical insulator as it is almost entirely non-conductive. It also exhibits a very high dielectric strength. These properties remain unchanged with frequency and temperature.

**Clean** samples refer to those that have been surface-cleaned using ethanol. Subsequently, the samples are stored in a protected atmosphere, although at ambient temperature and pressure, for at least one day, allowing the ethanol to fully evaporate and avoid interference with the measurements.

**Dried** samples refer to conditioned samples that have undergone a specific preparation process. Initially, the samples are disinfected using ethanol. They are then placed in an oven at  $65^{\circ}C$  under vacuum (less than  $10^{-2}$ mbar) for one month to reduce their moisture content. After

this drying period, the samples are transferred to a storage chamber where they are kept under vacuum to preserve their condition. This procedure is applied when samples are intended for use in controlled atmosphere environments.

The values considered for relative permittivity are shown in Table 1. The reference value ranges for the volumetric conductivity are shown in the Table 2.

Table 1: Values of Relative Permittivity  $\epsilon_r$  at 20°C and 50 Hz. Measurements taken with dielectric spectroscopy at G2Elab.

Material	$\epsilon_r$
PTFE	2,16
PP	2,51
PVC	3,83
PVDF	8,99

Table 2: Values of Volume Conductivity  $\sigma$ [S/m].

Material	$\sigma$
PTFE	$10^{-18} - 10^{-21}$
PP	$10^{-16} - 10^{-18}$
PVC	$10^{-13} - 10^{-15}$
PVDF	$10^{-13} - 10^{-16}$

#### 4.3 Results

### 4.3.1 Cartography

The data from The Software SPD (Figure 28), are organized in .csv files. These files were treated in Matlab to extract the relevant information. In particular, with AppDesigner the following interface was realized.

The app developed in MATLAB using the AppDesigner tool allows users to load multiple files in .csv or .xlsx format. The user can select the desired type of plot: either surface potential cartographies or potential decay curves over time. A table is also included, which displays the values from the Excel file for further analysis. The app can be exported and installed on different devices.

The following cartographies were realized before and after applying a Positive ionization of 2 seconds:  $V_{needle} = 6000V$  and  $V_{grid} = 2500V$ . The cartographies represent the spatial distribution of the surface potential.

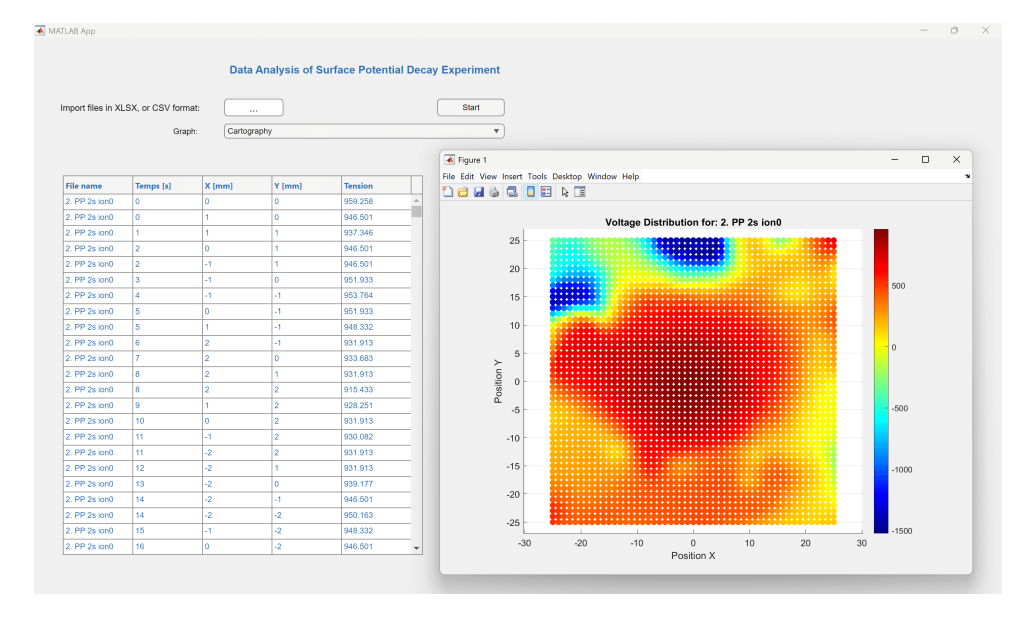


Figure 30: Interface realized on Matlab-AppDesign.

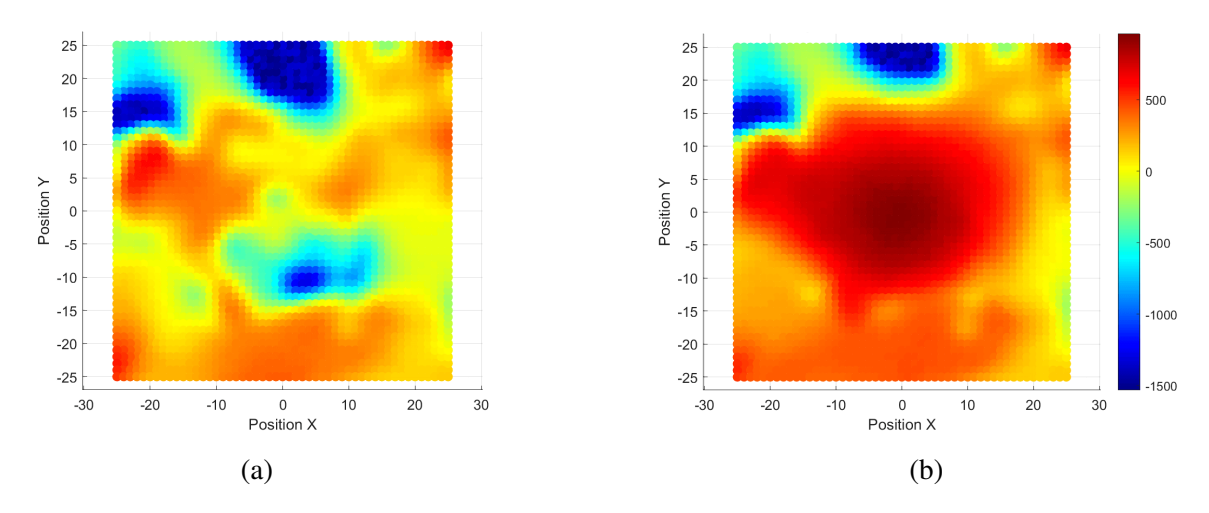


Figure 31: PP cartographies in millimeters over a 5 cm  $\times$  5 cm sample surface. (a) Before ionization and (b) immediately after ionization. Each cartography required 40 minutes.

Before ionization, PP exhibits a clearly irregular surface potential distribution, with alternating areas of positive and negative charge. After ionization, a marked concentration of positive potential is observed, indicating that the material has efficiently accumulated charge. It is well known that PP is capable of retaining charge for a long time while also easily accumulating it.

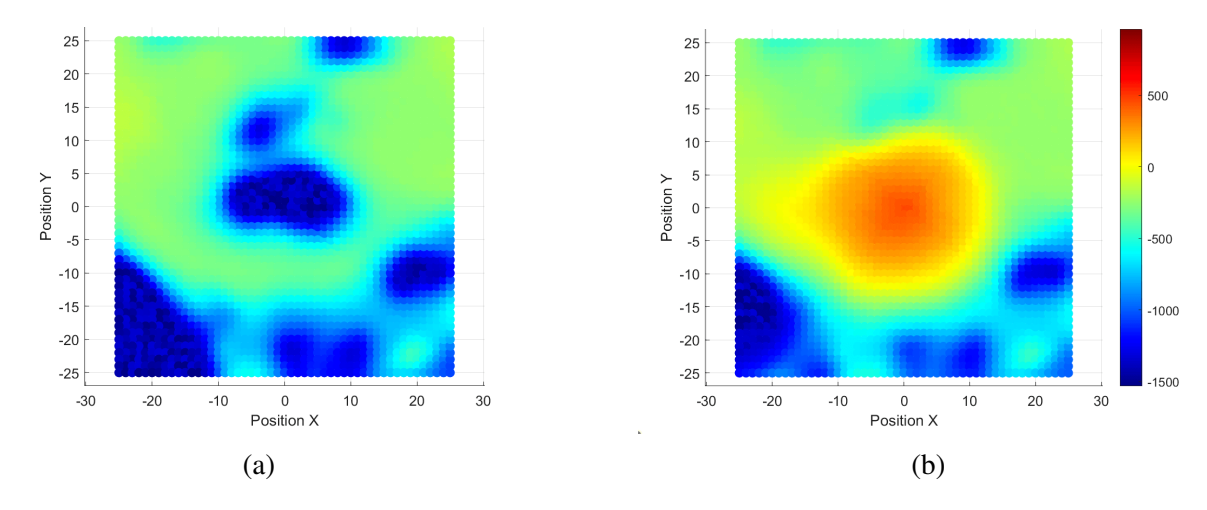


Figure 32: PVC cartographies in millimeters over a 5 cm  $\times$  5 cm sample surface. (a) Before ionization and (b) immediately after ionization. Each cartography required 40 minutes.

PVC is characterized by light tones, with a map showing discharged areas and weakly negative zones. After ionization, the material appears weakly charged. It is known that PVC accumulates charges with difficulty and retains them only for short periods.

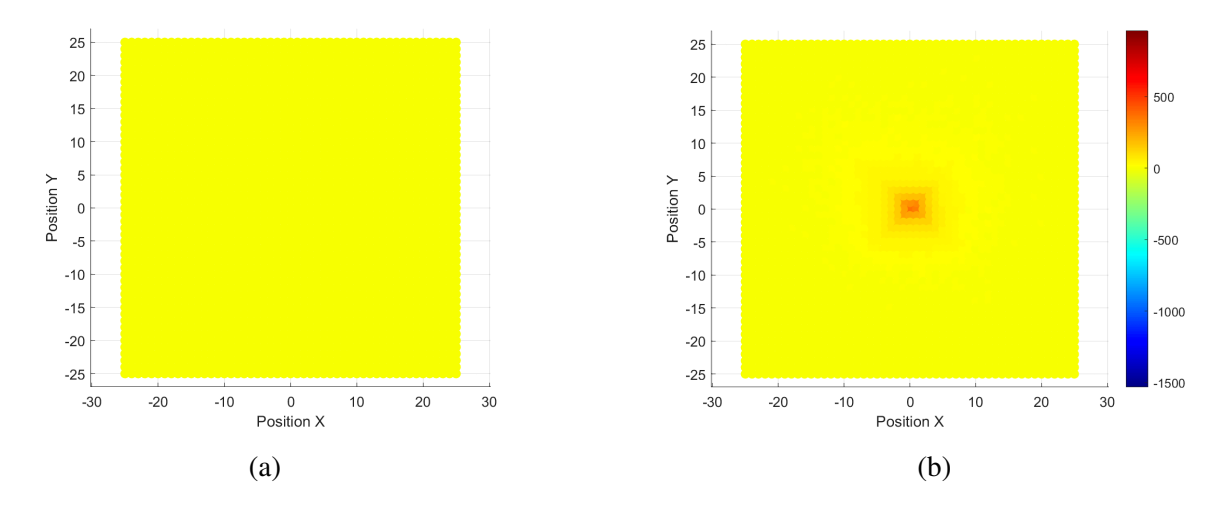
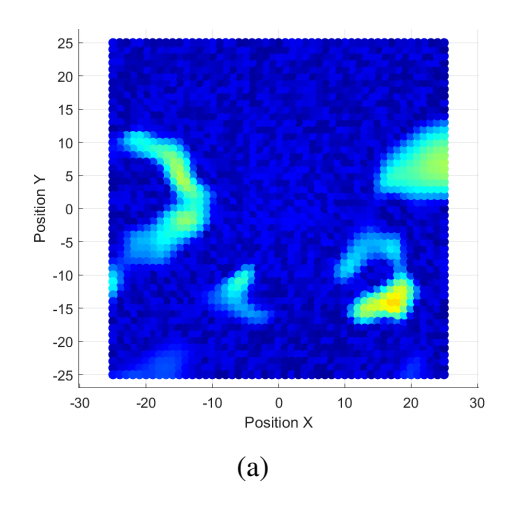


Figure 33: PVDF cartographies in millimeters over a 5 cm × 5 cm sample surface. (a) Before ionization and (b) immediately after ionization. Each cartography required 40 minutes.

PVDF stands out for the complete absence of charge before ionization, highlighting the material's high electrostatic stability. After ionization, an extremely localized effect is observed: a small charge accumulation at the center, without significant diffusion.



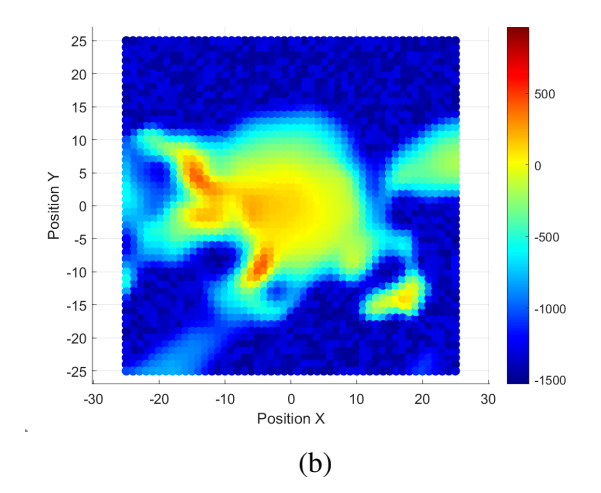


Figure 34: PTFE cartographies in millimeters over a 5 cm × 5 cm sample surface. (a) Before ionization and (b) immediately after ionization. Each cartography required 40 minutes.

PTFE exhibits a highly electronegative behavior. Following ionization, PTFE responds positively to the charge, showing a high sensitivity to surface charge accumulation.

In conclusion, we can say as follows. Triboelectric properties play a fundamental role in the initial formation of surface charge. For example, PTFE is well-known for its strong tendency to attract and retain electrons through contact or friction. This explains why a PTFE sample might appear already significantly charged even before ionization. Once the charge is present on the surface, the conductivity determines its ability to accumulate and retain it over time. Materials with low conductivity, such as PP and PTFE, tend to maintain a persistent surface charge, as the trapped charge has difficulty dissipating through the material. Consequently, a greater persistence of charge accumulation is observed on such materials. In contrast, those with higher conductivity, like PVDF, show less persistence of accumulated charge, as it is more effectively dissipated through the material. What we observe is influenced also by surface characteristics, such as environmental humidity or the way the sample was handled, also play a significant role both in the amount of charge initially accumulated and its subsequent distribution on the surface.

## 4.3.2 Decay Curves for Positive and Negative Ionization

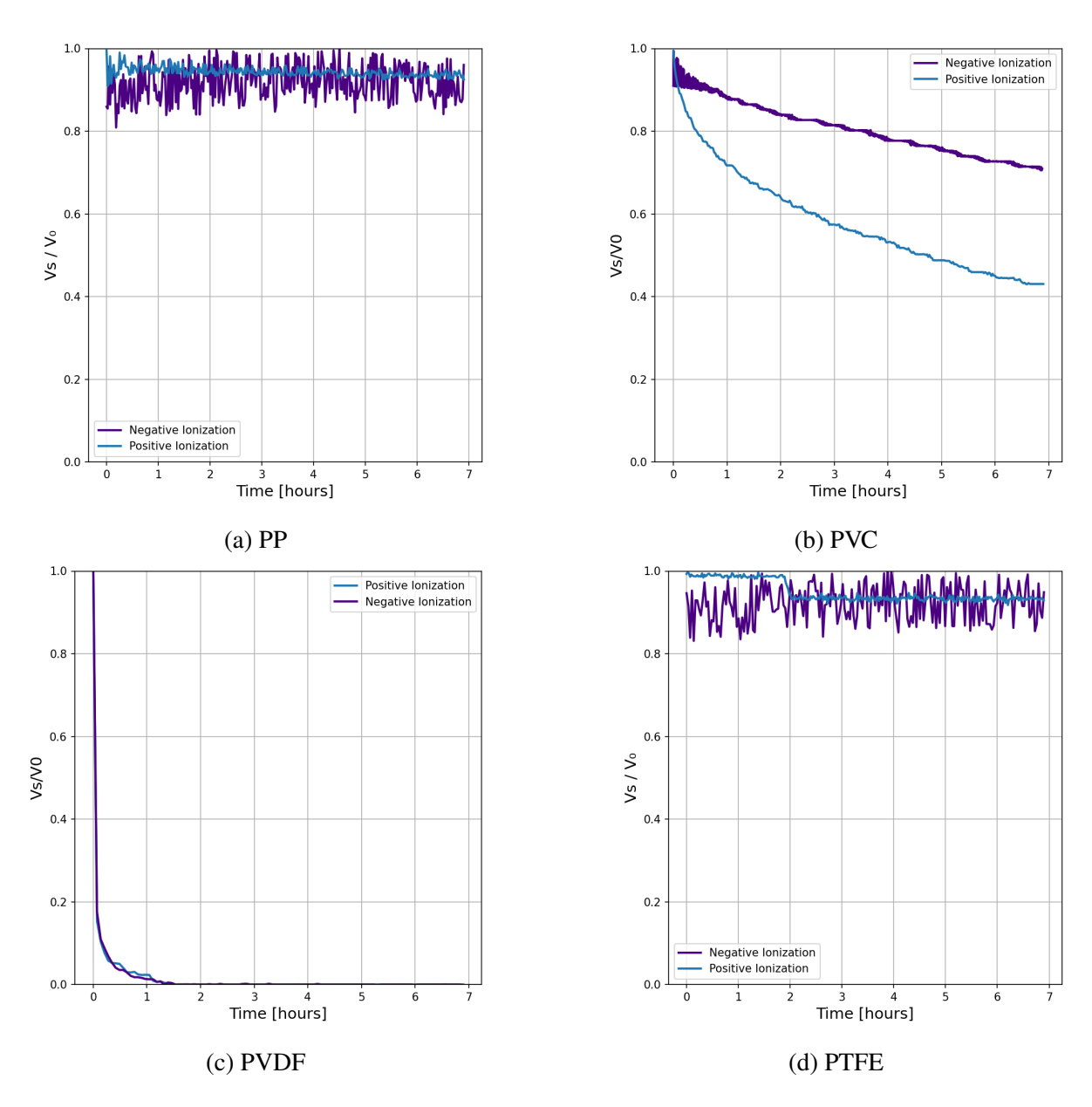


Figure 35: Normalized decay curves for the different samples. Voltage applied for positive ionization  $V_{needle} = +6000V$  and  $V_{grid} = +2500V$  for 2 seconds. Voltage applied for negative ionization  $V_{needle} = -6000V$  and  $V_{grid} = -2500V$  for 2 seconds.

In Figure 35 (a)-(d) surface potential decay curves recorded over 7 hours for the dielectric materials is shown. To reduce experimental noise and improve the clarity of the decay trends, a smoothing algorithm was applied to the surface potential data during the analysis.

While theoretical considerations suggest that electrons typically decay faster due to their higher mobility and tendency to penetrate into the polymer bulk, this trend is not universally observed. In particular, materials such as PVC exhibit slower and more irregular decay for negative charges. This suggests the presence of deep traps that retain electrons for extended periods, delaying the overall relaxation process.

The irregular shape of PP and PTFE decay curves for negative ionization indicate a non-uniform release of trapped charges, possibly involving trapping and de-trapping from deep and shallow states. This behavior is consistent with what is expected from negative corona discharge, which injects high-energy electrons into the material and results in more chaotic and unstable decay profiles. In contrast, smoother decay curves for positive ionization are observed for the same materials. This suggests a more regular charge de-trapping mechanism.

#### Overall:

- A chaotic decay profile may be a signature of negative charge injection and deep trapping;
- A smooth and monotonic decay suggests positive charge accumulation;
- The material properties, such as trap distribution and bulk conductivity, strongly influence the relaxation dynamics.

#### 4.3.3 Decay Curves for Different Time of Ionization

The Figures 36 (a)-(d) illustrate the influence of ionization time on the normalized surface potential decay for the different samples.

- PP exhibits a slow decay for both ionization times, with a slightly higher final potential for 10s. This suggests good charge retention. capability.
- PVC shows a very distinct difference: the decay for 2s is much faster.
- PVDF demonstrates extremely rapid decay for both times.
- PTFE exhibits very slow decay for both times. The difference between 2s and 10s is minimal, suggesting that even short times are sufficient to saturate its charge retention capacity.

Generally, it is observed that a longer ionization time (10 seconds) leads to a slower surface potential decay or a higher final potential compared to a shorter ionization time (2 seconds). This finding aligns with our previous observations, which indicate that a longer charging time increases the amount of charge trapped. Charge injection into the bulk  $(\rho_q)$ , promoted by corona discharge, is greater with longer ionization times, thereby slowing down the decay.

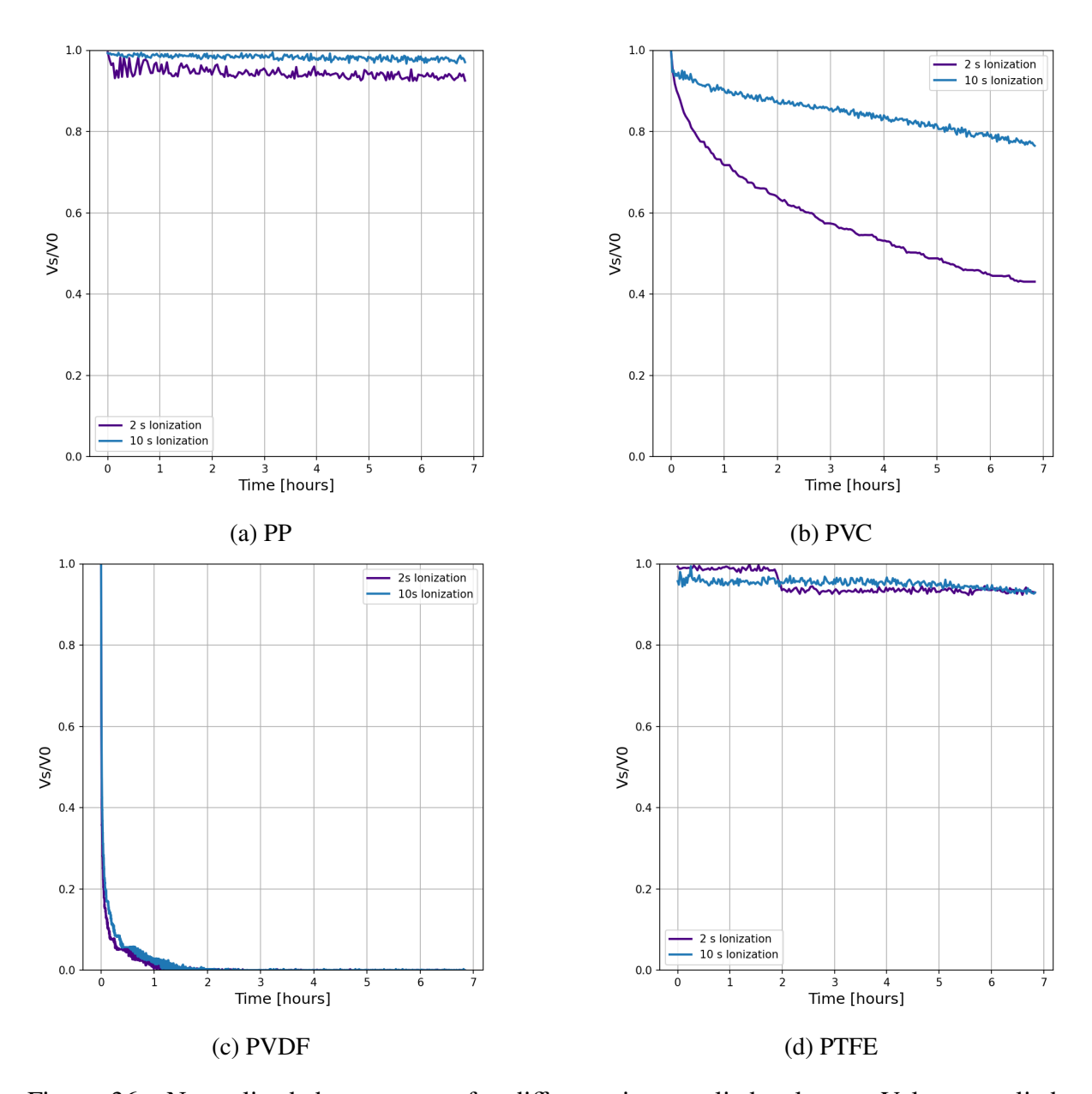


Figure 36: Normalized decay curves for different time applied voltage. Voltage applied:  $V_{needle} = +6000V$  and  $V_{grid} = +2500V$ . Time of ionization: 2 seconds and 10 seconds.

#### 4.3.4 Conductivity from Decay Curves

In this section, we will analyze the surface potential decay curves of our samples. The aim is to perform a bi-exponential fitting of these curves in order to extract the charge conductivity values.

A positive ionization of 2 seconds was applied:  $V_{needle} = 6000V$  and  $V_{grid} = 2500V$ . Subsequently, the sample was moved under the capacitive probe: the potential measurement was carried out over a period of 7 hours, with data recorded every 4 seconds.

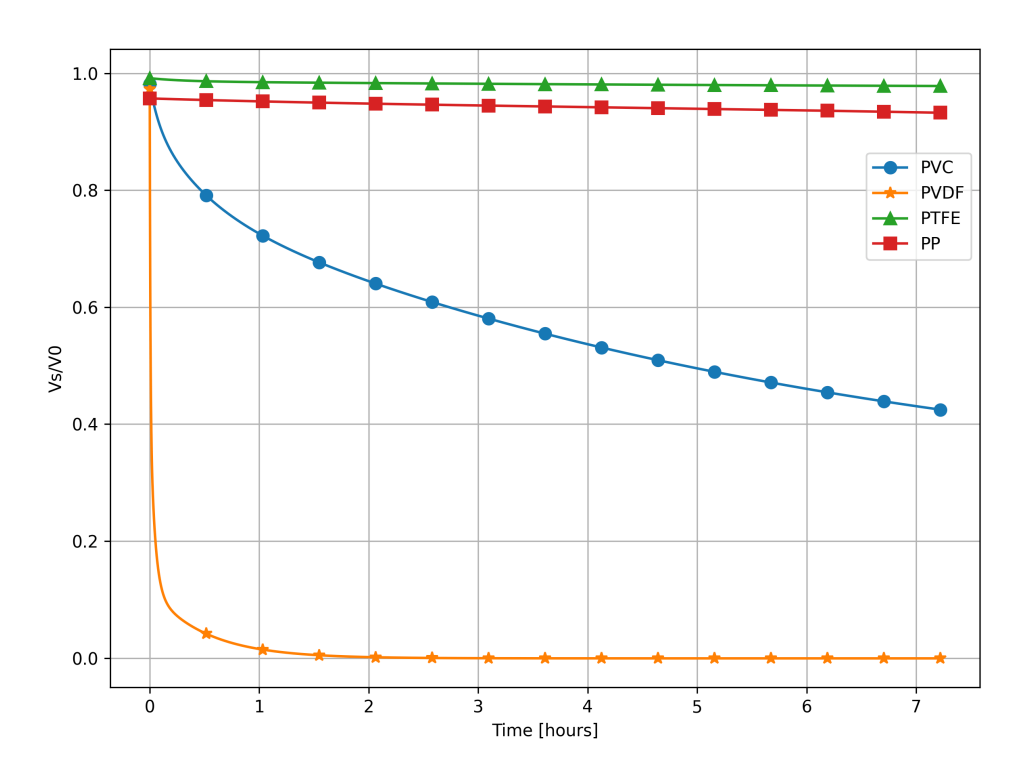


Figure 37: Normalized Decay for the different samples after positive ionization of 2 seconds. The bi-exponential fitting has been applied to the data.

In the Figure 37, the y-axis shows the normalized surface potential. This approach is commonly adopted in the context of surface potential decay studies, as it allows for evaluating the decay behavior independently of the sample's initial charge level. The normalized voltage  $V_s/V_0$  represents the proportion of residual voltage relative to the initial voltage. The x-axis represents time in hours. Although some authors [33] recommend using a logarithmic time scale, a linear scale was chosen here to ensure clearer graphical representation. We observe that:

PVDF exhibits the most rapid surface potential decay, losing approximately 90% of its initial potential within the first 10 minutes, and dropping below 1% after about 1 hour. This indicates that PVDF dissipates surface charge extremely quickly. PVC shows a significant but slower decay: after 7 hours, it retains around 43% of its initial potential, suggesting a gradual but continuous charge dissipation. In contrast, PTFE and PP maintain almost constant surface potential throughout the entire duration of the measurement, with a total decrease of less than 2% over 7 hours. This suggests that the two materials are very effective at retaining a charge after trapping it, and therefore, in addition to being excellent electrical insulators, they have very

low conductivity that prevents charge dissipation.

The surface potential decay curves were analyzed to derive a biexponential fitting in order to obtain the conductivities values. This choice is due to the fact that, as already widely illustrated in paragraphs 3.1.3 and 3.1.4 concerning the theoretical model of Static Potential Decay and its limitations, a biexponential solution is often used for the analysis of surface decay.

As done in [44], the solution is to consider the Surface potential as a sum of exponential as follows:

$$V_s(t) = \sum_{i=1}^n A_i \exp(-t/\tau_i)$$
(29)

where  $V_s(t)$  is the surface potential with time,  $\tau_i$  is the relaxation time. Considering shallow and deep traps involved in the de-trapping process, a double exponential function can be used to fit the surface potential decay curves:

$$V_s(t) = A_{fast} \exp(-t/\tau_{fast}) + A_{slow} \exp(-t/\tau_{slow})$$
(30)

where  $A_{fast}$  and  $A_{slow}$  represent the initial surface potential after charging due to charges captured by shallow and deep traps, and  $\tau_{fast}$  and  $\tau_{slow}$  are the relaxation time of charges captures by shallow and deep traps. At time t=0,  $A_{fast} + A_{slow} = V_0$ .

The bi-exponential fit to the normalized surface potential has been realized in Python.

In this section we are fitting the normalized potential because we want to get the value of  $\tau_{fast}$  and  $\tau_{slow}$  and we are not so interested in the amplitude  $A_{fast}$  and  $A_{slow}$ .

Fitting is a mathematical process used to find the parameters of a theoretical function that best approximates a set of experimental data. In Python, this is typically done using the *curve\_fit* function from the SciPy library. In the case of a bi-exponential fit,  $curve\_fit$  automatically finds the best-fit parameters  $A_1$ ,  $A_2$ ,  $\tau_{fast}$ ,  $\tau_{slow}$  that minimize the difference between the experimental data and the theoretical curve. Knowing that  $\tau = \epsilon/\sigma$  the values in the Table 3 has been found.

Table 3: Calculated conductivity values  $\sigma$  (in S/m).

Material	$\sigma_{ m fast}$	$\sigma_{ m slow}$
PTFE	$1.52 \cdot 10^{-14}$	$5.81 \cdot 10^{-18}$
PP	$9.33 \cdot 10^{-14}$	$2.20 \cdot 10^{-17}$
PVC	$1.72 \cdot 10^{-14}$	$7.96 \cdot 10^{-16}$
PVDF	$1.32 \cdot 10^{-12}$	$5.78 \cdot 10^{-14}$

The conductivity values are important for understanding the ability of insulating materials to retain electric charge over time. From the bi-exponential analysis, we obtain two conductivity values,  $\sigma_{\text{fast}}$  and  $\sigma_{\text{slow}}$ : the charge dissipation process involves mechanisms at different speeds, related to the type of trapping. From the Table 3, we can observe the different conduction properties of the materials. PP shows very low conductivity values. Compared to PTFE, however, it has a higher  $\sigma_{\text{fast}}$ , which suggests a brief initial charge decay, slightly faster. PVC presents intermediate conductivity values compared to the other polymers, with a larger slow component ( $\sigma_{\text{slow}}$ ) than PP and PTFE, indicating a more pronounced long-term charge dissipation. PVDF stands out for its visibly high conductivity values. This implies that it is not able to retain charge for a long time, as clearly observed in its decay curve in Figure 32. PTFE distinguishes itself for its absolutely lowest conductivity values. This makes it a material exceptionally resistant to

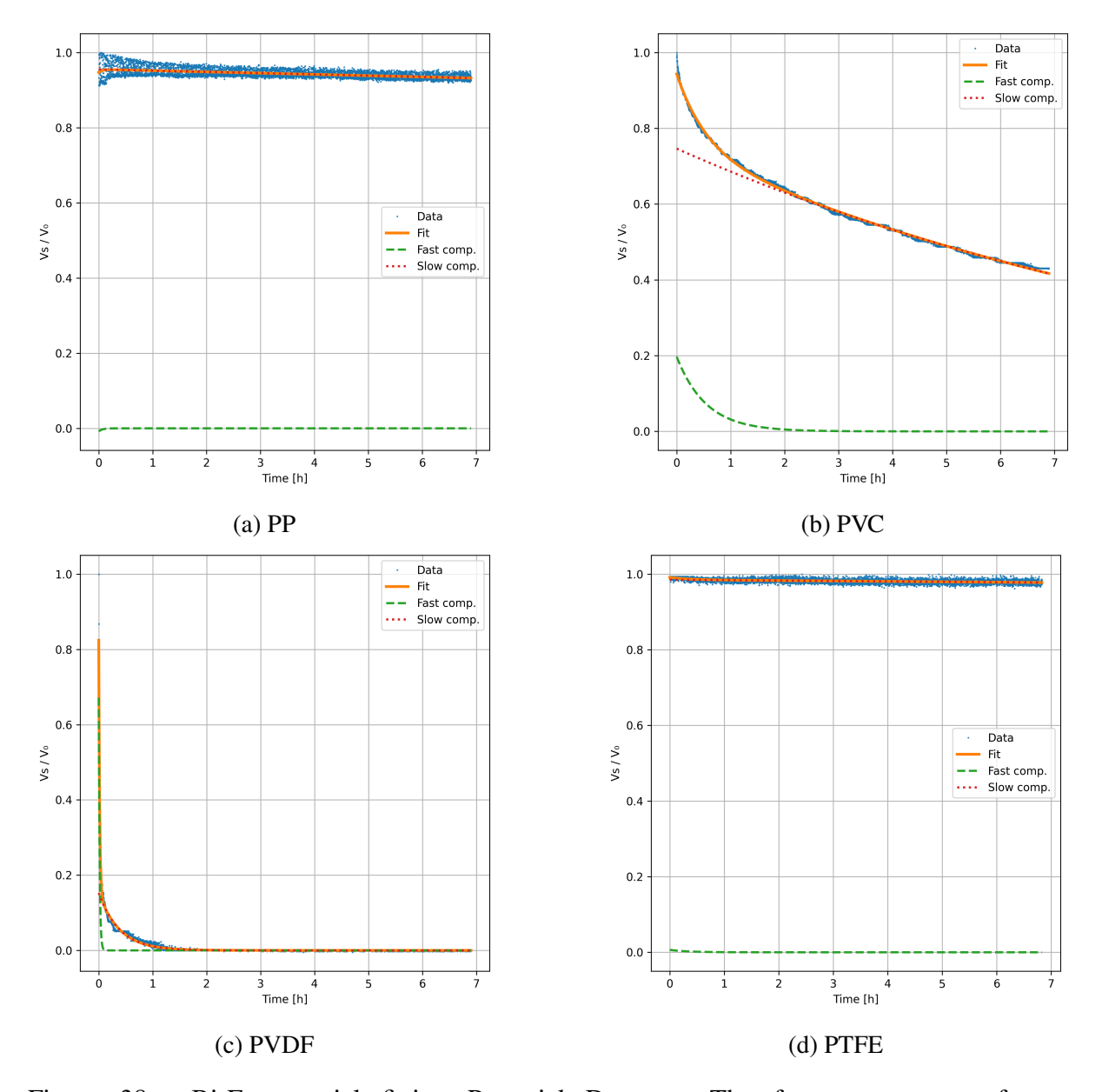


Figure 38: Bi-Exponential fitting Potential Decay. The fast component refers to  $A_{fast} \exp(-/\tau_{fast})$ , while the slow component corresponds to  $A_{slow} \exp(-t/\tau_{slow})$ .

charge movement, maintaining the surface potential almost unaltered over time. In summary, a rapid potential decay indicates a high conductivity value, while a slow decay indicates much smaller conductivity values.

### 4.3.5 Trap Energy Distribution

As explained in detail in paragraph 3.2.1, two different models can be used to analyze the trap energy distribution. The first model is more accurate, but it requires  $f_0$ , rate of initial occupancy of the traps, that is difficult to determine. The second model, on the other hand, does not give the exact number of traps, but it still provides the general trend. In this analysis, the second model is used.

This choice is based on the fact that even in the scientific literature it is difficult, if not impossible, to find the exact value of  $f_0$ , a constant that is often assumed to be equal to one. However, this assumption is unrealistic: it only applies when samples are exposed to ionization long enough to completely fill all traps. In our study, samples are charged for only 2 or 10 seconds, so assuming  $f_0 = 1$  is not realistic. Also, the SPD experiment alone is not enough to measure  $f_0$ .

For these reasons, I chose to use the second model explained in 3.2.1, as suggested by Philippe Molinié [33]. My analysis includes two methods: an analytical method and a numerical method, which are explained in detail below.

The **analytical method** is based on calculating  $t \cdot dV/dt$  for each time interval. This method is very sensitive to noise, both due to external measurement conditions (such as environmental factors), and because the data files often contain too many points, including repeated or identical values. For this reason (before calculating  $t \cdot dV/dt$ )  $V_s$  is first filtered in Python using the Savitzky-Golay filter. This filter smooths the data while preserving important features, such as peaks and slopes. This filter uses the least-squares method to fit a low-degree polynomial to a moving window of data points. Rather than just averaging points, it actually fits a curve and retrieves its value at the center of that window. This feature is great for reducing random noise, which can distort the shape of the signal. The size of the filter window can be changed depending on the data. If the data changes slowly or behaves in a quasi-static manner over time, a larger window is preferable for better noise smoothing. On the other hand, if the changes are happening quickly, smaller windows are better to capture all the important details without losing anything due to oversmoothing.

The **mathematical method**, is completely free of noise. It provides an estimate of the trend of the energy traps and is an important tool because it allows this estimate to be extended to much longer time intervals compared to those covered by the experimental SPD measurements.

Using this model, starting from the Vs measurements over time, a bi-exponential function  $V_s(t)$  (30) is constructed. The derivate of (30) is:

$$\frac{dV_s(t)}{dt} = -\frac{A_1}{\tau_1} e^{-t/\tau_1} - \frac{A_2}{\tau_2} e^{-t/\tau_2}$$
(31)

At this point  $t \cdot dV/dt$  over time is calculated.

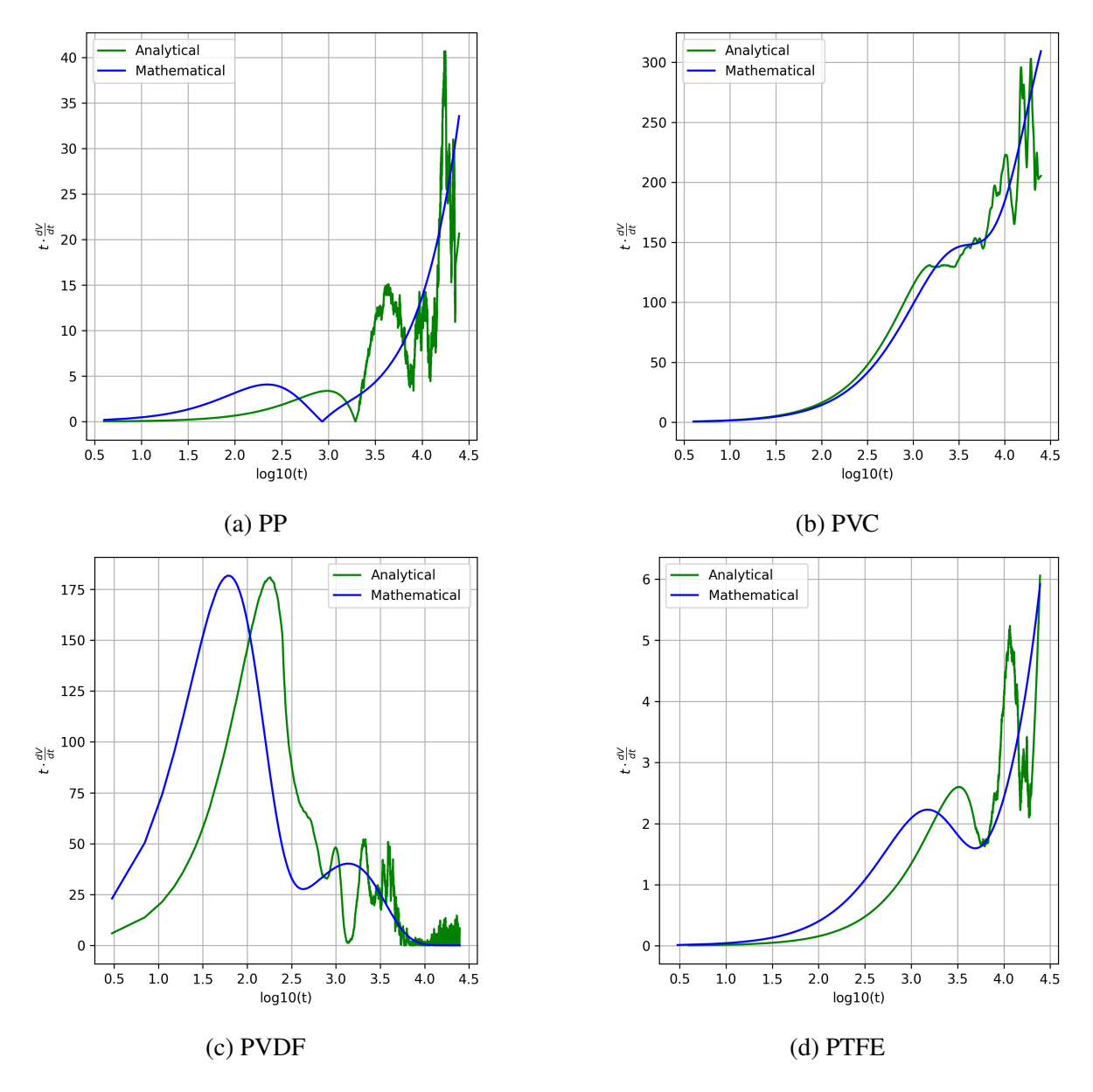


Figure 39: Comparison of Analytical and Mathematical Method.

In Figure 39 we compare the mathematical method with the analytical one obtained in the case of positive ionization lasting 2 seconds, with  $V_{needle} = 6000 \text{ V}$  and  $V_{grid} = 2500 \text{ V}$ . It is clear that, in the analytical method, the results are still strongly affected by noise. Before calculating  $t \cdot dV/dt$ , the data needs to be filtered, but this requires a balance between smoothing the curve and keeping the original shape of the signal. Since we don't want to change the signal too much, we have to use a smaller filter window, which means that some noise remains. For this reason, the mathematical model is a more effective and reliable tool for analyzing the trap density. However, comparing it with the analytical method is still useful, as it helps confirm that the bi-exponential model is valid.

In the Figure 40, the analyses is performed with mathematical method for positive ionization of 2 seconds and with  $V_{needle} = 6000 \text{ V}$  and  $V_{grid} = 2500 \text{ V}$ . Note that trap Depth has been calculated with (8).

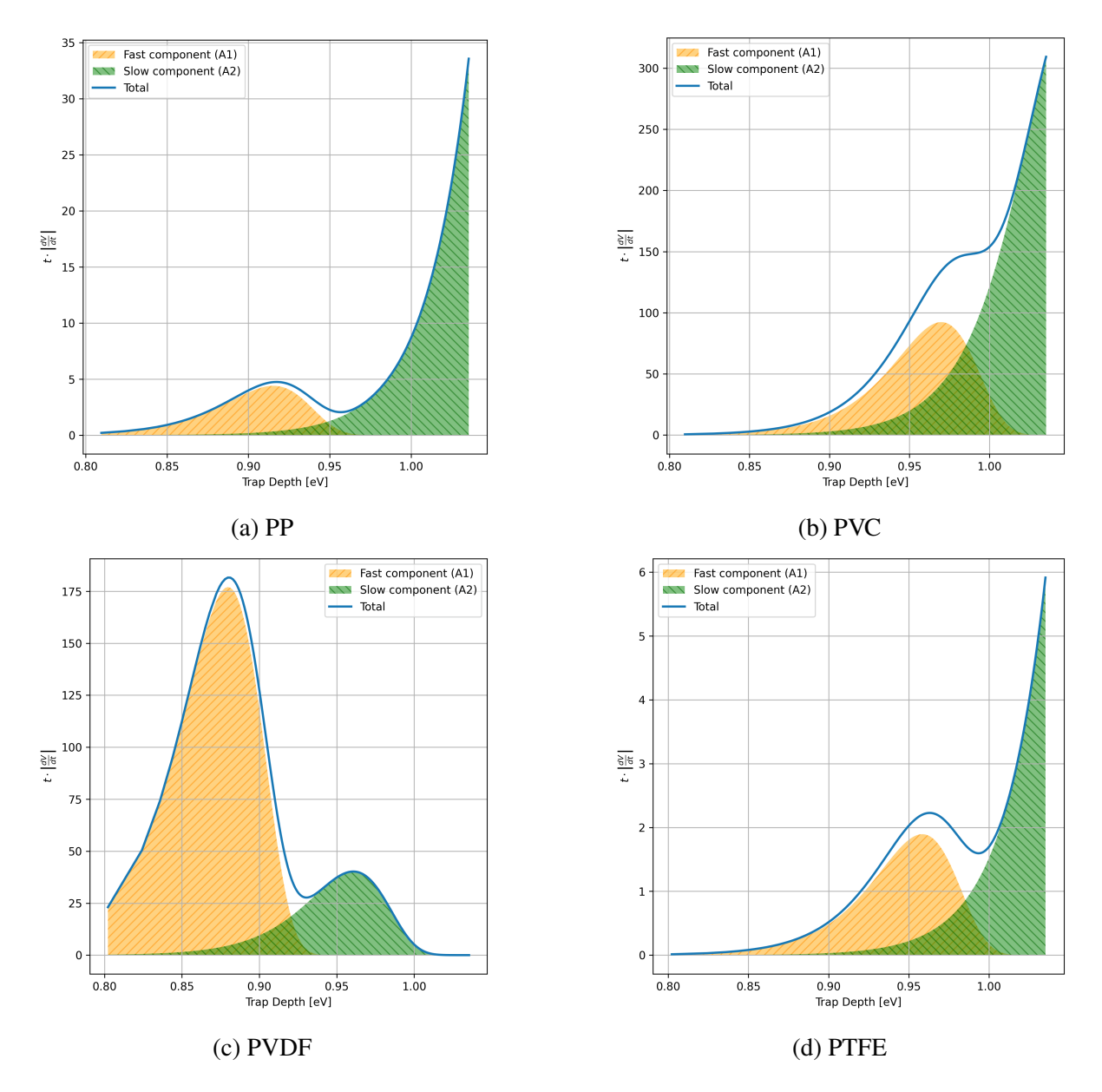


Figure 40: Fast and Slow components in *Vs* Decay.

The analysis of the  $t \cdot dV/dt$  curve allows us to infer the trap behavior in terms of density, depth, and charge release time, as previously explained in 3.2.1. In Figure 40 we see as follows.

PP shows a weakly pronounced fast component, which means that only a small amount of shallow traps released charge within the first hours of observation. The slow component is more significant and appears to increase with trap depth. Therefore, a substantial portion of the charge is still trapped, as suggested by the moderate total area under the curve.

In PVC, the fast component is much broader and more pronounced than in PP. This reflects a high density of shallow traps that release charge rapidly. The overall peak amplitude is large, indicating that a significant amount of charge has already been released. It is also reasonable to assume that the slow component continues to grow over time. PVC thus exhibits both a high initial charge release and a prolonged discharge behavior.

PVDF displays a very intense peak in the fast component, indicating a massive and rapid

release of charge from shallow traps with high density, as evidenced by the peak height. The slow component is much smaller, meaning the material has few deep traps active in the short term. As a result, PVDF is characterized by an extremely fast charge release.

In contrast, PTFE shows a visible but modest fast component. The slow component is barely developed within the 7-hour window, suggesting that the characteristic release time is well beyond 7 hours. The area under the curve is very small, reflecting the fact that most of the charge is still trapped. PTFE can thus be classified as an ultra-slow charge release insulator.

In the following, the analyses is performed with mathematical method for both positive and negative ionization. In positive ionization, positive ions are generated, whereas in negative ionization, electrons are produced. As consequence, it is possible to study electron trapping and positive ion trapping in the insulators. A positive and negative ionization of 2 seconds was applied:  $|V_{needle}| = 6000V$  and  $|V_{grid}| = 2500V$ . In particular, a time vector of 3 months, expressed in seconds, is applied to the mathematical model.

In the Figure 41, we can see as follows.

PP shows fewer holes traps (linked to positive ionization) compared to electron traps (linked to negative ionization). However, the positive traps seem to be deeper. For negative ionization, a significantly higher peak is observed in PP than in any other material. This means PP can hold large amounts of charge at very deep energy levels, so for a long time.

PVC responds to positive ionization by releasing positive ions from relatively shallow traps, which means this happens quite quickly. Its behavior is different for negative ionization; PVC holds negative charge for a long time, even though it doesn't accumulate as much charge as PP.

PVDF responds to positive ionization with two distinct charge releases, shown by two consecutive peaks at shallow energy levels. For negative ionization, two peaks are also observed in the charge release, but at slightly shallower energy levels than for positive ionization.

PTFE has very deep traps. Specifically, the traps observed in response to positive ionization are more numerous but present at shallower energy levels compared to those observed from negative ionization. This means PTFE accumulates electrons more easily, while positive ions remain in the material longer.

Overall, PP, PVC, and PTFE tend to accumulate more electrons than positive ions. PVDF is slightly different, as the peaks for both polarities are similar in height. This analysis suggests that in an environment where electrons are the main charge carriers, these materials might experience significant charge accumulation, which could affect their dielectric stability.

In conclusion, the mathematical method is an effective and reliable tool. Unlike the analytical model, it's robust against noise in experimental data, giving a clearer estimate of trap trends. Being able to predict over very long timeframes is important for forecasting total decay times, which can't be seen directly with short-term SPD measurements. Comparing it with the analytical model helped confirm that the bi-exponential model is valid.

On the other hand, analyzing the curves (Figures x and y) showed a consistent trend for PP, PVC, and PTFE: these materials all accumulate more electrons than positive ions. PVDF, however, is known for its very fast overall discharge times. This observation is crucial for how these polymers are used: in environments where electrons are the main charge carriers (for example, in high-voltage applications and certain types of electrical discharges), these materials are very prone to charge buildup. This charge buildup can affect their long-term dielectric stability, leading to an increase in internal electric fields in response to applied ones.

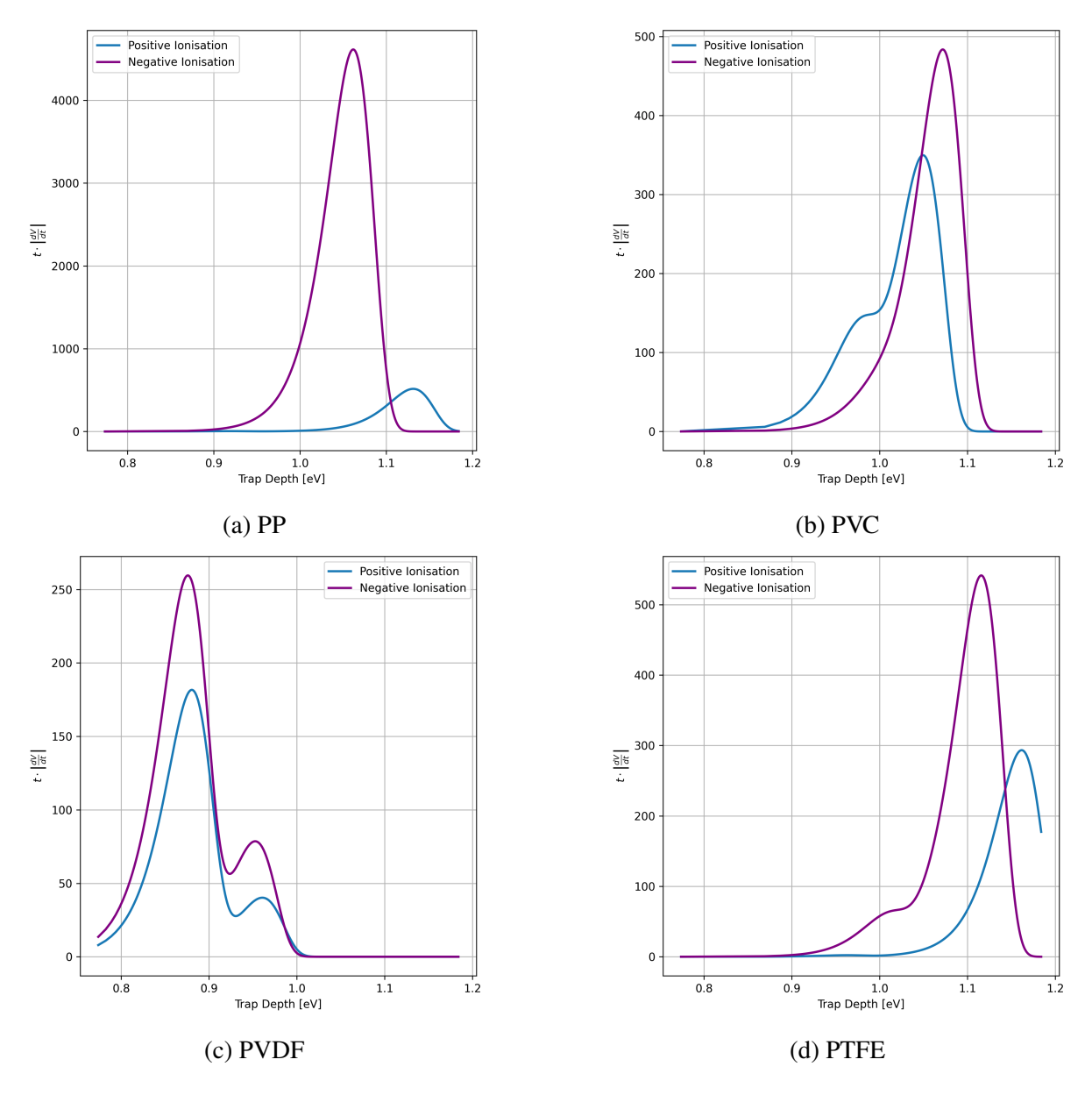


Figure 41: Application of Mathematical model over 3 months.

#### 4.3.6 Surface Charge Density

This section is necessary for the purpose of the simulation. The aim is to define the charge density on a sample, exactly after ionization. This charge density, which provides an indication of the charge accumulation, will be used in the following chapter for the simulation.

The charge density was measured using (27). This formula has been applied to the potential profile extracted along the line y=0 in the same files used for cartographies. After the data have been fitted with a Gaussian fit.

Gaussian fitting in Python consists of finding the best parameters for amplitude, mean, and standard deviation of a Gaussian function that best approximates a given dataset. This is done

by *curve\_fit* from *scipy.optimize*. The following formula as been implemented:

$$f(x) = A \cdot \exp\left(-\frac{(x-\mu)^2}{2\sigma^2}\right) + C \tag{32}$$

where C is the offset, necessary for negative values,  $\mu$  is the mean and  $\sigma$  is the standard deviation.

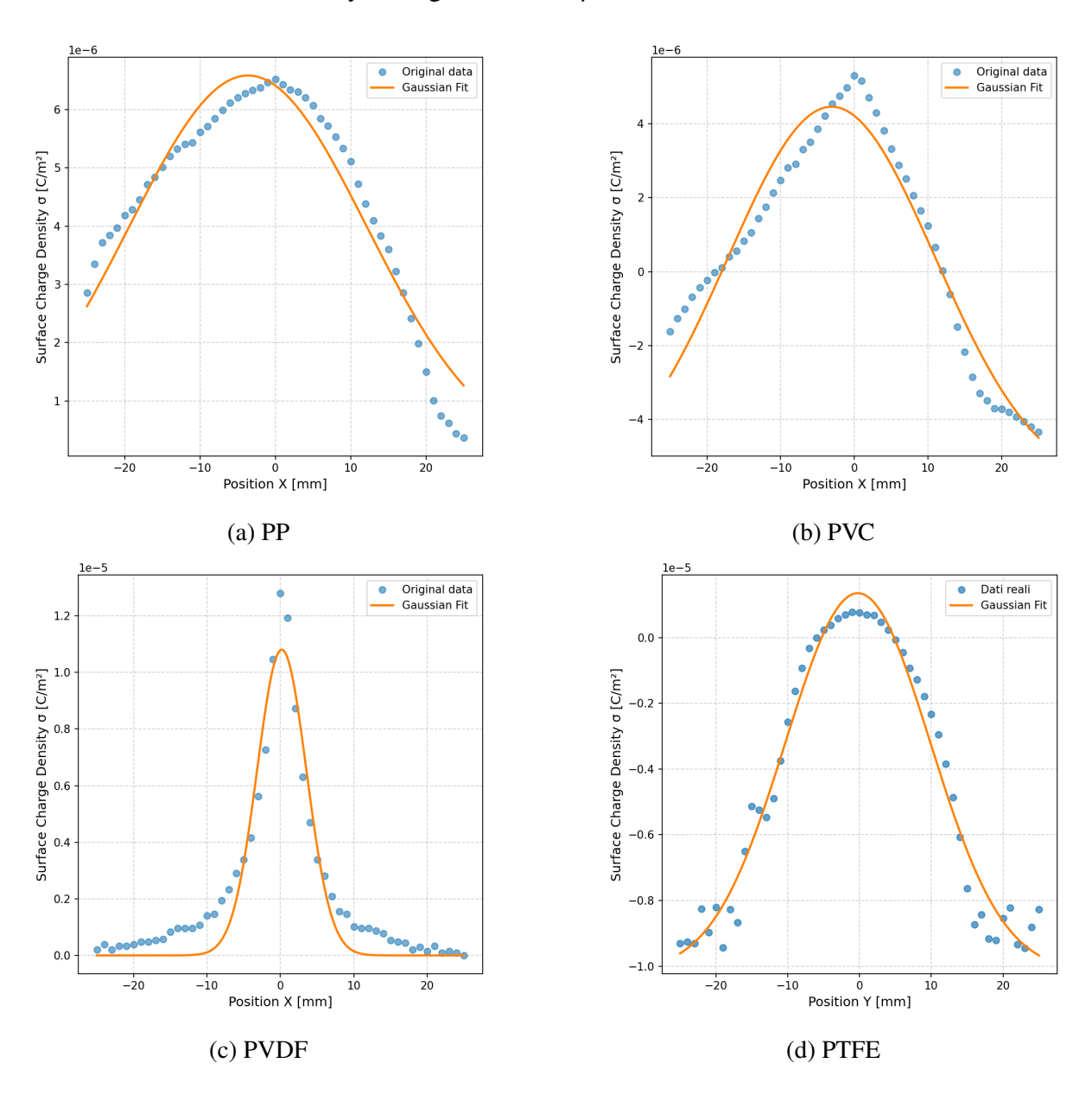


Figure 42: Gaussian Fit on Python.

The Gaussian function obtained can be seen in Figure 42. The following values in Table 4 were obtained.

Table 4: Gaussian Fit values.

Material	$A [C/m^2]$	$\mu$ [m]	$\sigma[m]$	$C[C/m^2]$
PP	$6.496 \cdot 10^{-6}$	$-1.361 \cdot 10^{-19}$		-
PVC	$8.597 \cdot 10^{-6}$	$-1.361 \cdot 10^{-19}$	$1.950 \cdot 10^{-2}$	$-2.182 \cdot 10^{-6}$
PVDF	$1.075 \cdot 10^{-5}$	$-1.361 \cdot 10^{-19}$	$3.382 \cdot 10^{-3}$	0
PTFE	$1.152 \cdot 10^{-5}$	$-1.361 \cdot 10^{-19}$	$1.007 \cdot 10^{-2}$	$-1.017 \cdot 10^{-5}$

## 5 Simulation

This study also involves a simulation part executed with COMSOL Multiphysics<sup>®</sup>. Following sections contain the studied models, in 3D. The aim is to develop the streamer criterion in air, first in the absence of any solid material, and then in the presence of a dielectric solid. In the case of the dielectric, the Gaussian distribution of surface charge density is used to simulate charge accumulation on the insulating material.

# 5.1 COMSOL Multiphysics®

COMSOL Multiphysics<sup>®</sup> is a numerical simulation software based on the Finite Element Method (FEM). In this work, the *Electrostatics* study, included in the *AC/DC Module*, was used to simulate electric fields in the presence of dielectric materials. This study solves **Poisson's equation**, which describes the relationship between the electric potential and the charge distribution within the domain:

$$\nabla \cdot (\varepsilon \nabla V) = -\rho_q \tag{33}$$

where V is the electric potential,  $\varepsilon$  is the material's permittivity, and  $\rho_q$  is the volume charge density. This equation is fundamental for describing the electrostatic behavior of dielectric materials. In fact, it is possible to determine the electric potential V at any point in space and consequently the electric field from the definition  $E = -\nabla V$ .

COMSOL Multiphysics<sup>®</sup> is a very powerful tool, but because of this, simulations often can take a long time. Therefore, it is necessary to find a compromise between simulation time and good meshing to obtain results as close as possible to reality. It is thus essential, during data analysis, to validate the simulation with a theoretical model.

#### 5.2 Electrode in Air without Solid

#### 5.2.1 Geometry

In Figure 43 below, the pointed electrode used in the G2Elab laboratory for breakdown inception analysis without a solid is showed. The gas used is air.

The symmetry of the electrode around its own axis was exploited: a 2D axisymmetric geometry was therefore performed, and subsequently the geometry was rotated by  $360^{\circ}$  to obtain the corresponding 3D model.



Figure 43: Point electrode used in G2Elab for breakdown experiment in air.

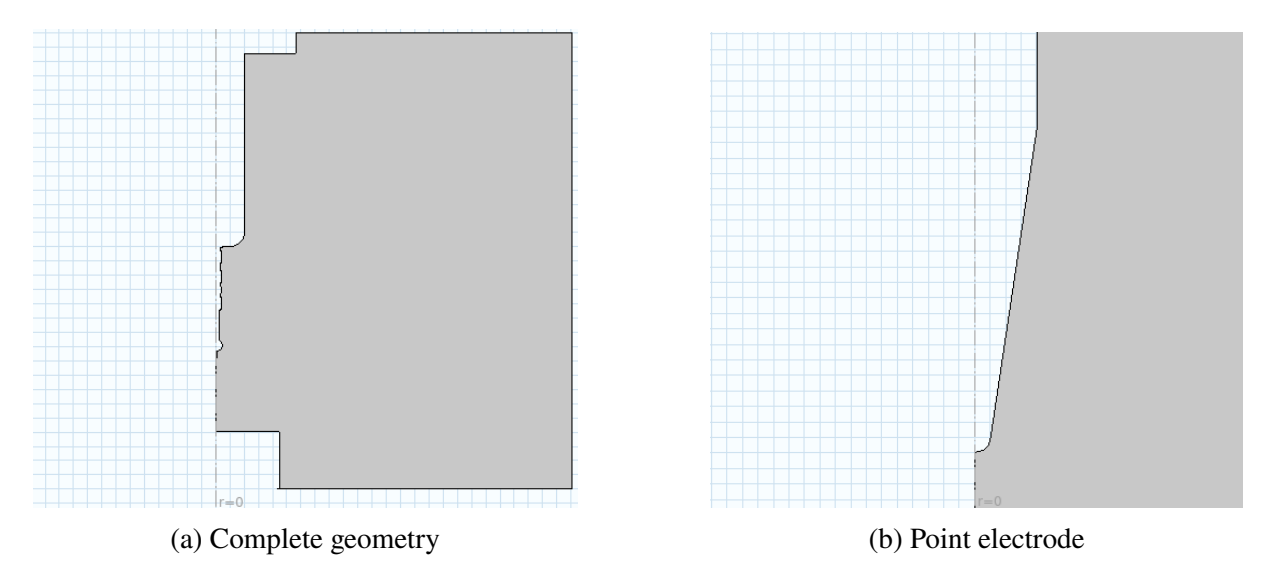


Figure 44: 2D axisymmetric Geometry.

In Figure 45 we can see the electrode of Figure 43 realized in 2D axialsymmetric geometry. At the end of the electrode body, there is a tip 45 (b).

The geometry was therefore imported into a new COMSOL file for the three-dimensional study. In *Geometry > Work Plane > Plane Geometry*, it is possible to import the geometry from another COMSOL file. Using the *Revolve* section available in *Work Geometry*, a full rotation around the axis was selected.

A voltage of 29kV has been applied to the HV electrode (Figure 46 (a)), and the other electrode is the ground (Figure 46 (b)).

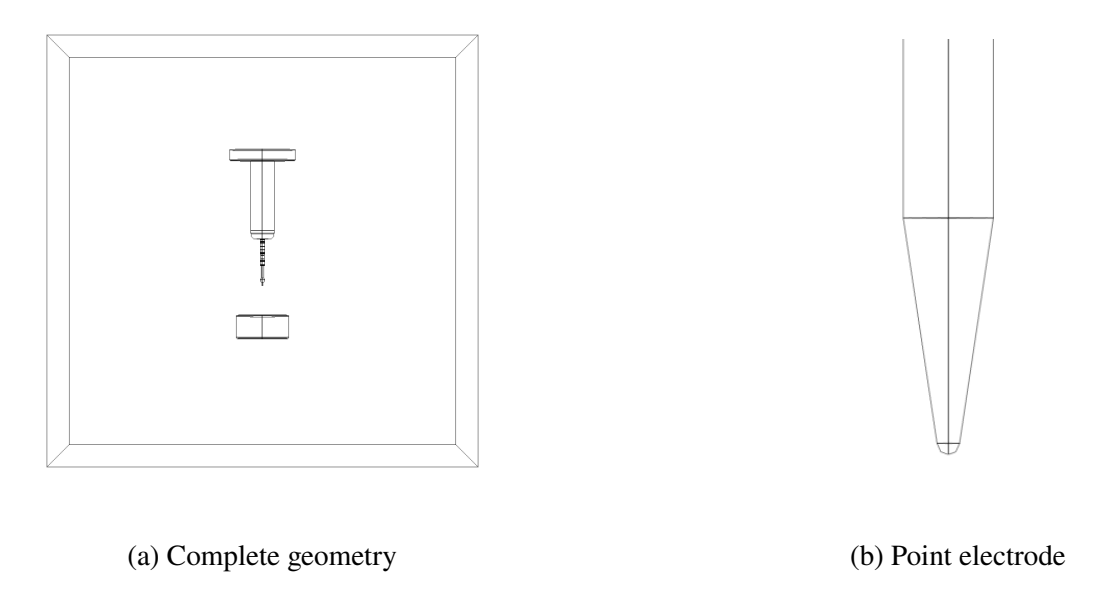


Figure 45: 3D Geometry.



Figure 46

Meshing in the case of complex geometries must be carried out with particular attention to the thinnest and sharpest regions of the structure. Consequently, the tip of the electrode was meshed with great care.

For the body of the electrode, a free tetrahedral mesh was applied, adjusting the values of the minimum and maximum element sizes to achieve a high-quality mesh.

The tip, on the other hand, required a more detailed approach. Among the available strategies, the most effective appeared to be the use of the Partition with Ball. This technique allows to inserting a spherical subdomain around a specific point of interest, the point of the electrode in this case. So the mesh is refined in that area (Figure 47).

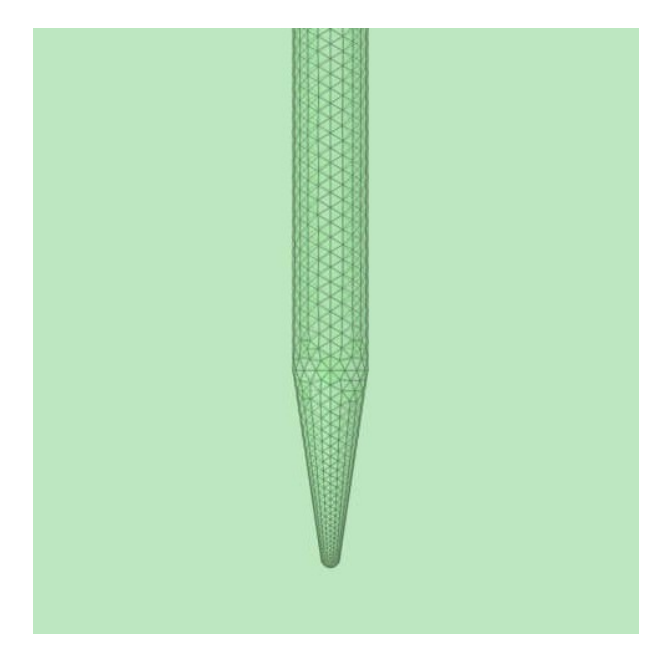


Figure 47: Mesh point electrode

#### 5.2.2 Validation of the model

The theoretical reference for the tip-plane configuration is typically found in [45].

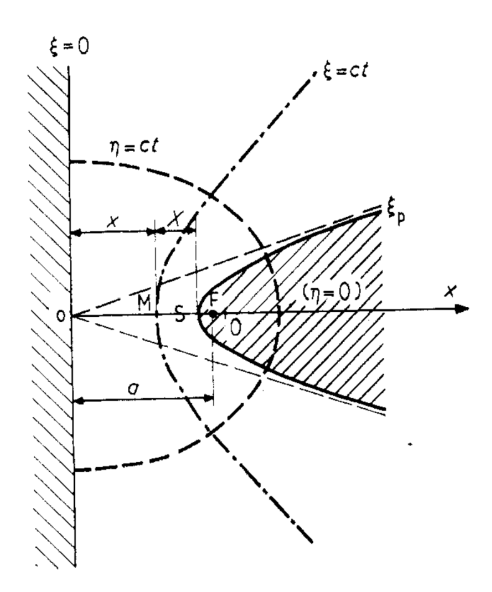


Figure 48: Tip-Plane [45].

Considering the geometry in Figure 48, the Electric field is expressed as:

$$E(X) = \frac{aC}{X(2a - X) + (a - X)r} \text{ with } C = \frac{V}{\ln\left\{2\left(\frac{a}{r}\right)^{1/2}\right\}}$$

In Figure 49 the Electric Field is evaluated in COMSOL along a 2D line from the tip of the point electrode to the grounded electrode (Simulation 1) and is compared with the theoretical

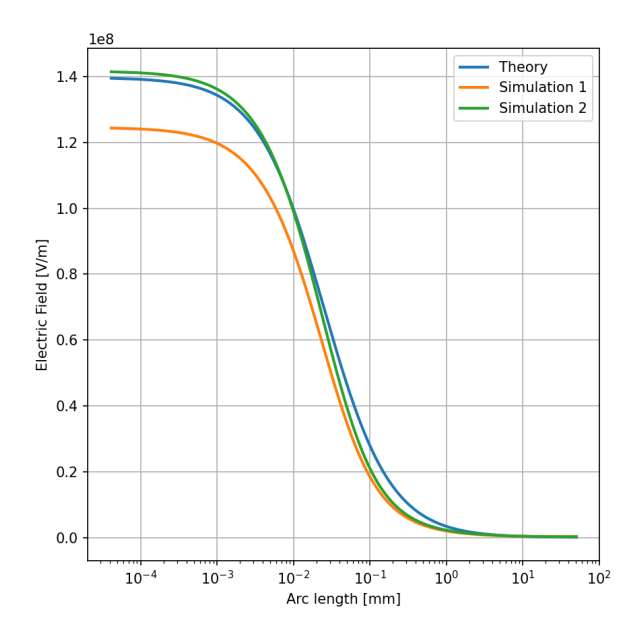


Figure 49: Electric field evaluated along a 2D line from the tip electrode to the ground. Simulation 1 corresponds to the original grounded electrode, while Simulation 2 corresponds to a larger grounded electrode.

model. The results show that the models are in excellent agreement; therefore, the meshing used represents a good compromise between the accuracy of the results and the computational time. Additionally, the figure includes Simulation 2 in which the grounded electrode is larger. This is intended to observe how the width of the grounded electrode impacts the maximum electric field value at the tip. Indeed, the theoretical model assumes an infinite grounded electrode, and this comparison helps to evaluate the validity of that assumption in the numerical simulation.

#### 5.2.3 Results

It is necessary to perform a study of the electric field in the geometry for the evaluation of the streamer criteria. Obviously, the electric field will be maximum at the tip of the electrode because the curvature radius there is very small, causing a local concentration of the electric field lines and as a consequence the field increases.

The electric potential of  $29 \, kV$  has been applied to the point electrode, the grounded electrode has an electric potential of  $0 \, V$ . The electric field was evaluated along the streamlines exported from COMSOL, see Figure 50. There are several methods to generate these streamlines. In the comparison between the different approaches, the most advantageous method is found to be the selection of streamlines originating from a specific boundary (the tip in our case) combined with a mesh-controlled distribution. The streamlines originate at the tip and extend down to the ground. This strategy was shown to obtain the highest values of the streamer criterion, thus representing the most critical scenario in terms of discharge formation.

Consequently, the electric field is evaluated along the streamlines in order to compute the integral of the streamer criterion, which is defined as:

$$\int_{L} \alpha_{eff}(E(s)) ds \approx k \tag{34}$$

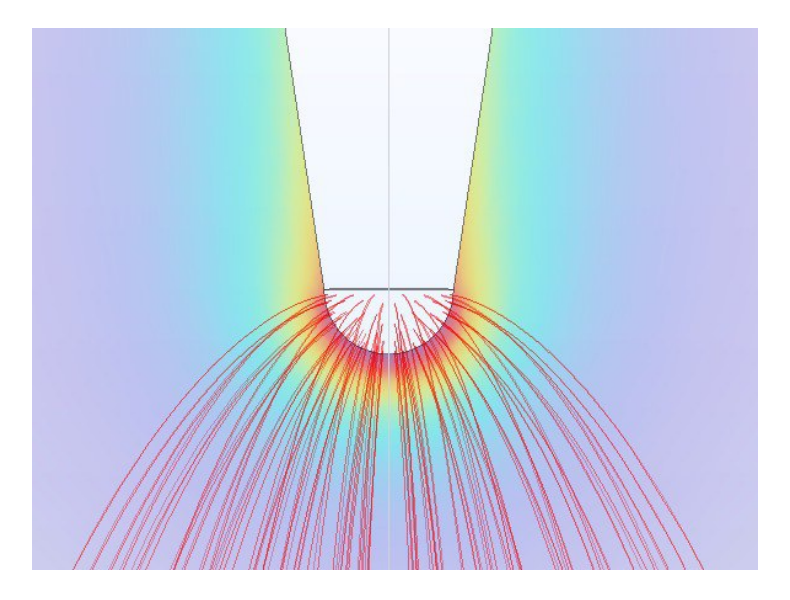


Figure 50: Mesh controlled streamline on selected boundary.

This equation has already been discussed in paragraph 2.1.4. It should be recalled that for  $k \ge 20$ , breakdown in air occurs.

In this simulation, a Electric Potential of 29kV has been applied to the point-electrode. The integral was computed for the different streamlines in MATLAB, and the following result was obtained. At atmospheric pressure (1 atm = 1.01325 bar), in air:  $V_{max} = 8, 2 [kV]$ .

These results imply that all streamlines considered are well above the critical breakdown threshold in air. Thus, under the applied conditions (29 kV, 1 atm), the generation of a streamer discharge is possible and highly likely, and the streamline of  $k_{max}$  is the best favorable path of inception.

#### 5.3 Electrode in Air with Solid

#### 5.3.1 The triple point

As already discussed,  $SF_6$  has insulating properties that are difficult to find in other gases because of his dielectric withstand. The major challenge is the issue of the 'triple point' (Figure 51) where two insulating materials with different dielectric properties meet a conductor. The triple point is a critical area of the system: it facilitates discharge initiation, which could lead to equipment failure.

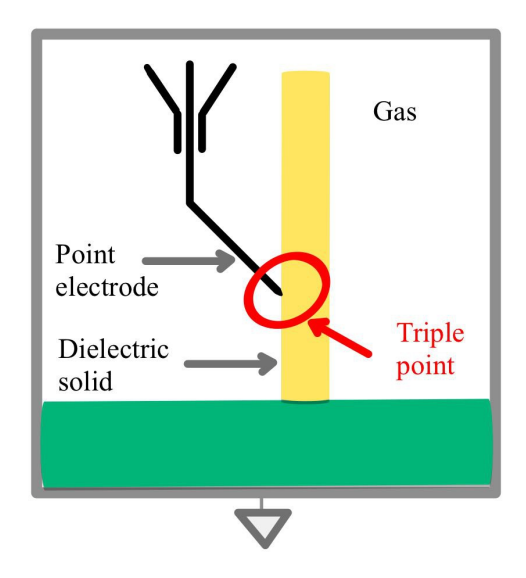


Figure 51: Triple point

In G2Elab, the scenario seen in figure 51 is studied experimentally by applying high voltage to the electric holder using a Marx generator. The distance between the electrode tip and the ground plane is 5 cm. Additionally, the solids analyzed are PTFE, PVC, PVDF, PP. The experiment can be conducted either at atmospheric pressure or under increased pressure. A highly sensitive camera captures the discharge or any breakdowns, while the emitted light is measured by a photomultiplier connected to an oscilloscope.

## 5.3.2 Geometry

In Figure 52 below, the pointed electrode used in the G2Elab laboratory for breakdown inception analysis with a solid is showed. The gas used is air. Figure 53 shows the geometry realized in COMSOL Multiphysics<sup>®</sup>.



Figure 52: Point electrode used in G2Elab for breakdown experiment in air with solid.

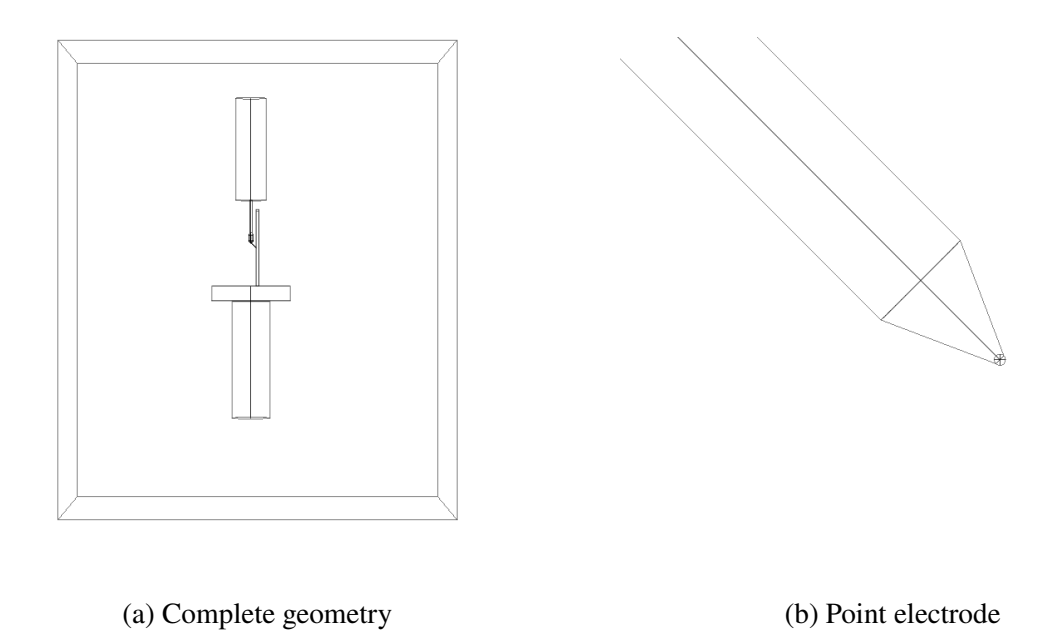


Figure 53: 3D Geometry.

In this section, the charge accumulation in the insulating material is also evaluated through

the surface charge density,  $\sigma_q$ . In paragraph 4.3.4, a Gaussian distribution of the charge density was found for the different insulating solids. This distribution refers specifically to the line at y=0, so along the central cross-section of the solid. On the solid's surface in COMSOL, the Gaussian distribution is applied not only along the x-axis but also along the z-axis, resulting in a two-dimensional surface distribution, as shown in the Figure 54.

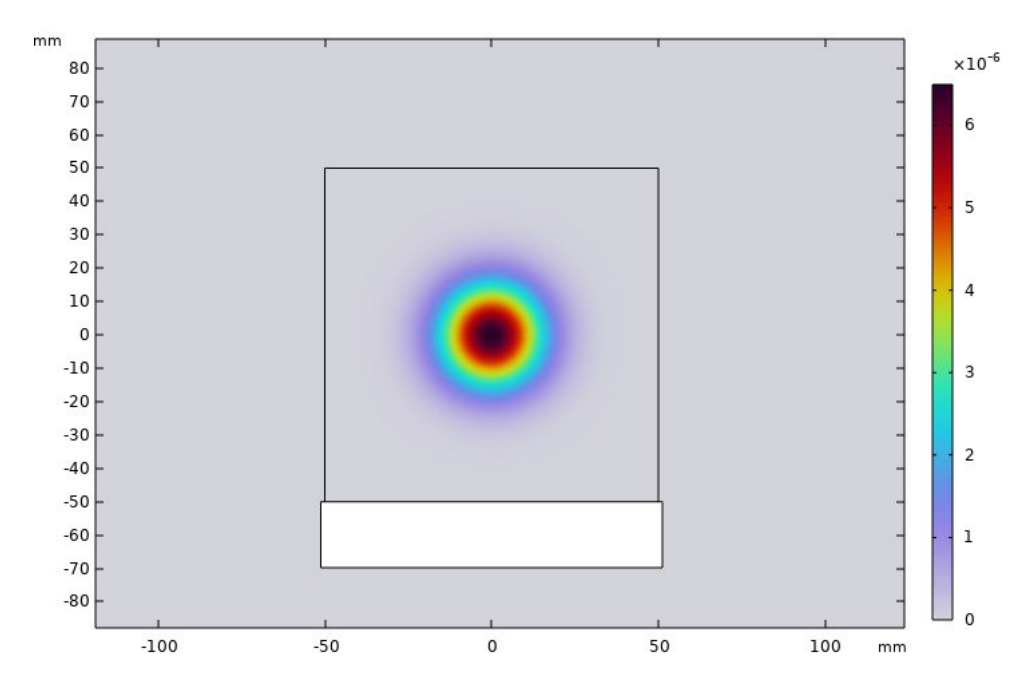


Figure 54: Charge density on surface of PP. Values for Gaussian distribution taken from Table 3.

It is important to note that this distribution will influence the sample's response to the externally applied electric field, which will be simulated in COMSOL in the following steps. A voltage of 29kV has been applied to the HV electrode (Figure 55 (a)), and the other electrode is the ground (Figure 55 (b)).

The same meshing applied for 3D Geometry without solid has been used for this geometry: the tip of the electrode was meshed with great care with Partition with Ball, centered in the point, and the body of the electrode was meshed with a free tetrahedral, adjusting the values of the minimum and maximum element sizes to achieve a high-quality mesh. Figure 56 shows the meshing of the point.

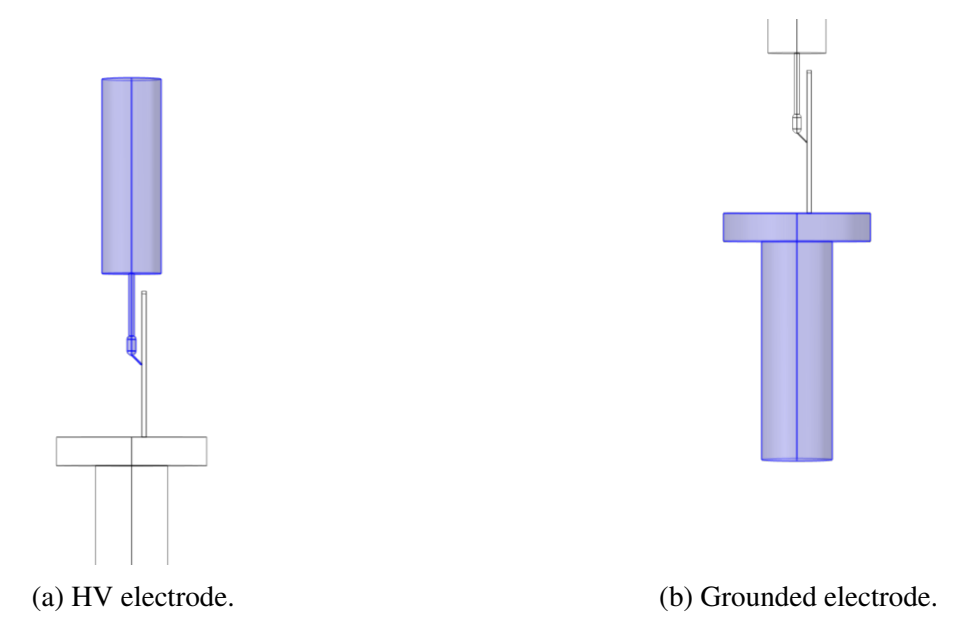


Figure 55

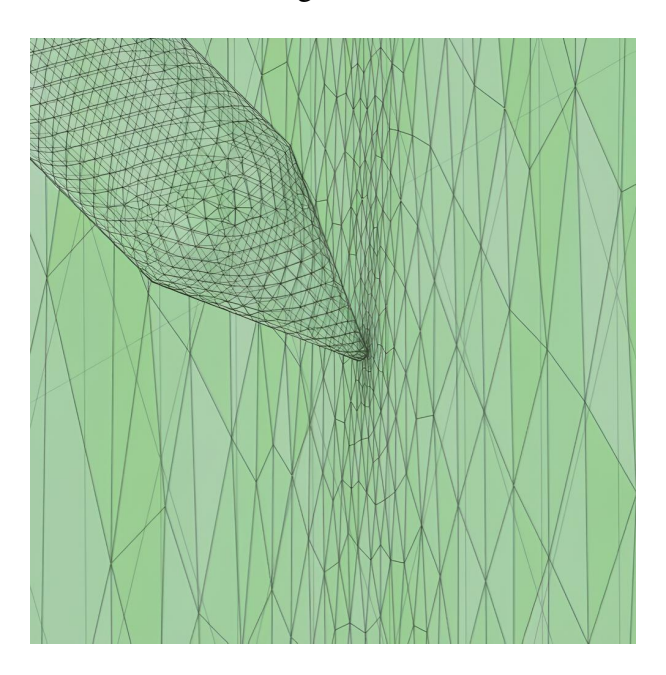


Figure 56: Mesh point electrode.

### **5.3.3** Validation of the model

For the validation of the following model, it is not possible to refer to an established theoretical formulation, as was done in the case of the electrode in air without any solid material, in paragraph 5.2.2. In the literature, an analytical description of the electric field distribution in the presence of complex geometries—such as the one considered in this study has not yet been rigorously defined.

However, the validation of the previous model, performed on a simplified configuration, allows us to adopt the same meshing scheme for the more complex geometry.

#### **5.3.4** Results

#### 1. Effect of the Relative Permittivity on the Electric Field

Placing a dielectric solid parallel to an electrode axis alters the electric field lines due to the solid's higher relative permittivity compared to air. This difference in permittivity causes the field lines to concentrate towards the dielectric's surface. The introduction of the solid causes the material to polarize in the presence of an electric field. This process generates an internal electric field that opposes the applied external field, resulting in the divergence of field lines and a reduction in the field intensity inside the solid. Consequently, if the electrode features a sharp point, this concentration of field lines becomes particularly pronounced at the tip, resulting in a significantly more intense electric field in that localized region.

The phenomenon of electric field line distortion along the solid can be observed through a 3D simulation in COMSOL Multiphysics<sup>®</sup>. Figure 57 illustrates the distribution of electric field lines in air and when the solid material is present.

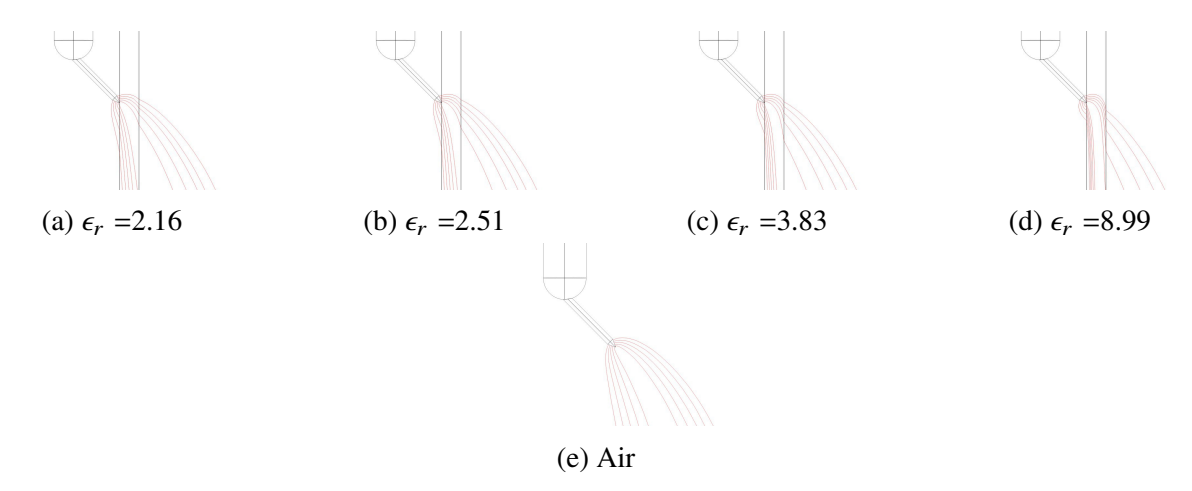


Figure 57: Streamline with solid of different  $\epsilon_r$  and in air.

Among the materials considered, PTFE exhibits a relatively low relative permittivity ( $\epsilon_r = 2.16$ ), while PVDF has a significantly higher relative permittivity ( $\epsilon_r = 8.99$ ). An higher  $\epsilon_r$  amplifies the effect as we can see comparing PTFE ( $\epsilon_r = 2.16$ ) to PVDF ( $\epsilon_r = 8.99$ ).

The intensified Electric field near the tip creates a preferential path for discharge, characterized by a higher electric field. The maximum Electric field is evaluated in the geometry and the values are shown in the Table 5.

Table 5: Maximum Electric Field for different  $\epsilon_r$ . Domain: All Geometry, Applied Voltage 29 kV, Position: Triple point.

$\epsilon_r$	Maximum Electric Field [V/m]
1 (Air)	$1.04 \cdot 10^9$
2.16	$2.50 \cdot 10^9$
2.51	$2.91 \cdot 10^9$
3.83	$4.47 \cdot 10^9$
8.99	$8.69 \cdot 10^9$

From the COMSOL simulation, it is observed that the maximum electric field always occurs at the tip of the electrode. In the presence of a solid, this corresponds to the triple point. This is due to the extremely small radius of curvature of the electrode tip (0.05 mm), which causes a strong intensification of the electric field in that region.

Applying the same voltage, Table 4 shows that the maximum electric field values strongly depend on the permittivity of the solid. When  $\varepsilon_r$  increases, the electric field near the tip intensifies significantly. This is because, when the relative permittivity of the solid increases, the material attracts more electric field lines, concentrating them more strongly near its surface. This increases the risk of breakdown from the tip.

Before proceeding with the following analysis, it is necessary to clarify that the case considered in Table 4, which does not include charge accumulation, does not represent the actual behavior of the sample in response to ionization. This is because the model used is simplified and is primarily intended to observe how the electric field varies with the permittivity parameter. In reality, insulating samples, as shown by the cartographies in 4.3.1, already have a pre-existing charge distribution before any charge deposition from ionization occurs. The charge present inside the sample obviously influences the subsequent charge accumulation related to the ionization process.

#### 2. Effect of the Charge Density of the sample on the Electric Field

Considering the Charge Density on the solid, we get the following value for the Maximum Electric Field.

Table 6: Maximum Electric Field for different  $\epsilon_r$  with density of charge. Domain: All Geometry, Applied Voltage 29 kV, Position: Triple point.

$\epsilon_r$	Maximum Electric Field with $\sigma_q$ [V/m]
2.16	$1.99 \cdot 10^9$
2.51	$2.62 \cdot 10^9$
3.83	$4.21 \cdot 10^9$
8.99	$14.62 \cdot 10^9$

From the comparison between Tables 5 and 6, we observe that for PP, PVC, PVDF the electric field slightly decreases in the presence of charge density. For PTFE, the total measured electric field increases. It is important to note that the electric field is given by:

$$E_{tot} = E_{external} + E_{accumulated\ charges} \tag{35}$$

The simulation, conducted under a positive applied voltage, shows that the effect of surface charge accumulation on the total electric field depends on the sign of the charges. When positive charges accumulate on the surface of the sample, they create an electric field that opposes the one produced by the positively charged electrode. This results in a reduction of the total electric field. Conversely, the accumulation of negative charges reinforces the external field, leading to an overall increase. This behavior is particularly evident in highly electronegative materials like PTFE, where the field generated by the trapped charges is aligned with the applied field, enhancing the electric field near the electrode. In contrast, the other polymers tend to accumulate charges that oppose the applied field, which leads to a reduction of the electric field in the most

critical area.

In the Figure 58, the Electric Field streamlines are shown. A uniform distribution of streamlines over the entire bottom surface of the tip was selected in order to achieve better visibility of the streamlines.

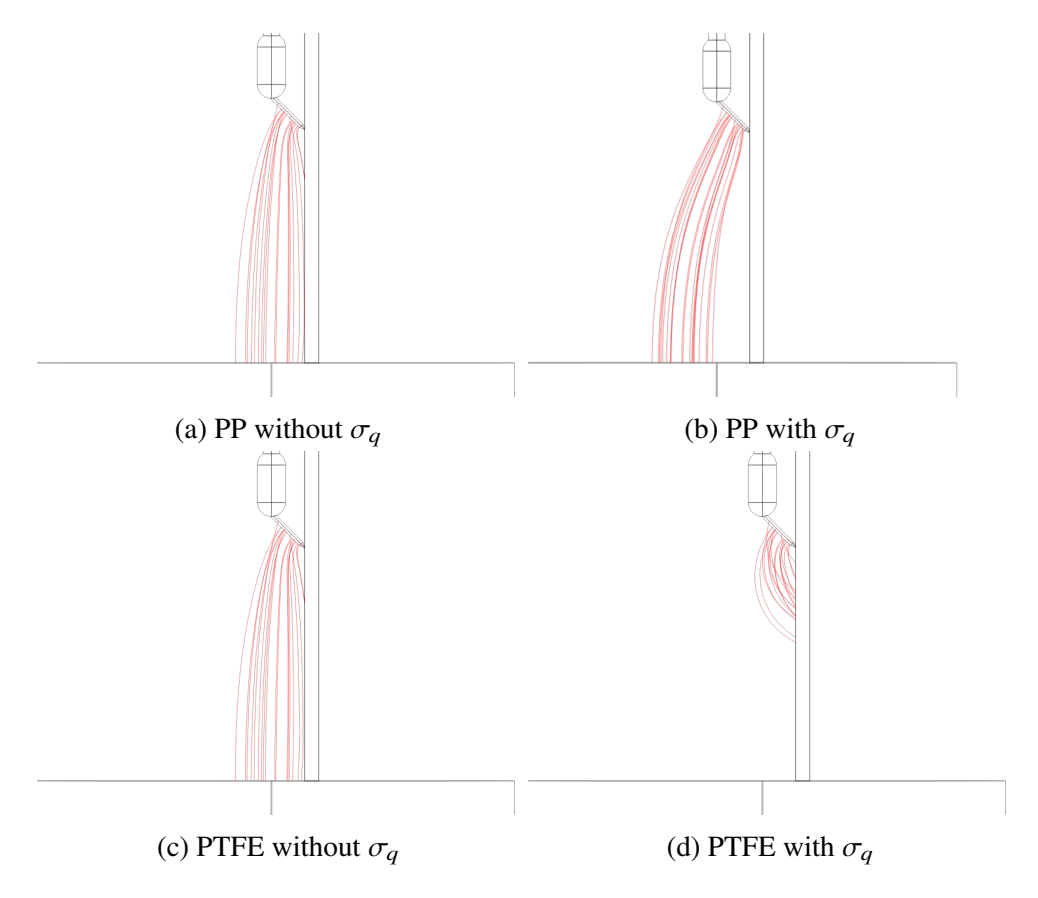


Figure 58: Streamline for Streamer Criteria analysis. Voltage applied to the electrode: +29 kV

For PP, it can be observed that with the addition of surface charge density, the streamlines curve slightly more, in response to the electric field generated by the accumulated charge within the material. What happens with PTFE is particularly interesting. Without surface charge density, the streamlines are comparable to those observed for PP: they follow the typical path from the electrode tip to ground. However, when the surface charge density is introduced, the streamlines become strongly concentrated in the area near the tip, and the electric field is much more intense.

The streamlines curve because the electric field is distorted by the presence of negative charges on the surface of the PTFE. These charges modify both the intensity and the local direction of the field, resulting in a deviation of the streamlines from the one without density of charge.

Logically, the effect will be reversed in the case where a negative voltage is applied to the electrode. As an example, the streamlines for negative applied voltage are shown in Figure 59.

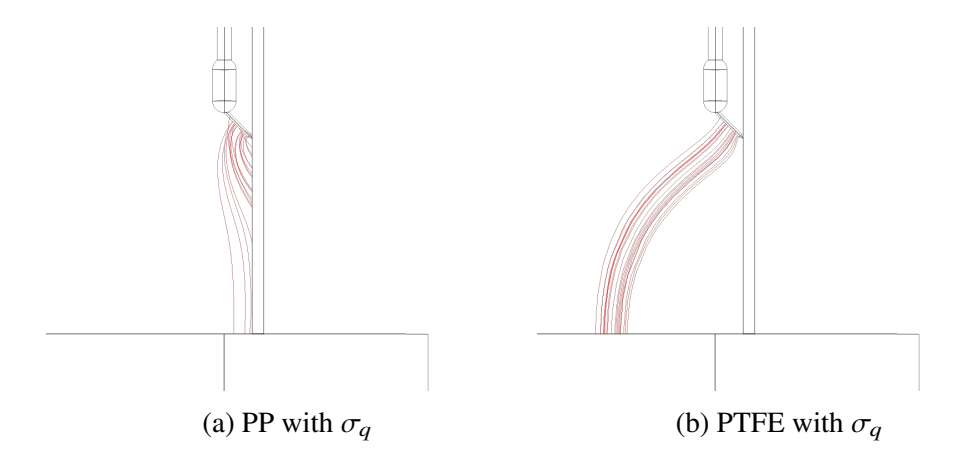


Figure 59: Streamline for applied voltage to the electrode: -29 kV

The streamlines in the Figure 59 are directed toward the surface of the insulating solid for the PP case. This occurs because the electric field generated by the charge density adds to the field generated by the electrode along the surface of the solid. The electric field increases  $(E_{max} = 3.47 \cdot 10^9 \text{ [V/m]})$ .

In contrast, for PTFE, a reduction of the electric field along the surface is observed ( $E_{max} = 6.19 \cdot 10^8$  [V/m]), and the field lines move away from the solid compared to the case without surface charge (Figure 58 (c)).

#### 3. Streamer Criteria

As done in the paragraph 5.2.3, also in this paragraph the aim is to solve the streamer criterion to understand how is affected by the charge accumulation. To do this, different streamline configurations available in COMSOL were examined in order to identify the most suitable one for the geometry in Figure 52. In this case, the streamlines were generated at the tip of the point, since we are interested in studying the electric field in the region where it is at its maximum. Therefore, in the streamline settings, the following options were selected: *Positioning* > On selected items, *Point distribution* > Uniform, Number > 20.

In this simulation an Electric Potential of 29kV has been applied to the point-electrode and the simulation is performed at atmospheric pressure (1 atm = 1.01325 bar), in air. The obtained streamlines in the case of PTFE are shown in the Figure 60. Note that in the figure, the right side in white is the solid: in fact, it was extract from the domain of study because the streamer propagates in air.

The integral (34) is computed for the different streamlines in MATLAB, and the results in Table 6 are obtained.

In agreement with what was observed previously, PP, PVC, and PVDF show a reduction in the total electric field when space charge density is considered. PTFE, however, exhibits the opposite behavior.

Indeed, we observe in Table 6 that the  $V_{max}$  that can be applied, slightly increases when the space charge density is considered. Conversely, this value decreases in the case of PTFE because, as observed, the electric field increases and, consequently, the probability of streamer inception.

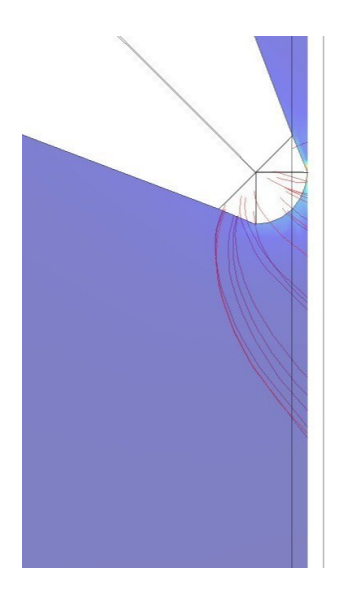


Figure 60: Streamline on point. Case of PTFE sample with  $\sigma_q$ . Applied voltage: +29 kV.

Table 7: Results of streamer criteria. Applying  $V_{max}$  we get k = 20.

Sample Material	$\sigma_q$	$V_{max} [kV]$
PP	X	4.70
PP	<b>√</b>	5.87
PVC	X	3.44
PVC	<b>√</b>	3.73
PVDF	X	2.13
PVDF	<b>√</b>	2.20
PTFE	X	4.70
PTFE	<b>√</b>	2.68

However, this comparison is not realistically complete. In fact, as previously stated, the case without space charge density is a simplified scenario, and thus at this stage, the aim was to observe the impact of such a simplification.

The realistic and more important comparison is to be made in the presence of a solid (and thus space charge density) and in the absence of a solid. Comparing the results obtained in the previous paragraph for  $V_{max}$  in the absence of a solid, it is easy to observe that the introduction of the solid decreases the value of  $V_{max}$ , favoring streamer inception. In particular, PTFE shows a very small value of  $V_{max}$ , indicating that its use may facilitate the onset of streaming.

However, a limitation of the model should be noted. The simulation is purely electrostatic, meaning that it was performed by applying a fixed surface charge density (specific to each material) and a constant voltage of  $29 \ kV$ . This approach only allows for evaluating the electric field distribution in response to the applied potential and the density of charge. As discussed in the sections related to surface potential decay, the charge density evolves over time. Therefore, in a time-dependent analysis, the assumption of a constant surface charge would no longer hold. For instance, in the case of PVDF, which is known for its rapid charge decay, the obtained  $V_{max}$  value is only representative of the initial condition, before any significant discharge occurs.

# **Conclusions**

The high environmental impact of  $SF_6$ , widely used for electrical insulation, drives the search for more sustainable alternatives. Hybrid gas/solid systems, combining compressed air and polymeric materials as solid insulators, represent a promising solution.

This thesis focused on studying surface charge accumulation in polymers under high electric fields to understand how it affects the local electric field and the risk of discharge initiation, using a combined experimental and numerical simulation approach.

In this study, the following were utilized: experimental measurements using SPD on PP, PVC, PVDF, and PTFE; analysis via bi-exponential fitting to estimate charge density and traps; COMSOL simulations with a triple point configuration; and calculation of the streamer criterion as a predictive measure.

In the analysis of experimental data, a clear preference emerged for defining a mathematical model for their treatment. This necessity is particularly evident due to the large volume of collected data. During the data processing phase, for instance in the study of trap density, the abundance of data, combined with the numerical differentiation, introduces significant noise into the analysis. Mathematical modeling, specifically the application of bi-exponential fitting, proved to be an extremely useful and effective tool for overcoming these challenges and improving the accuracy of data analysis. Specifically, the mathematical model employed, extensively validated by the literature, posits the existence of two distinct components: one with fast dynamics and one with slow dynamics. These two components respectively describe a fast and a slow charge release mechanism.

From the surface potential decay curves and the fitting model, it is observed (in order from highest to lowest charge retention) that:

- Polytetrafluoroethylene PTFE: Retains charge for an extended period; its complete discharge for positive ionization requires more than three months. It presents a large number of deep traps and a reduced number of shallow traps, resulting in some of the lowest conductivity values among the other studied samples.
- Polypropylene PP: Strongly retains charge during the analyzed period. Its conductivity
  values are extremely low, comparable only to those obtained for PTFE. It exhibits fewer
  fast-release traps than PVC but more than PTFE. Both positive and negative charges are
  completely released within approximately three months.
- Polyvinyl Chloride PVC: Shows a faster surface potential decay compared to PP and PTFE. Consequently, it has a higher number of fast-release traps than PP and PTFE. However, it still presents a significant number of slow-release traps. It completely discharges in about one month.
- Polyvinylidene Fluoride PVDF: Exhibits a very rapid surface voltage discharge, occurring
  in about one hour. This indicates a high number of low-energy traps and a reduced number
  of deep traps.

Experimental measurements highlighted the surface charge dynamics of the different polymers, while COMSOL simulations provided a detailed picture of the interaction between the electric field and the accumulated charge. This integrated approach allowed for a more comprehensive evaluation of how the material properties influence the streamer criteria.

The results obtained from the electrostatic simulations in COMSOL Multiphysics<sup>®</sup> show that the presence of a dielectric solid alters the electric field distribution near the electrode tip, especially at the triple point. The presence of the solid causes a concentration of field lines near the solid surface and consequently leads to an intensification of the electric field in that region.

A realistic representation of hybrid insulation must account the accumulated surface charge on the solid dielectric, which originates from prior charge deposition processes. The inclusion of surface charge density modifies the local electric field in different ways depending on the nature of the material.

For PP, PVC, and PVDF, the accumulated surface charge tends to oppose the externally applied electric field, resulting in a net reduction of the total electric field at the triple point. This phenomenon is consistent with a positive polarization of the dielectric, where the internal field generated by the charge distribution partially screens the external field.

In contrast, for PTFE, which is known for its strong ability to trap negative charges due to its high electronegativity and deep trap levels, the accumulated surface charge enhances the local electric field. In this case, the field produced by the space charge is aligned with the external field, leading to a reinforcement of the total electric field and an increase in k (Streamer criteria). This effect directly correlates with a higher risk of streamer inception, making PTFE less favorable in applications where discharge mitigation is critical.

In the perspective of designing safer and more efficient hybrid systems:

PP appears to be a good compromise between low conductivity and a neutral behavior with respect to the electric field, with moderate charge retention that helps reduce the risk of discharge inception.

PTFE, while excelling in charge retention due to the presence of deep traps, can be problematic in critical configurations (such as the triple point) because of the local reinforcement of the electric field and the high risk of streamer inception.

PVDF shows low charge stability over time, with rapid release that can be advantageous in applications where quick dissipation of accumulated charge is preferred to avoid discharge phenomena.

PVC is a material with balanced characteristics for applications requiring a compromise between charge accumulation and release.

#### Some suggestions for future studies:

- The simulation conducted is electrostatic and stationary, which means it does not take into account how the charge accumulated on the materials changes over time. To have a more complete and realistic assessment of the materials' reliability under operating conditions, it will be essential to develop time-dependent models to study how the charge dissipates over time and how streamers may form and propagate.
- Another interesting aspect to explore is the environmental impact and sustainability of
  the insulating materials we analyzed. It is important to examine in detail the recycling
  and end-of-life management processes of these polymers to evaluate more sustainable
  solutions for hybrid gas/solid systems, integrating both technological and environmental
  aspects.

# References

- [1] D. Halliday, R. Resnick, and J. Walker, *Fundamentals of Physics, 10th ed.* Hoboken, NJ, USA: John Wiley and Sons, 2014.
- [2] IPCC, Climate Change 2021: The Physical Science Basis. Contribution of Working Group I to the Sixth Assessment Report of the Intergovernmental Panel on Climate Change V. Masson-Delmotte et al., Eds. Cambridge University Press, 2021.
- [3] B. H. Crichton, Gas Discharge Physics Glasgow, UK: University of Strathclyde, 1996.
- [4] F. Llewellwyn-Jones, *Ionization and Breakdown in Gases*, Methuen, London, 1957.
- [5] S. Rahmanzadeh and M. S. Pishvaee *Electron radar search algorithm: a novel developed meta-heuristic algorithm*, vol. 32, no. 15, pp. 10989-11005, Oct. 2019.
- [6] E. E. Kunhardt and Y. Tzeng, *Development of an electron avalanche and its transition into streamers*, Polytechnic University, Route 110, Farmingdale, New York 11735, Auburn University, Auburn, Alabama, 36849-3502, 1987.
- [7] S. Nijdam, J. Teunissen, U. Ebert, *The physics of streamer discharge phenomena*, Plasma Sources Science and Technology, vol. 29, no. 10, 103001, Oct. 2020
- [8] T. Liu, I. Timoshkin, J. MacGregor, M. Wilson, J. Given, N. Bonifaci, R. Hanna, *Field-Time Breakdown Characteristic of Air, N2, CO<sub>2</sub> and SF*<sub>6</sub> IEEE transiction on plasma science, VOL. 48, 2020.
- [9] L. B. Loeb, Electrical Coronas: Their Basic Physical Mechanisms, University of California Press, United States, 1965.
- [10] A. von Keudell and V. Schulz-von der Gathen Foundations of low-temperature plasma physics—an introduction Plasma Sources Sci. Technol., vol. 26, no. 10, p. 103001, Oct. 2017.
- [11] Laure Tremas. *Pre-breakdown and breakdown phenomena in air along insulating solids*, Electric power. Université Grenoble Alpes, 2017.
- [12] N. A. Popov, Formation and Development of a Leader Channel in Air, Plasma Physics Reports, vol. 29, no. 8, pp. 695–708, 2003.
- [13] C. L. da Silva and V. P. Pasko, *Dynamics of streamer-to-leader transition at reduced air densities and its implications for propagation of lightning leaders and gigantic jets* J. Geophys. Res. Atmos, vol. 118, no. 21, pp. 12,041-12,054, Nov. 2013.
- [14] Mose Akyuz, *Positive streamer discharge in air and along insulating surface:experiment and simulation*, Faculty of Science and Technology, 2002.
- [15] I. Gallimberti and N. Wiegart, Streamer and leader formation in SF<sub>6</sub> and SF<sub>6</sub> mixtures under positive impulse conditions. II. Streamer to leader transition Journal of Physics D: Applied Physics, vol. 19, no. 12, pp. 2363–2377, Dec. 1986.

- [16] V. Babrauskas *Arc Breakdown in Air over Very Small Gap Distances* Fire Science and Technology Inc., Issaquah, WA, USA.
- [17] E. Husain and R. S. Nema, *Analysis of Paschen curves for air, N2 and SF*<sub>6</sub> using the *Townsend breakdown equation* Proceedings of the International Conference on Gaseous Dielectrics, Bangalore, India, Aug. 1982.
- [18] P. K. Watson, *The Transport and Trapping of Electrons in Polymers* IEEE Transactions on Dielectrics and Electrical Insulation, vol. 2, no. 5, pp. 916-924, Oct. 1995.
- [19] D. A. Seanor, Electrical Properties of Polymers Elsevier, 2013.
- [20] W.-W. Shen, H.-B. Mu, G.-J. Zhang, J.-B. Deng, and D.-M. Tu, *Identification of electron and hole trap based on isothermal surface potential decay model* J. Appl. Phys., vol. 113, no. 8, p. 084102, 2013.
- [21] I. Gallimberti, G. Marchesi, and L. Niemeyer, textitStreamer corona at an insulator surface in Proc. 7th Int. Symp. on High Voltage Engineering, Dresden, Germany, paper 41.10, pp. 47-50, Aug. 1991.
- [22] X. Meng, H. Mei, L. Wang, Z. Guan, and J. Zhou, *Characteristics of Streamer Propagation along Insulation Surface: Influence of Shed Configuration* China Electric Power Research Institute, Beijing, China.
- [23] Dubinova, Modeling of streamer discharges near dielectrics, Phd Thesis Applied Physics and Science Education, Technische Universiteit Eindhoven, 2016.
- [24] N. L. Allen and P. N. Mikropoulos, *Streamer Propagation along Insulating Surfaces* IEEE Trans. Dielectr. Electr. Insul., vol. 6, no. 3, pp. 357-362, June 1999.
- [25] Giacometti, J. A., Fedosov, S., Costa, M. M. Corona Charging of Polymers: Recent Advances on Constant Current Charging. Brazilian Journal of Physics, 29(2), 1999.
- [26] Li J, Zhou F, Min D, Li S and Xia R 2015 The energy distribution of trapped charges in polymers based on isothermal surface potential decay model IEEE Trans. Dielectr. Electr. Insul. 22 1723–32.
- [27] I. D. Baikie, E. Venderbosch, J. A. Meyer, and P. J. Z. Estrup, *Analysis of stray capacitance in the Kelvin method* J. Appl. Phys., vol. 69, no. 5, pp. 2754-2759, Mar. 1991.
- [28] S. Boisseau, *Récupération d'énergie vibratoire à électrets*, phdthesis, Université de Grenoble, 2011.
- [29] A. Crisci, B. Gosse, J.-P. Gosse, and V. Ollier-Duréault, *Surface-potential decay due to surface conduction* J. Electrostatics, vol. 44, no. 4, pp. 249-261, Oct. 1998.
- [30] P. Molinié, A Review of Mechanisms and Models Accounting for Surface Potential Decay IEEE Trans. Plasma Sci., vol. 40, no. 2, pp. 167-175, Feb. 2012.
- [31] P. Molinié, *How fast does a static charge decay? An updated review on a classical problem* Laboratoire de Génie Electrique et Electronique de Paris (GeePs), Université Paris-Saclay, CentraleSupélec, CNRS, Gif-sur-Yvette, 91192, France, 2024.

- [32] Y. Han, S. Li and D. Min *Trap Energy Distribution in Polymeric Insulating Materials through Surface Potential Decay Method* IEEE Transactions on Dielectrics and Electrical Insulation, vol. 25, no. 2, pp. 639-, April 2018.
- [33] P. Llovera and P. Molinié, New Methodology for Surface Potential Decay Measurements: Application to Study Charge Injection Dynamics on Polypropylene Films IEEE Transactions on Dielectrics and Electrical Insulation, vol. 11, no. 6, pp. 1049–1056, Dec. 2004.
- [34] P. K. Watson, *The energy distribution of localized states in polystyrene, based on isothermal discharge measurements* Journal of Electrostatics, vol. 24, pp. 25–36, 1990.
- [35] J. Belcher et al., Capacitance and Dielectrics, MIT OpenCourseWare, 2007.
- [36] G. Li, K. Hu, W. Sun, Y. Wei, S. Li, and Q. Lei, *Surface trap characteristics of polyimide and effect of surface charge accumulation on surface flashover* Journal of Applied Physics, vol. 132, no. 21, p. 213301, Dec. 2022.
- [37] M. Tschentscher, D. Graber, and C. M. Franck, *Influence of humidity on conduction processes in gas-insulated devices* IET High Volt., vol. 5, no. 3, pp. 290–296, 2020.
- [38] L. Gu, W. Tan, J. He, Z. Jiang, X. Chen, W. Ren, and Z. Jin *Relationship between Corona Discharge Thrust and Applied Voltage's Polarity* Energies, vol. 16, no. 8, p. 3569, Apr. 2023
- [39] E. A. Baum, T. J. Lewis, and R. Toomer, *Decay of electrical charge on polyethylene films* Journal of Physics D: Applied Physics, vol. 10, no. 4, pp. 487–495, Apr. 1977.
- [40] E. Manias, A. Touny, L. Wu, K. Strawhecker, B. Lu, and T. C. Chung, *Polypropylene/Montmorillonite Nanocomposites. Review of the Synthetic Routes and Materials Properties* Chem. Mater., vol. 13, no. 10, pp. 3516–3529, Sep. 2001.
- [41] Ahmad, N., Kausar, A., Muhammad, B. *Perspectives on Polyvinyl Chloride and Carbon Nanofiller Composite: A Review* Polymer-Plastics Technology and Engineering, 55(10), 2016
- [42] Dallaev, R.; Pisarenko, T.; Sobola, D.; Orudzhev, F.; Ramazanov, S.; Trčka, T. Brief *Review of PVDF Properties and Applications Potential*. Polymers 2022, 14, 4793.
- [43] G. J. Puts, P. Crouse, and B. M. Ameduri, *Polytetrafluoroethylene: Synthesis and Characterization of the Original Extreme Polymer* Chem. Rev., vol. 119, no. 1, pp. 176–313, Jan. 2019.
- [44] N. Amiour, Z. Ziari, and S. Sahli *Traps energy distribution in Kapton HN poly-imide films through surface potential decay model under humidity conditions* Proc. CIRFE'23—International Conference on Electrical and Electronics Engineering, Constantine, Algeria, Oct. 2023.
- [45] R. Coelho and J. Debeau *Properties of the tip-plane configuration* Laboratoire de Génie Electrique, Faculté des Sciences de Paris, and Laboratoire Central des Industries Électriques, Paris, France, Dec. 29, 1970.